PB86-155033

Development of CBM-X (Carbon Bond Mechanism) for Urban and Regional AQSMs (Air Quality Simulation Models)

Systems Applications, Inc.
San Rafael, CA

Prepared for

Environmental Protection Agency
Research Triangle Park, NC

Feb 86

U.S. Department of Commerce
National Technical Information Service
NTIS

PB86-155033

EPA/600/3-86/012
February 1986

DEVELOPMENT OF CBM-X MECHANISMS FOR URBAN AND REGIONAL AQSMs

by

G. Z. Whitten
M. W. Gery

Systems Applications, Incorporated
101 Lucas Valley Road
San Rafael, California 94903

Contract No. 68-02-3738

Project Officer

Marcia C. Dodge

Atmospheric Chemistry and Physics Division
Atmospheric Sciences Research Laboratory
Research Triangle Park, North Carolina 27711

ATMOSPHERIC SCIENCES RESEARCH LABORATORY
OFFICE OF RESEARCH AND DEVELOPMENT
U.S. ENVIRONMENTAL PROTECTION AGENCY
RESEARCH TRIANGLE PARK, NORTH CAROLINA 27711

REPRODUCED BY
NATIONAL TECHNICAL
INFORMATION SERVICE
U.S. DEPARTMENT OF COMMERCE
SPRINGFIELD, VA. 22161

TECHNICAL REPORT DATA
(Please read Instructions on the reverse before completing)

1. REPORT NO. EPA/600/3-86/012	2.
3. RECIPIENT'S ACCESSION NO. PB86 155033/AS	
4. TITLE AND SUBTITLE DEVELOPMENT OF CBM-X MECHANISMS FOR URBAN AND REGIONAL AQSMs	5. REPORT DATE February 1986
	6. PERFORMING ORGANIZATION CODE
7. AUTHOR(S) G. Z. Whitten and M. W. Gery	8. PERFORMING ORGANIZATION REPORT NO.
9. PERFORMING ORGANIZATION NAME AND ADDRESS Systems Applications, Inc. 101 Lucas Valley Road San Rafael, California 94903	10. PROGRAM ELEMENT NO. CDWA1A/02/2046 (FY-86)
	11. CONTRACT/GRANT NO. Contract 68-02-3738
12. SPONSORING AGENCY NAME AND ADDRESS Atmospheric Sciences Research Laboratory-RTP, NC Office of Research and Development U.S. Environmental Protection Agency Research Triangle Park, North Carolina 27711	13. TYPE OF REPORT AND PERIOD COVERED Final (7/82 - 10/85)
	14. SPONSORING AGENCY CODE EPA/600/09
15. SUPPLEMENTARY NOTES	

16. ABSTRACT

A series of chemical kinetic mechanisms, each of which describes the formation of photochemical smog from nitrogen oxide and multiple organic precursors has been developed. The most condensed version of the mechanism series now available is known as CBM-IV. The formulation and testing of CBM-IV is the subject of this report. This mechanism has been carefully tested against results obtained with an expanded CBM mechanism and several intermediately condensed mechanisms to ensure that the condensation steps did not contain compensating factors and to verify that the CBM-IV performed well under a range of conditions. The condensation of the expanded mechanism was tested in an incremental manner by simulating seven days of outdoor smog chamber data from two different experimental facilities. The data provided a wide range of time, temperature, light intensity, and concentration conditions for comparing simulation results from increasingly condensed mechanisms with the expanded mechanism. This approach was used to minimize compensating errors and to verify the operating boundaries of the mechanism at each condensation step. This development yielded a mechanism containing 28 species and 70 reactions.

17. KEY WORDS AND DOCUMENT ANALYSIS		
a. DESCRIPTORS	b. IDENTIFIERS/OPEN ENDED TERMS	c. COSATI Field/Group

18. DISTRIBUTION STATEMENT RELEASE TO PUBLIC	19. SECURITY CLASS (This Report) UNCLASSIFIED	21. NO. OF PAGES 139
	20. SECURITY CLASS (This page) UNCLASSIFIED	22. PRICE

EPA Form 2220-1 (9-73)

NOTICE

The information in this document has been funded by the United States Environmental Protection Agency under contract No. 68-02-3738 to Systems Applications, Inc. It has been subject to the Agency's peer and administrative review, and it has been approved for publication as an EPA document.

Mention of trade names or commercial products does not constitute endorsement or recommendation for use.

ABSTRACT

A series of chemical kinetic mechanisms based on the Carbon-Bond Mechanisms (CBM), each of which describes the formation of photochemical smog from nitrogen oxide and multiple organic precursors, has been developed. The most condensed version of the mechanism series now available is known as CBM-IV. The formulation and testing of the CBM-IV is the subject of this report. This mechanism has been carefully tested against results obtained from an expanded version of the CBM and several other versions that represent intermediate steps of condensation to ensure that the condensation steps do not contain compensating factors and to verify CBM-IV performance under a range of conditions. The condensation of the expanded CBM mechanism to CBM-IV was tested in an incremental manner by simulating seven days of outdoor smog chamber data from two different experimental facilities. These data provide a wide range of time, temperature, light intensity, and concentration conditions with which to compare simulation results from increasingly condensed mechanisms with those of the exapanded mechanism. This approach was used to minimize compensating errors and to verify the operating boundaries of the mechanism at each condensation step. The development effort yielded a mechanism containing 28 species and 70 reactions.

CONTENTS

Abstract iii

1. Introduction 1
   - Development of Carbon-Bond Mechanisms 1
   - Report Structure 4

2. Ranges of Mechanisms 6
   - Mechanism Choice 6
   - Stages of Condensation 13

3. Demonstration of Mechanism Condensation 26
   - Mechanism Validation 26
   - Test of Condensation Steps 26
   - Verification of Temperature Effects with PNA and MPNA 34
   - Condensation of Isoprene Chemistry 43

4. Summary and Recommendations 48
   - Summary 48
   - Recommendations 49

References 51

Appendix Simulation Results for Mechanism Condensation Steps ... 53

FIGURES

Number		Page
1	Schematic diagram of heirarchical levels of chemical species in photochemical smog	3
2	Ozone simulation results for UCR 80283 two-day experiment	30
3	Ozone simulation results for UCR 101083 four-day experiment	31
4	Ozone simulation results for UNC 92081 one-day experiment	33
5	CBM-X simulation results for UNCR 122677 (with PNA and MPNA chemistry)	35
6	CBM-X simulation results for UNCR 122677 (without PNA and MPNA chemistry)	37
7	CBM-X simulation results for UNCR 102477 (with PNA and MPNA chemistry)	39
8	CBM-X simulation results for UNCR 102477 (without PNA and MPNA chemistry)	41
9	Simulation results for UNCB 71680 using the CBM-RR mechanism	44
10	Simulation results for UNCB 71680 using the CBM-IV mechanism	46
A-1	Base case simulation results for UCR-80283 two-day experiment	57
A-2	Base case simulation results for UCR-101083 four-day experiment	62
A-3	Base case simulation results for UNC-92081 one-day experiment	81

A-4 Case one simulation results for UCR-80283 two-day experiment..... 83

A-5 Case one simulation results for UCR-101083 four-day experiment..... 91

A-6 Case one simulation results for UNC-92081 one-day experiment..... 107

A-7 Case two simulation results for UCR-80283 two-day experiment..... 109

A-8 Case two simulation results for UCR-101083 four-day experiment..... 117

A-9 Case two simulation results for UNC-92081 one-day experiment..... 133

A-10 CBM-IV (case three) simulation results for UCR-80283 two-day experiment..... 135

A-11 CBM-IV (case three) simulation results for UCR-101083 four-day experiment..... 143

A-12 CBM-IV (case three) simulation results for UNC-92081 one-day experiment..... 159

TABLES

Number		Page
1	The Carbon Bond Mechanism series	2
2	The Carbon Bond Mechanism-RR	7
3	The Carbon Bond Mechanism-IV	21
4	Species used in the CBM-IV	25
5	Initial conditions used for mechanism condensation experiments	28

SECTION 1

INTRODUCTION

DEVELOPMENT OF CARBON-BOND MECHANISMS

Since 1976, Systems Applications has been developing Carbon Bond Mechanisms (CBM) for use in urban and regional air quality simulation models. The series of mechanisms developed to date is given in Table 1. The main objective of the mechanism development effort reported here was to prepare a highly condensed version (CBM-IV) of the expanded Carbon Bond Mechanism (CBM-X) for use in complex atmospheric models such as the EPA Regional Oxidant Model (ROM). A further objective was to develop new methods for condensing and testing chemical mechanisms. Thus, in addition to documenting the development and testing of the CBM-IV mechanism, this report also outlines a potential protocol for mechanism condensation and discusses a set of condensation techniques (some of which are new) and tests that can be used to condense and test other chemical kinetic mechanisms.

The development of the mechanisms shown in Table 1 has been guided by the concept of a hierarchy of chemical species in which each species involved in oxidant formation is assigned to a hierarchical level on the basis of the number of systems in which it occurs, with the most ubiquitous species occupying the lowest, or foundation, level. An example would be the reactions of butane and acetaldehyde. Acetaldehyde is formed in significant quantitites during the photochemical oxidation of butane/NO_x systems; therefore, the reactions of acetaldehyde must be included in an explicit mechanism for butane. The reverse is not true. Little or no butane is formed in the photochemical oxidation of acetaldehyde/NO_x systems; therefore, butane reactions need not be included in an explicit mechanism for acetaldehyde. Thus, butane is assigned to a higher hierarchical level than acetaldehyde. The hierarchical levels used in the Carbon-Bond Mechanism (CBM) are shown schematically in Figure 1.

As shown in Table 1, the first version of the Carbon Bond Mechanism (CBM-I) was formulated in 1977. The mechanism was highly parameterized due to the limited state of knowledge existing at the time. Since then our knowledge of the photochemical process has expanded considerably.

TABLE 1. The Carbon-Bond Mechanism series.

Mechanism	Description	Number of Reactions/Species	Reference
CBM-I	Original CBM	35/20	Whitten and Hogo (1977) Whitten et al. (1980a)
CBM-II	Update/Expansion of CBM-I	65/27	Whitten et al. (1980b)
CBM-III	Update of CBM-II with improved aromatics chemistry	75/36	Killus and Whitten (1982)
CBM-X	Expanded version of CBM-III suitable for use in EKMA	146/67	Whitten et al. (1985a)
CBM-XR	CBM-X with isoprene chemistry for regional scale modeling	170/78	Whitten et al. (1985b)
CBM-RR	Condensed version of CBM-XR	113/47	Whitten et al. (1985b)
CBM-IV	Highly condensed version of CBM-RR	70/28	This work

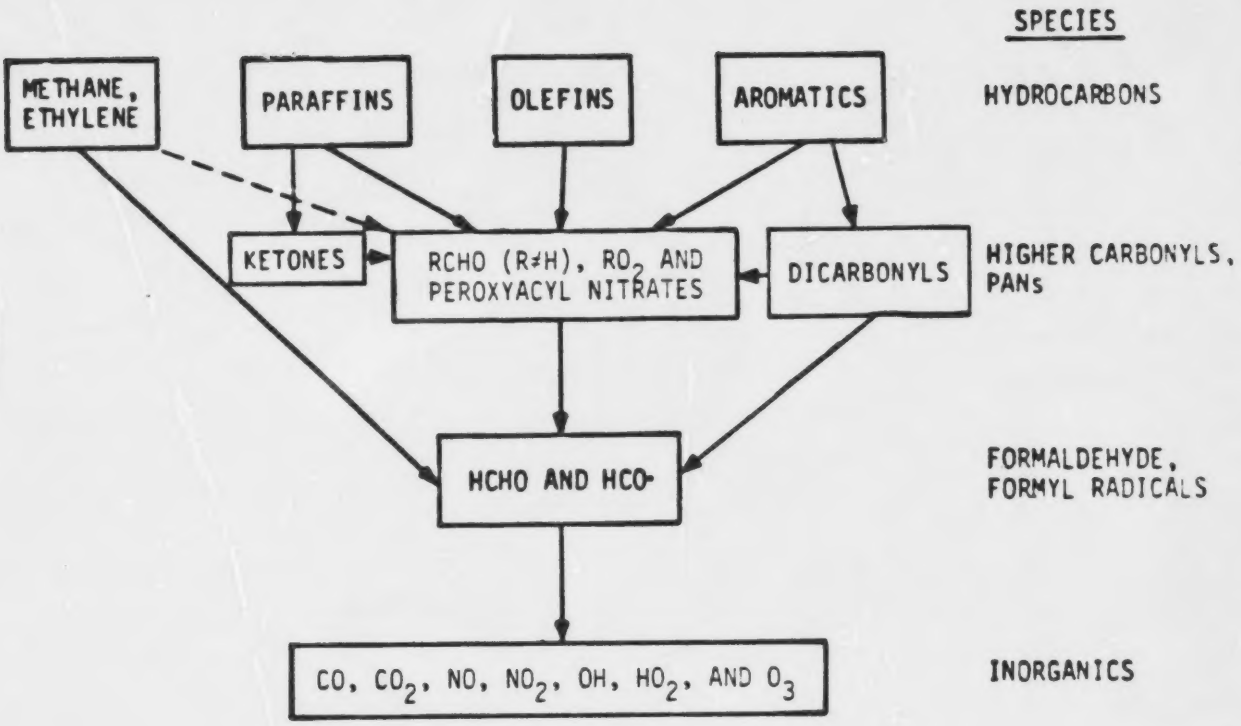

Figure 1. Schematic diagram of hierarchical levels of chemical species in photochemical smog.

This increased knowledge is reflected in the two updates to the CBM (CBM-II and CBM-III). All three of these mechanisms were developed for use in sophisticated AQSMs; therefore, they are highly condensed. A recent version of the CBM was developed specifically for use in the Empirical Kinetics Modeling Approach (EKMA). As indicated in Table 1, this expanded Carbon-Bond Mechanism is called CBM-X. Because the computational demands of EKMA are minimal, the CBM-X includes considerably more chemical detail than it was possible to include in the earlier versions of the mechanism.

The validation of the CBM-X has been presented in Whitten, Killus, and Johnson (1985a). The chemistry of species common to almost all organic systems (e.g., formaldehyde, acetaldehyde, PAN, and methylglyoxal) was tested against the results of numerous smog chamber experiments containing those compounds. In addition, the explicit chemistry of ethene, toluene, and m-xylene, and the 1-olefin (OLE) and alkyl group (PAR) formulations were validated through simulations of the appropriate experimental data. The complete CBM-X mechanism was then used to successfully simulate a series of automobile exhaust experiments (Jeffries et al., 1985) performed at the University of North Carolina (UNC) smog chamber facility.

Whitten, Johnson, and Killus (1985b) then extended the CBM-X mechanism for regional use (CBM-XR) by including and testing an isoprene reaction subset. In addition, the CBM-XR mechanism was validated against a new set of smog chamber data obtained at the University of California at Riverside (UCR) (Carter et al., 1985). These experiments provided a multi-day testing environment in which nighttime reactions could be investigated for both accuracy and importance to condensation procedures. Also, mechanism development using a large data set from this second outdoor chamber led to a clearer description of significant smog chamber reactions.

The next stage in our mechanism series development produced a condensed version of the CBM-XR suitable for use in EPA's Regional Oxidant Model (ROM). As shown in Table 1, the resulting mechanism, called the CBM-RR, contains 113 reactions and 47 species. Although the CBM-RR is appropriate for use in the ROM, it is still a very large and complex mechanism. The work reported here was undertaken with the goal of producing a more compact regional oxidant mechanism to reduce the computational time required to run to the ROM. The mechanism resulting from this effort is called CBM-IV because in terms of complexity the mechanism is comparable to the CBM-I through III series of mechanisms.

REPORT STRUCTURE

Section 2 contains a discussion of (1) the range of CBM mechanisms and their applications and (2) the various stages of condensation involved

in developing the most current version--CBM-IV. Section 3 discusses mechanism validation and the testing of the condensation steps. Section 4 contains a summary of the work and recommendations for further development and evaluation efforts. Complete plots of the test simulations are contained in an appendix.

SECTION 2

RANGES OF MECHANISMS

MECHANISM CHOICE

As our understanding of the chemical processes that occur in the atmosphere has become more complete, photochemical kinetics mechanisms have become more comprehensive. Unfortunately, limited computer resources still require that some compression of the chemistry occur for all mechanisms, even those used in simple atmospheric models. The expanded CBM-X mechanism was designed to simulate urban photochemistry (Whitten, Johnson, and Killus, 1985a). It was validated against a large set of smog chamber data and can be used effectively in atmospheric models with simple physical and meteorological descriptions such as trajectory models.

When model complexity increases, however, due either to larger temporal and spatial requirements or to more complete physical and meteorological descriptions, a more compact chemistry module is usually required. Whitten, Johnson, and Killus (1985b) developed and tested a condensed version of the CBM-X (CBM-RR) for inclusion in the EPA Regional Oxidant Model (ROM). The CBM-RR is shown in Table 2. The condensation undertaken to achieve this mechanism involves simple algebraic transformations that decrease the time needed to perform simulations without affecting the solution.

It is possible to condense The CBM-RR even further by making assumptions concerning the bounding conditions of various functions and variables (reactions and species). However, this procedure is not trivial and requires stepwise verification over a large range of possible conditions. In the remainder of this section we discuss various condensation techniques and assumptions, and their limits and benefits, and outline the condensation steps used to achieve the final, highly condensed mechanism called CBM-IV. This mechanism contains the essential qualities of the CBM-X and CBM-XR mechanisms in a highly compressed format. The CBM-IV mechanism should be suitable for use in simulating urban and regional oxidant chemistry within a model that requires a very concise chemistry module in order to function efficiently.

TABLE 2. THE CARBON-BOND MECHANISM--RR

	Reactions	Rate constant[a]	Activation energy[b]
1	NO2 = NO +O	vary	
2	O = O3	$4.65 \times 10^{+6}$	-690.
3	O3 +NO = NO2	26.6	1430.
4	O +NO2 = NO	13800.	
5	O +NO2 = NO3	2320.	-600.
6	O +NO = NO2	3120.	-411.
7	NO2 +O3 = NO3	0.0474	2450.
8	O3 = O1D	vary	
9	O3 = O	0.042	
10	O1D = O	$4.29 \times 10^{+10}$	-100.
11	O1D +H2O = 2. OH	326000.	
12	O3 +OH = HO2	100.	940.
13	O3 +HO2 = OH	3.0	580.
14	NO3 +NO = 2. NO2	28100.	-250.
15	NO3 +NO2 = NO +NO2	0.59	1230.
16	NO3 +NO2 = N2O5	1780.	60.
17	N2O5+H2O = 2. HNO3	1.9×10^{-6}	
18	N2O5 = NO3 +NO2	3.12	10840.
19	NO +NO2 +H2O = 2. HNO2	1.6×10^{-11}	
20	HNO2+HNO2 = NO +NO2 +H2O	1.5×10^{-5}	
21	HNO2 = NO +OH	0.18 x k1	

TABLE 2. CONTINUED.

	Reactions		Rate constant[a]	Activation energy[b]
22	NO2 +OH	= HNO3	16300.	-560.
23	NO +OH	= HNO2	9770.	-427.
24	HO2 +NO	= OH +NO2	12300.	-240.
25	NO +NO	= 2. NO2	1.52×10^{-4}	-530.
26	H2O2	= 2. OH	0.0014 x k1	
27	OH +H2O2	= HO2	2520.	187.
28	OH +HNO2	= NO2	9770.	
29	OH +HNO3	= NO3	192.	-778.
30	NO3	= 0.85NO2 +0.85 O +0.15NO	30.6 x k1	
31	HO2 +HO2	= H2O2	4144.	-1150.
32	HO2 +HO2 +H2O	= H2O2 +H2O	0.218	-5800.
33	HO2 +NO2	= PNA	1630.	-617.
34	PNA	= HO2 +NO2	5.12	10420.
35	OH +CO	= HO2	400.	
36	FORM+HO2	= FROX	14.8	
37	FORM+OH	= HO2 +CO	15000.	
38	FORM	= 2. HO2 +CO	vary	
39	FORM	= CO	vary	
40	FORM+O	= OH +HO2 +CO	237.	1550.
41	FORM+NO3	= HNO3 +HO2 +CO	0.93	
42	FROX+NO	= NO2 +HO2	10400.	
43	FROX	= FORM +HO2	90.	
44	ALD2+O	= C2O3 +OH	636.	986.
45	ALD2+OH	= C2O3	24000.	-250.
46	ALD2+NO3	= C2O3 +HNO3	3.7	
47	ALD2	= MEO2 +HO2 +CO	vary	

TABLE 2. CONTINUED.

	Reactions		Rate constant [a]	Activation energy [b]
48	ALD2+HO2	= MEO2 +FORM	5.	
49	C2O3+NO	= MEO2 +NO2	16500.	-250.
50	C2O3+NO2	= PAN	9000.	-250.
51	PAN	= C2O3 +NO2	0.0222	14000.
52	MEO2+NO2	= MPNA	6000.	-735.
53	MPNA	= MEO2 +NO2	92.	10400.
54	MEO2+NO	= MEO +NO2	11000.	-180.
55	MEO +NO	= MNIT	44400.	-200.
56	MEO +NO	= FORM +HO2 +NO	1920.	
57	MEO +NO2	= MEN3	22200.	
58	MEO	= FORM +HO2	394000.	1313.
59	MEN3+OH	= FORM +NO2	2220.	360.
60	MNIT+OH	= FORM +NO	2370.	340.
61	MNIT	= MEO +NO	0.3 x k1	
62	MEO2+MEO2	= 0.70MEO +0.65FORM	503.	-220.
63	MEO2+C2O3	= MEO +MEO2	4400.	
64	C2O3+C2O3	= 2. MEO2	3700.	
65	MEO2+HO2	=	8900.	-1300.
66	C2O3+HO2	=	9600.	
67	AONE	= MEO2 +C2O3	0.00004 x k1	
68	AONE+OH	= XO2 +FORM +C2O3	580.	
69	GLY	= 1.79CO +0.21FORM + 0.19HO2	0.0075 x k1	
70	GLY +OH	= HO2 +2. CO	15000.	
71	MGLY	= C2O3 +HO2 +CO	0.02 x k1	
72	MGLY+OH	= XO2 +C2O3	26000.	

TABLE 2. CONTINUED.

	Reactions		Rate constant [a]	Activation energy [b]
73	OH	= ME02	21.	
74	PAR +OH	= 0.93X02 +0.80ROR + 0.13H02 +0.13ALD2 + 0.067X02N -0.13PAR	1150.0	
75	ROR +N02	=	22000.	
76	ROR	= 0.38KET +0.38H02 + 0.62AONE +0.62D + -1.24PAR	390000.	
77	ROR	= ALD2 +D -PAR	90000.	7000.
78	D +PAR	= X02 +H02 +0.7AONE + 0.3ALD2 -1.7PAR	10000.	
79	D +KET	= C203 -PAR	10000.	
80	X02 +NO	= N02	12000.	
81	KET	= C203 +X02 +H02 +ALD2 + -3.0PAR	0.0003 x k1	
82	O +OLE	= 0.95ALD2 +0.30H02 + 0.15X02 +0.15CO + 0.05ME02 +0.05C203 + -0.35PAR	5920.	324.
83	OH +OLE	= ME02 +ALD2 -PAR	42000.	-537.
84	03 +OLE	= 0.5ALD2 +0.516FORM + 0.3MCRG +0.3CRIG + 0.212CO +0.136H02 + 0.144ME02 +0.080H -PAR	0.018	1897.
85	N03 +OLE	= 0.91X02 +0.91H02 + 0.09X02N	11.4	
86	O +ETH	= ME02 +H02 +CO	1080.	800.
87	OH +ETH	= ME02 +FORM	12000.	-382.
88	03 +ETH	= FORM +0.37CRIG + 0.37CO +0.13H02	0.0027	2840.
89	CRIG+NO	= FORM +N02	10000.	
90	CRIG+N02	= FORM +N03	1000.	
91	CRIG+H20	=	0.006	

TABLE 2. CONTINUED.

	Reactions		Rate constant[a]	Activation energy[b]
92	CRIG+FORM	=	30.	
93	CRIG+ALD2	=	30.	
94	MCRG+NO	= ALD2 +NO2	10000.	
95	MCRG+NO2	= ALD2 +NO3	1000.	
96	MCRG+H2O	=	0.006	
97	MCRG+FORM	=	30.	
98	MCRG+ALD2	=	30.	
99	TOL +OH	= HO2 +0.64XO2 +1.13GLY + 0.56MGLY +0.36PHEN + 0.36PAR +0.077BZA	9750.	
100	PHEN+NO3	= PHO +HNO3	14000.	
101	BZA +OH	= BZO2	20000.	
102	BZO2+NO2	= PBZN	2500.	
103	BZO2+NO	= XO2 +PHO +CO +NO2	3700.	
104	PBZN	= BZO2 +NO2	0.022	14000.
105	BZA	=	0.004	
106	PHO +NO2	=	20000.	
107	XYL +OH	= HO2 +0.72XO2 +0.67GLY + 1.33MGLY +0.28PHEN + 0.56PAR +0.06TLA	36000.	
108	TLA +OH	= XO2 +PHO +2. PAR	20000.	
109	ISOP+O	= HO2 +0.8ALD2 +0.55OLE + 0.5XO2 +0.5CO +0.2KET + 0.45ETH -0.3PAR	28000.	
110	ISOP+OH	= 0.87XO2 +0.87FORM + 0.87HO2 +0.58KET 0.29OLE +0.58ETH 0.29ALD2 -0.29PAR	126000.	
111	ISOP+O3	= FORM +0.45ALD2 + 0.55ETH +0.98HO2 + 0.10OLE +0.2KET + 0.06CO -0.45PAR	0.018	

TABLE 2. CONCLUDED.

	Reactions		Rate constant [a]	Activation energy [b]
112	ISOP+NO3	= XO2N	165.	
113	XO2N+NO	=	1000.	

a All rate constants are in appropriate ppm and min units at 298K and one atmosphere of air. That is, all unimolecular and photolysis reactions (+ $h\nu$) are in units of min^{-1}; all bimolecular reactions are in units of ppm^{-1} min^{-1}; and all termolecular reactions are in units of ppm^{-2} min^{-1}. Rate constants designated as "vary" are defined in Whitten, Killus, and Johnson, 1985a and b.

b The numbers listed are Arrhenius temperature coefficients in degrees Kelvin for B in the expression $k_T = k_{298} \exp(B \times (\frac{1}{298} - \frac{1}{T}))$.

STAGES OF CONDENSATION

The CBM-RR Mechanism

As noted, the CBM-RR mechanism shown in Table 2 was developed for use in the EPA Regional Oxidant Model by condensing the CBM-XR. As discussed in Section 1, the CBM-XR is a a regional version of the CBM-X that includes isoprene chemistry. The CBM-RR is computationally more efficient than the CBM-XR without sacrificing the function of the chemistry. The condensation that was used to achieve the CBM-RR involved a number of basic steps:

(a) Lumping of constant concentration species M and O_2 into rate constants; e.g.,

$$O + O_2 + M \rightarrow O_3 + M \qquad k = 2.22 \times 10^{-5}\ ppm^{-2}\ min^{-1}$$

can be written

$$O \rightarrow O_3 \qquad k = 4.65 \times 10^{6}\ min^{-1}$$

(b) Elimination of stable products such as FACD, ACAC, PROX, NTR, OZD, DNIT, NPHN, ISN1, ISN2, PROD, and MEOH. Removal of these species eliminates nitrogen and carbon products that may be of importance in some parallel modeling exercises. For instance, the simulation of atmospheric acid formation would require inclusion of organic acid and nitrate products, and the total conservation of nitrogen mass. Although this would not be a difficult revision, the reader is advised that use of a model to simulate conditions for which it has not been tested can result in unforseen difficulties.

(c) Elimination of species X by utilizing negative stoichiometry. X was a mass balance counter that reacted with one PAR to remove the PAR and conserve mass, i.e.,

$$X + PAR \rightarrow .$$

In the CBM-RR, X has simply been redefined as -PAR. Thus,

$$ROR \rightarrow ALD2 + D + X$$

is now

$$ROR \rightarrow ALD2 + D - PAR \ .$$

(d) Combination of parallel reactions using fractional product stoichiometry. For example, the photolysis of NO_3 was changed from

$$NO_3 \rightarrow NO_2 + O \qquad k = 26.0 \times K_1 \ min^{-1}$$

$$NO_3 \rightarrow NO \qquad k = 4.6 \times K_1 \ min^{-1}$$

to

$$NO_3 \rightarrow 0.85\ NO_2 + 0.85\ O + 0.15\ NO \qquad k = 30.6 \times k_1 \ min^{-1} \ .$$

(e) Inclusion of fixed pathway splits for intermediate products formed during oxidation reactions. As examples, the species HOTA and HTMA represented the energetically excited intermediates formed during ozone-ethene and ozone-propene reactions. These products and their reactions were eliminated through a combination of reactions using fractional stoichiometries. Similar condensations were performed for the O_3-isoprene species INT, MVK, and MACR.

(f) Creation of a universal peroxy radical, XO_2. This species is an operator that reacts to convert NO to NO_2:

$$XO_2 + NO \rightarrow NO_2$$

Use of XO_2 requires that the stable products formed during NO to NO_2 conversion be included in the initial reaction that forms the peroxy radical. Thus, in the CBM-RR

$$MGLY + OH \rightarrow MGPX$$

$$MGPX + NO \rightarrow NO_2 + C_2O_3$$

was represented by

$$MGLY + OH \rightarrow XO_2 + C_2O_3$$

$$XO_2 + NO \rightarrow NO_2$$

(g) Inclusion of a nitrate operator similar to XO_2. This operator--XO_2N--accounts for the formation of a nitrate from the reaction of NO with a peroxy radical. As an example, the reaction set

$$NO_3 + OLE \rightarrow PNO_2$$

$$PNO_2 + NO \rightarrow DNIT \qquad k = 1000\ ppm^{-1}\ min^{-1}$$

$$PNO_2 + NO \rightarrow NO_2 + HO_2 + NTR \qquad k = 10000\ ppm^{-1}\ min^{-1}$$

was expressed as

$$NO_3 + OLE \rightarrow 0.91\ XO_2 + 0.91\ HO_2 + 0.09\ XO_2N$$

$$XO_2 + NO \rightarrow NO_2$$

$$XO_2N + NO \rightarrow \ .$$

These condensation techniques do not affect the mathematical results of simulations using the mechanisms over the widest range of conditions for which atmospheric models might be applied. Although the techniques used to this point may require some verification, the type of test required is usually easy to define from the technique itself. For example, the operator technique using XO_2 causes the products of the NO-to-NO_2 conversion reactions to appear earlier in time since they are assumed to appear along with XO_2 rather than after the NO-to-NO_2 reactions. The change in time of appearance would be exaggerated when NO approaches zero and the peroxy radicals can build up in concentration so that radical-reduced reactions compete with the NO reactions. Whitten, Johnson, and Killus (1985b) used a special multiple-day smog chamber experiment to test the XO_2 operator. This special four-day experiment ran out of NO_x four times and fresh NO_x was added on three days. Hence, the experiment tested the XO_2 technique under exaggerated conditions yet the results were favorable. The next section discusses more extensive steps used to further condense the regional CBM-X.

Condensation Requiring Extensive Testing

Certain routine changes that involve minimal perturbation to the mechanism can yield a high level of condensation. These include elimination of unimportant products, insignificant chemistry, and species that can be shown to be in steady state. These techniques were used to develop the CBM-RR from the CBM-XR mechanism as reported by Whitten, Johnson, and Killus (1985b). We next discuss the techniques used to condense the CBM-RR to the CBM-IV.

Species Eliminated from CBM-RR

Hydroxy Methylperoxy Radical (FROX). All simulations to date indicate that the species FROX and its reactions are insignificant. The FROX cycle (Reactions 36, 42, and 43 in Table 2) is trivial except for conditions of high NO, since entry into the cycle is generally prohibited by the low rate of Reaction 36. Therefore, reactions containing this species, including Reaction 36, were removed in the CBM-IV.

Benzaldehyde (BZA). BZA and its subsequent reaction products, peroxybenzoyl radical (BZO_2) and peroxybenxoyl nitrate (PBZN), represent the chemistry of the OH-toluene abstraction pathway. Very little of the product mass of reacted toluene occurs in these species and they contribute far less reactivity than do the dicarbonyl products formed from OH addition to toluene; therefore, the mass of the abstraction pathway is comparatively unreactive, allowing elimination of these three species. Such a practice appears to be more realistic than assuming that 100 percent of toluene reacts through the OH addition pathway.

CRIG, MCRG. Reactions 89 to 98 (Table 2) represent the chemistry of the biradical intermediate species (CRIG, MCRG) formed from ozone-olefin reactions. Estimates of these reaction rate constants are highly uncertain. Theoretical and experimental evidence (Kerr and Calvert, 1984) appear to indicate that reaction of biradicals with water is the most important loss mechanism. This reaction becomes even more dominant under regional modeling conditions for which NO concentrations are lower. Thus, the biradical species and their reactions have been totally eliminated. This assumption transfers all biradical carbon to stable species (the ozonides). As noted, however, this chemistry may be reinstated at a later date when more accurate reaction rates for NO are determined. Biradical oxidation of SO_2 may also be considered.

Peroxynitric Acid (PNA) and Methyl-peroxynitric Acid (MPNA). PNA and MPNA form and thermally decompose in a manner similar to PAN, providing chemical cycles for storage and possible later release of NO_2 and radicals. At temperatures below 280 K, the rates of decomposition are slow compared to formation resulting in stable products. This limits ozone formation since these acid species are sinks for NO_2 and peroxy radicals. As will be demonstrated in the next section, thermal decomposition rates are much more rapid above 290 K and the initial reactants are quickly returned to the reacting system. Thus, in mechanistic compression for use above 290 K these species and the reactions that form them can be eliminated. For simulations below 280 K, however, PNA and MPNA should be included since a mechanism without these sinks may overpredict ozone concentrations.

Steady-State Approximations

Ozone Photolysis. Reactions 8, 10, and 11 in Table 2 represent the ozone photolysis channel leading to formation of the hydroxyl radical. The O^{1D} reactions are very fast:

$$O^{1D} \xrightarrow{+ M} O \qquad k_{10} = 4.29 \times 10^{+10} \text{ min}^{-1} \text{ at } 298 \text{ K} ,$$

$$O^{1D} + H_2O \rightarrow 2\ OH \qquad k_{11} = 3.26 \times 10^{+5} \text{ ppm}^{-1} \text{ min}^{-1} .$$

The constant value of [M] = 1×10^6 ppm has been included in the rate constant for Reaction 10. If water concentration is included in a similar way for rate constant 11, Reactions 10 and 11 may be eliminated in favor of a constant formation ratio between O and OH in Reaction 8. This reaction then becomes:

$$O_3 \rightarrow (2\ \alpha)\ OH + (1.0 - \alpha)\ O$$

where

$$\alpha = [H_2O] \cdot k_{11} / ([H_2O] \cdot k_{11} + [M] k_{10})$$

with

$$k_{10} = 42900 \exp[-100(1/298 - 1/T)] \text{ ppm}^{-1} \text{ min}^{-1} ,$$

$$k_{11} = 326000 \text{ ppm}^{-1} \text{ min}^{-1} .$$

The assumption of $[H_2O]$ = 15000 ppm at 298 K yields

$$O_3 \rightarrow 0.205\ OH + 0.897\ O .$$

If water concentration is assumed to be constant, then H_2O can be eliminated from the species list and the reaction rates for Reactions 17, 19, and 32 can be multiplied by the appropriate concentrations.

MEO Chemistry. The dominant reaction of MEO in the atmosphere is Reaction 58:

$$MEO \xrightarrow{+ O_2} FORM + HO_2$$

Therefore, MEO can be considered a steady-state species that can be represented by its rapidly formed reaction products. This assumption results in the elimination of MEO, MNIT, and MEN3.

Parameterization of Specific Compounds

Peroxy Radical Chemistry. Prior to condensation, there were 19 different organic peroxy radicals in the CBM-XR: MEO_2, C_2O_3, ANO_2, MGPX, BO_2, OPEN, BZO_2, PHO_2, TLO_2, XYLO, RO_2, RO_2R, AO_2, PNO_2, ISO1, ISO2, ISO3, ISO4, and ISO5. In the presence of NO, the predominant fate of these radicals is oxidation of NO to form NO_2 and a variety of organic products. In the CBM-IV, all reactions that produce these organic peroxy radicals (with the exception of those producing C_2O_3) have been altered by condensation to yield XO_2 and stable products in the manner discussed earlier. Because of the special importance of the C_2O_3/PAN cycle, C_2O_3 is handled explicitly in this condensation; and HO_2 chemistry is separate. The special case of MEO_2 and alteration of XO_2 chemistry is discussed next.

MEO2. MEO2 can be represented by XO_2 and steady-state MEO (FORM + HO_2) since MEO_2 reaction with NO to form NO_2 and MEO is normally predominant. The only condition in which this substitution would produce a change in predictions is when NO concentrations approach zero. In this case, FORM and HO_2 would be produced in the model even if no NO were available for oxidation. It is known that when NO concentrations are low, peroxy radical termination reactions compete with NO oxidation reactions. Studies of some of these reactions for the species MEO_2 and C_2O_3 (Baulch et al., 1984) indicate that the products of termination reactions are often identical or similar to those formed in NO to NO_2 conversion. That is, the product mass is not always lost to nonreactive species. Thus, peroxy radicals are represented as XO_2 and stable products in CBM-IV.

The operator XO_2 can be kept from unrealistically depleting NO at low NO concentrations by accounting for the competition between NO and peroxy radicals for the XO_2 operation. Therefore, XO_2 reaction with the two remaining peroxy radicals (HO_2 and C_2O_3) has been accounted for in the CBM-IV. Consider the original reactions:

$$MEO_2 + C_2O_3 \rightarrow MEO + MEO_2 \quad ,$$

$$MEO_2 + HO_2 \rightarrow \quad .$$

Recall that MEO ≡ FORM + HO_2 and MEO_2 ≡ XO_2 + FORM + HO_2. After production of FORM and HO_2 in the original MEO_2-forming reaction, the XO_2 operator in the condensed version is similarly represented by

$$XO_2 + C_2O_3 \rightarrow FORM + XO_2 + HO_2 \quad ,$$

$$XO_2 + HO_2 \rightarrow \quad .$$

Although XO_2 manifests function but no mass, the competition for peroxy radicals under various conditions is now accounted for by competition for the XO_2 operator.

Acetone (AONE). AONE is a minor product of paraffin chemistry. Both the photolysis and OH reactions of acetone are slow (Atkinson and Lloyd, 1984). Since the central carbon is inaccessable during OH attack, the reactivity of AONE has been set to that of 2 PAR. This allows elimination of the AONE species and its reactions, and alters the product representation in the PAR + OH reaction.

Ketone (KET). KET represents the carbonyl carbon that forms when an alkoxy radical (ROR) stabilizes upon loss of a hydrogen atom. The treatment of acetone (AONE ≡ 2 PAR) just discussed assumes no reactivity for this carbon. Simulation results indicate that the mass throughput rates for the two KET reactions are slow; at least two orders of magnitude less than the D + PAR reaction. Therefore, approximating the reactivity of KET as 1 PAR, and elimination of Reactions 92 and 94 should not affect mechanism performance.

Glyoxal (GLY). Under atmospheric conditions, the most important reaction of glyoxal is hydroxyl radical oxidation:

$$GLY + OH \rightarrow H_2O + 2\ CO + HO_2$$

This is analogous to:

$$FORM + OH \rightarrow H_2O + CO + HO_2$$

Previous evaluation (McRae, Leone, and Seinfeld, 1983) indicates that the parameterization of glyoxal as FORM + CO appears to be appropriate.

Paraffin (PAR). Condensation of the paraffin chemistry proved to be more complex than that of most other species. As shown in Reaction 74 of Table 1, about 80 percent of the carbon mass results in ROR. The remaining chemistry of this species is represented in Reactions 75 through 78 (recall that KET has been replaced by 1 PAR). These reactions can initially be condensed to:

$$ROR + NO_2 \rightarrow \qquad (75)$$

$$ROR \rightarrow 0.385\ HO_2 + 0.615\ D + 0.385\ PAR \qquad (76)$$

$$ROR \rightarrow ALD_2 + D - PAR \qquad (77)$$

$$D + PAR \rightarrow XO_2 + HO_2 + 0.3\ ALD_2 - 0.3\ PAR \qquad (78)$$

Reaction 78 allows a simple steady-state representation of D:

$$D \equiv XO_2 + HO_2 + 0.3\ ALD2 - 1.3\ PAR$$

In addition, examination of k_{75} reveals that even at high NO_2 concentrations (0.5 ppm) Reaction 75 would account for only about 2 percent of the ROR loss. Thus, an expression for ROR can be created by substituting for D and combining reactions:

$$ROR \rightarrow HO_2 + 0.615\ XO_2 + 0.185\ ALD2 - 0.415\ PAR$$

$$+ f_{(T)}[0.385\ XO_2 + 1.115\ ALD2 - 1.885\ PAR]$$

where $f_{(T)}$ is the temperature-dependent fraction of ROR reacting through reaction 77, and the product yields in brackets represent the difference in yields between that reaction and Reaction 76. $f_{(T)}$ may be defined as

$$f_{(T)} = \frac{K_{77}}{K_{76} + K_{77}} = \frac{90000\ \exp(7000(1/298 - 1/T))}{390000 + 90000\ \exp(7000(1/298 - 1/T))}$$

$$f_{(298)} = 0.1875$$

At 298 K:

$$ROR = HO_2 + 0.687\ XO_2 + 0.394\ ALD2 - 0.768\ PAR$$

This value will vary somewhat with temperature and new product ratios should be recalculated for changes from 298 K. For example: f(283) = 0.06, f(293) = 0.13 and f(303) = 0.25.

With ROR defined at 298 K, the expression for products of OH + PAR can be calculated as

$$PAR + OH \rightarrow 1.485\ XO_2 + 0.933\ HO_2 + 0.446\ ALD2$$

$$+ 0.067\ XO_2N - 0.747\ PAR$$

When all of these changes are made to the CBM-RR, the CBM-IV mechanism shown in Table 3 is obtained; the species used in CBM-IV are listed in Table 4.

TABLE 3. THE CARBON-BOND MECHANISM--IV

	Reactions		Rate constant[a]	Activation energy[b]
1	NO2	= NO +O	vary	
2	O	= O3	$4.65 \times 10^{+6}$	-690.
3	O3 +NO	= NO2	26.6	1430.
4	O +NO2	= NO	13800.	
5	O +NO2	= NO3	2320.	-600.
6	O +NO	= NO2	3120.	-411.
7	NO2 +O3	= NO3	0.0474	2450.
8	O3	= 0.205 OH + 0.897 O	vary	
9	O3	= O	0.042 X k1	
10	O3 +OH	= HO2	100.	940.
11	O3 +HO2	= OH	3.0	580.
12	NO3 +NO	= 2. NO2	28100.	-250.
13	NO3 +NO2	= NO +NO2	0.59	1230.
14	NO3 +NO2	= N2O5	1780.	60.
15	N2O5	= 2. HNO3	0.0285	
16	N2O5	= NO3 +NO2	3.12	10840.
17	NO +NO2	= 2. HNO2	2.4×10^{-7}	
18	HNO2+HNO2	= NO +NO2	1.5×10^{-5}	
19	HNO2	= NO +OH	0.18 X k1	
20	NO2 +OH	= HNO3	16300.	-560.
21	NO +OH	= HNO2	9770.	-427.

TABLE 3. CONTINUED.

	Reactions		Rate constant[a]	Activation energy[b]
22	HO2 +NO	= OH +NO2	12300.	-240.
23	NO +NO	= 2. NO2	1.52×10^{-4}	-530.
24	H2O2	= 2. OH	0.0014 X k1	
25	OH +H2O2	= HO2	2520.	187.
26	OH +HNO2	= NO2	9770.	
27	OH +HNO3	= NO3	192.	-778.
28	NO3	= 0.85NO2 +0.85 O +0.15NO	30.6 X k1	
29	HO2 +HO2	= H2O2	4144.	-1150.
30	HO2 +HO2	= H2O2	3270.	-5800.
31	OH +CO	= HO2	400.	
32	FORM+OH	= HO2 +CO	15000.	
33	FORM	= 2. HO2 +CO	vary	
34	FORM	= CO	vary	
35	FORM+O	= OH +HO2 +CO	237.	1550.
36	FORM+NO3	= HNO3 +HO2 +CO	0.93	
37	ALD2+O	= C2O3 +OH	636.	986.
38	ALD2+OH	= C2O3	24000.	-250.
39	ALD2+NO3	= C2O3 +HNO3	3.7	
40	ALD2	= XO2 +2.HO2 +CO +FORM	vary	
41	ALD2+HO2	= XO2 +2.FORM +HO2	5.	
42	C2O3+NO	= NO2 +XO2 +FORM +HO2	16500.	-250.
43	C2O3+NO2	= PAN	9000.	-250.
44	PAN	= C2O3 +NO2	0.0222	14000.
45	C2O3+C2O3	= 2. XO2 +2.FORM +2.HO2	3700.	
46	C2O3+HO2	=	9600.	

TABLE 3. CONTINUED.

	Reactions		Rate constant [a]	Activation energy [b]
47	MGLY	= C2O3 +HO2 +CO	0.02 X k1	
48	MGLY+OH	= XO2 +C2O3	26000.	
49	OH	= XO2 +FORM +HO2	21.	
50	PAR +OH	= 1.49XO2 +0.067XO2N + 0.93HO2 +0.45ALD2 -0.75PAR	1150.0	
51	O +OLE	= 0.95ALD2 +0.35HO2 + 0.20XO2 +0.15CO + 0.05FORM +0.05C2O3 + -0.35PAR	5920.	324.
52	OH +OLE	= FORM +ALD2 +XO2 +HO2 -PAR	42000.	-537.
53	O3 +OLE	= 0.5ALD2 +0.66FORM + 0.212CO +0.28HO2 + 0.144XO2 +0.08 OH -PAR	0.018	1897.
54	NO3 +OLE	= 0.91XO2 +0.91HO2 + 0.09XO2N	11.4	
55	O +ETH	= FORM +XO2 +CO +2.HO2	1080.	800.
56	OH +ETH	= XO2 +2.FORM +HO2	12000.	-382.
57	O3 +ETH	= FORM +0.37CO + 0.13HO2	0.0027	2840.
58	TOL +OH	= HO2 +0.64XO2 +1.13FORM + 0.56MGLY +0.36PHEN + 0.36PAR +1.13CO	9750.	
59	PHEN+NO3	= PHO +HNO3	14000.	
60	PHO +NO2	=	20000.	
61	XYL +OH	= HO2 +0.72XO2 +0.67CO + 1.33MGLY +0.28PHEN + 0.56PAR +0.06TLA + 0.67FORM	36000.	
62	TLA +OH	= XO2 +PHO +2. PAR	20000.	
63	ISOP+O	= HO2 +0.8ALD2 +0.55OLE + 0.5XO2 +0.5CO + 0.45ETH -0.1PAR	28000.	

TABLE 3. CONCLUDED.

	Reactions		Rate constant [a]	Activation energy [b]
64	ISOP+OH	= 0.87XO2 +0.87FORM + 0.87HO2 +0.29PAR 0.29OLE +0.58ETH 0.29ALD2	126000.	
65	ISOP+O3	= FORM +0.45ALD2 + 0.55ETH +0.98HO2 + 0.10OLE +0.06CO -0.25PAR	0.018	
66	ISOP+NO3	= XO2N	165.	
67	XO2N+NO	=	1000.	
68	XO2 +NO	= NO2	12000.	
69	XO2 +HO2	=	5000.	-1300.
70	XO2 +C2O3	= XO2 +HO2 +FORM	2400.	

a All rate constants are in appropriate ppm and min units at 298K and one atmosphere of air. That is, all unimolecular and photolysis reactions (+ $h\nu$) are in units of min^{-1}; all bimolecular reactions are in units of ppm^{-1} min^{-1}; and all termolecular reactions are in units of ppm^{-2} min^{-1}. Rate constants designated as "vary" are defined in Whitten, Killus, and Johnson, 1985a and b.

b The numbers listed are Arrhenius temperature coefficients in degrees Kelvin for B in the expression $k_T = k_{298} \exp(B \times (\frac{1}{298} - \frac{1}{T}))$.

TABLE 4. SPECIES USED IN THE CBM-IV

Mechanistic Symbol	Chemical Structure	Name
NO	NO	Nitric oxide
NO2	NO_2	Nitrogen dioxide
NO3	NO_3	Nitrogen trioxide
N2O5	N_2O_5	Dinitrogen pentoxide
HNO2	HONO	Nitrous acid
HNO3	$HONO_2$	Nitric acid
O	O(3P)	Atomic oxygen
O3	O_3	Ozone
OH	OH	Hydroxyl radical
HO2	HO_2	Hydro peroxy radical
CO	CO	Carbon monoxide
H2OZ	HOOH	Hydrogen peroxide
PAN	$CH_3C(O)OONO_2$	Peroxyacyl nitrate
FORM	HC(O)H	Formaldehyde
ALD2	$CH_3C(O)H$	Acetaldehyde
MGLY	$CH_3C(O)C(O)H$	Methyl glyoxal
PAR	C-C	Paraffin carbon bond
OLE	C=C	Olefin carbon bond
ETH	$H_2C=CH_2$	Ethylene
TOL	ϕ-CH_3	Toluene surrogate
XYL	CH_3-C_6H_4-CH_3	Xylene surrogate
TLA	HC(O)-C_6H_4-(CH_3)	Tolualdehyde surrogate
ISOP	$CH_2=CH-C(CH_3)=CH_2$	Isoprene
C2O3	$CH_3C(O)OO$	Peroxy acyl radical
PHEN	ϕ-OH	Phenol (cresol) surrogate
PHO	ϕ-O	Phenoxy radical surrogate
XO2		NO → NO_2 operation
XO2N		NO → nitrate operation

* ϕ represents an aromatic ring.

SECTION 3

DEMONSTRATION OF MECHANISM CONDENSATION

MECHANISM VALIDATION

The CBM-IV mechanism is based on the reactions found in the CBM-X and CBM-XR (Whitten, Johnson, and Killus, 1985a and 1985b). As explained earlier, these latter two mechanisms were developed and tested through a hierarchical approach to minimize accumulation of compensating errors. The full reaction sets were then verified through extensive testing with data from the University of North Carolina, Battelle, and University of California at Riverside smog chambers. These data encompass a large range of temperature, light intensity, concentration, and hydrocarbon reactivity conditions in single and multi-day experiments, making the CBM-X and CBM-XR the most comprehensively validated mechanisms available.

During the condensation exercise, we did not attempt further validation of the chemical reaction schemes; rather, the goal was to produce a highly condensed version of the expanded mechanism (CBM-X). Therefore, though we were interested in the ability of the chemistry to simulate the experimental test data, the primary purpose throughout the condensation procedure was to develop the CBM-IV such that each mechanistic compression step yielded nonvarying simulation results. The steps eventually utilized have been presented in Section 2 and are documented in the appendix. In this section, we demonstrate the testing procedure.

TEST OF CONDENSATION STEPS

Three multi-component outdoor smog chamber experiments encompasing a wide range of chemical, temporal, and meteorological conditions are used to demonstrate verification of the condensation steps. Two of these experiments were multiday tests performed in the UCR outdoor Teflon Chamber (Carter et al., 1984); the other was a single-day experiment in the UNC outdoor chamber (Jeffries et al., 1985b) involving a more complex hydrocarbon mixture. Almost all of the condensation steps discussed in the previous section were tested individually to minimize the accumulation

of compensating errors. For the purpose of this demonstration, only the base mechanism (CBM-RR, Table 2) and the three successively condensed mechanisms (the final being CBM-IV) are considered here. Even with this limitation, however, the three smog chamber experiments created a test case encompassing seven days of data. Thus, the complete set of simulation results is presented as an appendix and a selected subset of these results is presented in this section.

The two UCR experiments provide a good testing environment because they employed a wide range of hydrocarbon and NO_x conditions, and large variations in temperature and water concentration. The UCR light and temperature data do not follow typical diurnal patterns since the dark period was often extended. These conditions complement the more natural UNC conditions under which the original mechanism was primarily developed because they create a wider range of conditions with which to test condensation of the mechanism. Initial concentrations for all tests are shown in Table 5.

The mechanism presented in Table 2 (CBM-RR) was used in the base-case simulations for the three experiments. Simulation of the UCR-80283 experiment was typically the most sensitive with respect to predicted first-day ozone concentrations. Complete base-case simulation results are contained in the appendix (Figures A-1 through A-3).

Case 1 (Figures A-4 through A-6) represents simulation results obtained when the following changes were made to the base case mechanism:

(1) PNA and MPNA cycles removed
(2) FROX cycle removed
(3) O^{1D} assumed to be a steady-state species
(4) MEO assumed to be a steady-state species (causing the elimination of MEO as well as MNIT and MEN3).
(5) AONE, GLY, and KET parameterized
(6) CRIG and MCRG removed
(7) H_2O concentration included in reaction rates.

These changes resulted in the elimination of 43 reactions and 13 of the 47 species. Examination of the base case and case 1 figures for all experiments (appendix) indicates that very little alternation in the results of the plotted species occurred after these changes were made.

The case 1 mechanism was altered to the case 2 mechanism (Figures A-7 through A-9) by

TABLE 5. INITIAL CONDITIONS USED FOR MECHANISM CONDENSATION EXPERIMENTS

Species	Concentrations (ppm)		
	UCR-80283	UCR-101083	UNC-92081
NO	0.250	0.098	0.117
NO_2	0.160	0.042	0.052
H_2O	2500.	12000.	16000.
Toluene	0.031	0.054	0.036
m-Xylene	0.025	0.047	0.025
1,2,4-Trimethylbenzene	--	--	0.007
Ethene	0.062	0.136	0.055
Propene	0.037	0.069	0.060
1-Butene	0.067	0.125	0.013
c-2-Butene	--	--	0.010
2-Methyl-1-butene	--	--	0.009
2-Methyl-2-butene	--	--	0.011
n-Butane	0.075	0.142	0.067
n-Pentane	0.072	0.135	
i-Pentane	--	--	0.040
2-Methyl-pentane	--	--	0.026
2,4-Dimethyl-pentane	--	--	0.033
2,2,4-Trimethyl-pentane	--	--	0.021
i-Octane	0.035	0.072	--

(1) Expansion of the function of XO_2 to include MEO_2.

Although this change led to the elimination of only one additional species and two reactions, the case 2 alteration was tested separately because we felt it constituted a fundemental alteration of the mechanism. No important variations in results were found between case 1 and case 2 simulations (see appendix).

Case 3 (Figures A-10 through A-12) constitutes the final condensed version--CBM-IV--presented in Table 3. The condensation from case 2 to Case 3 consisted of

(1) Elimination of BZA chemistry (causing the deletion of BZA, BZO2, and PBZN).

(2) Condensation of PAR chemistry (causing the elimination of ROR and D).

This final condensation yielded 28 species (an elimination of 19) and 70 reactions (an elimination of 43) after condensation. To facilitate comparison of the effect of condensing the CBM-RR mechanism, a subset of the simululations presented in the appendix is repeated in Figures 2 through 4 (in all plots, solid lines represent CHEMK simulation results and individual points represent experimental measurements). These figures compare the ozone predictions obtained with the CBM-RR and CBM-IV mechanisms for all three experiments. Examination of these figures and those in the appendix (which show the simulation profiles for all species measured in the experiments) indicates very little change in predictions throughout all condensation steps.

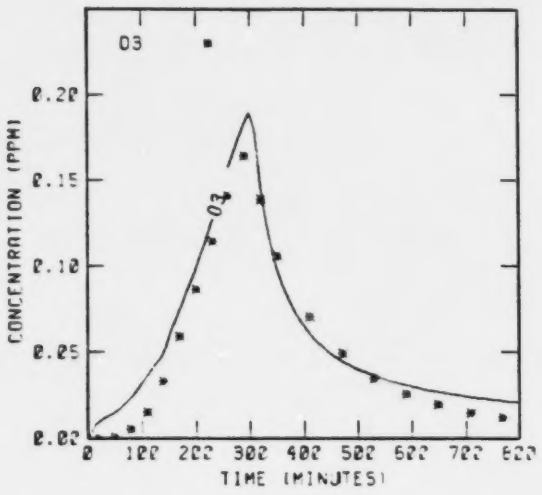

Day 1: CBM-RR

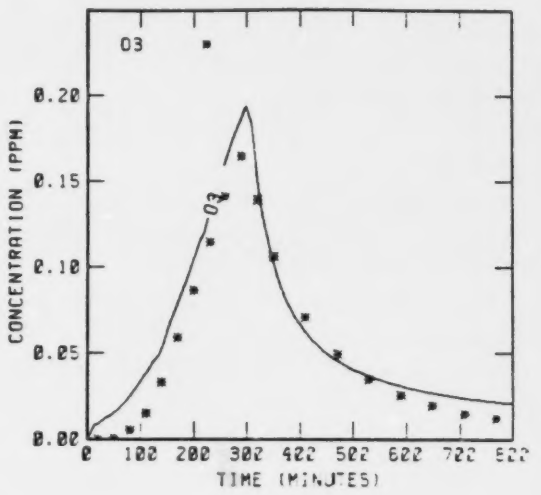

Day 1: CBM-IV

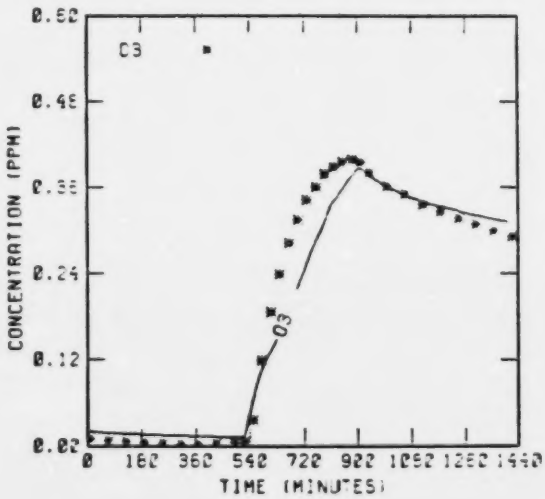

Day 2: CBM-RR

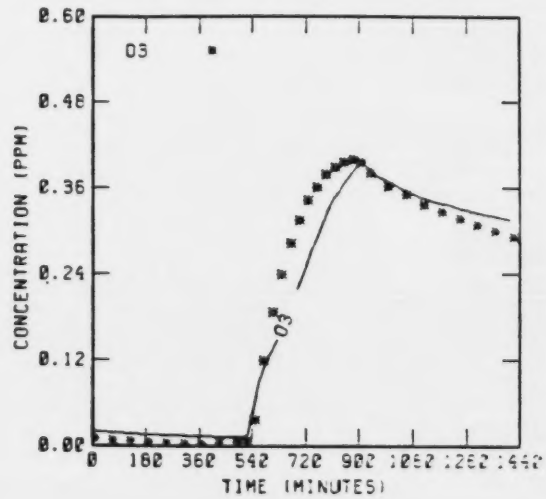

Day 2: CBM-IV

Figure 2. Ozone simulation results for UCR 80283 two-day experiment.

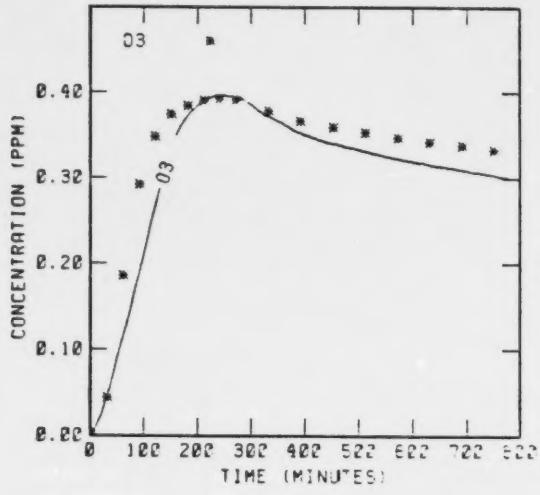

Day 1: CBM-RR

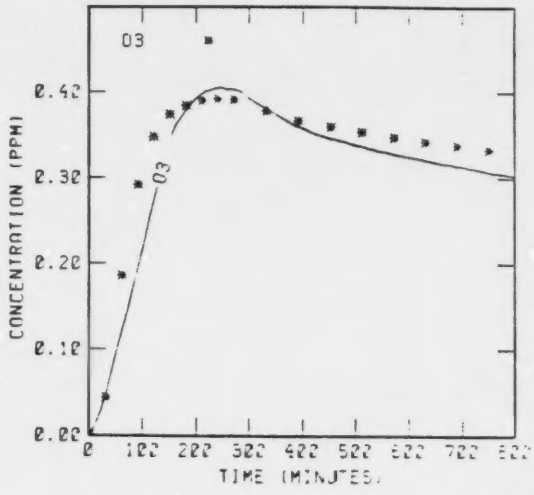

Day 1: CBM-IV

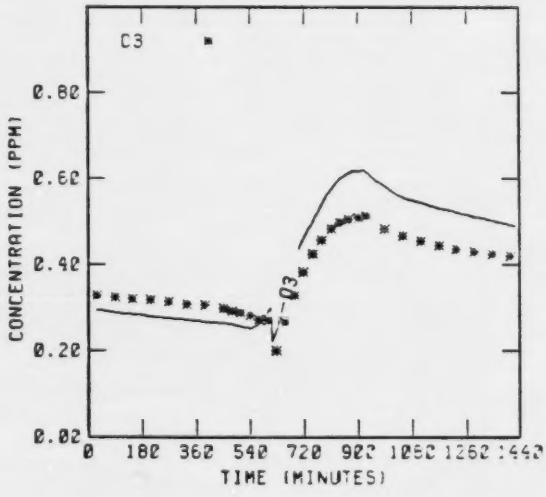

Day 2: CBM-RR

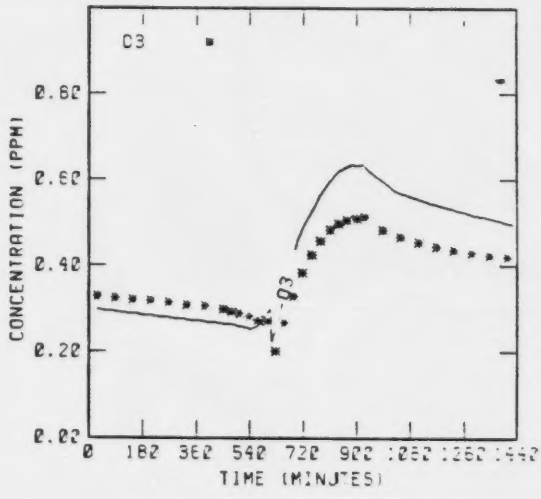

Day 2: CBM-IV

Figure 3. Ozone simulation results for UCR 101083 four-day experiment.

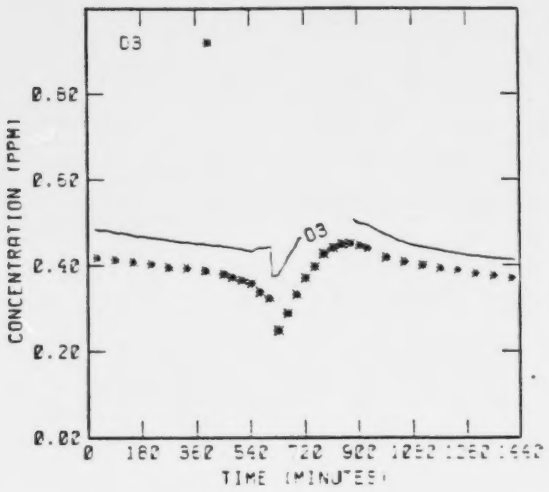

Day 3: CBM-RR

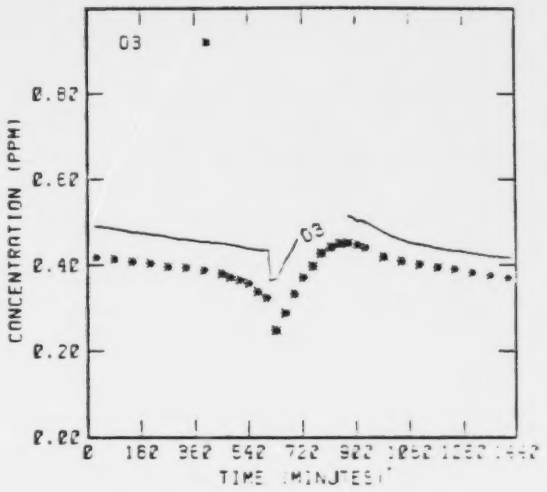

Day 3: CBM-IV

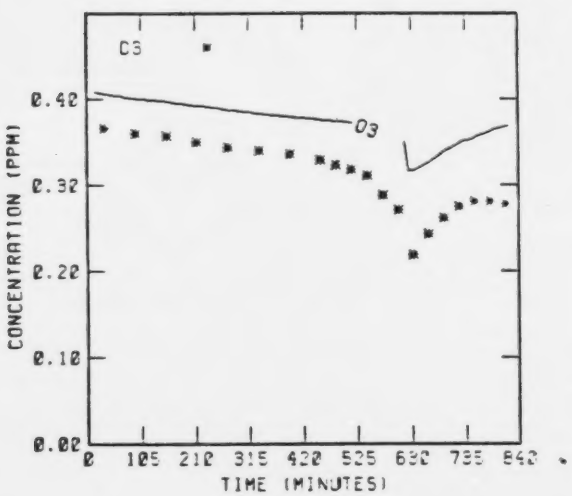

Day 4: CBM-RR

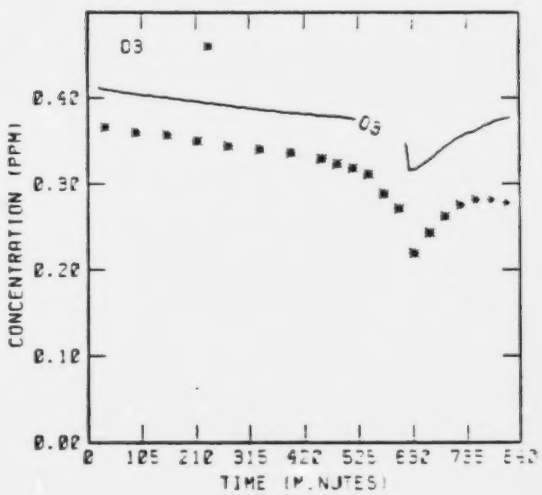

Day 4: CBM-IV

Figure 3 (concluded)

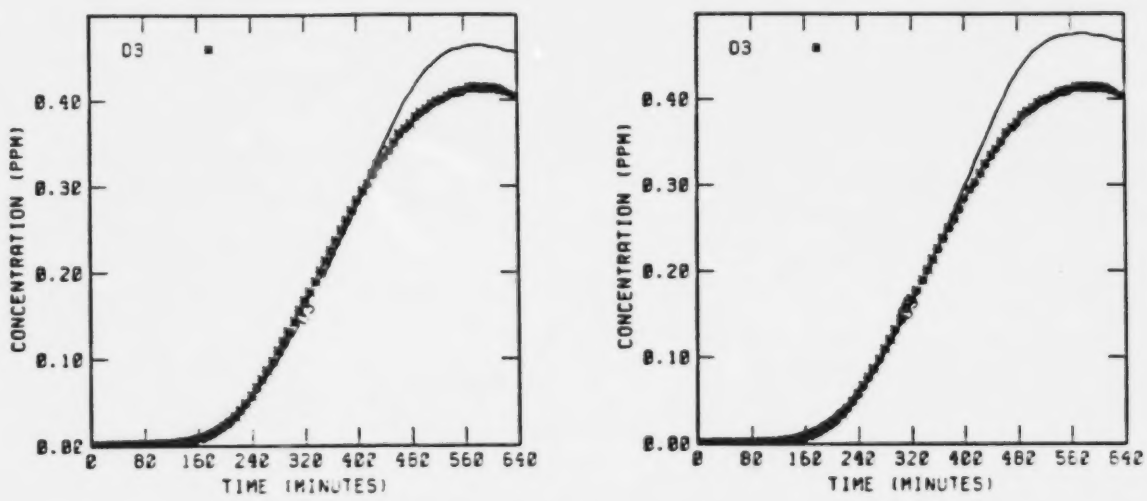

CBM-RR

CBM-IV

Figure 4. Ozone simulation results for UNC 92081 one-day experiment.

VERIFICATION OF TEMPERATURE EFFECTS WITH PNA AND MPNA

As noted earlier, the rates of PNA and MPNA thermal decomposition vary greatly with temperature. As temperature rises and decomposition dominates, the average interval over which these cycles "store" peroxy radicals and NO_2 diminishes and the reactions become less important. Several UNC smog chamber experiments have been performed on cold days, facilitating variable temperature testing of these processes.

Figure 5 presents experimental and simulation results for the UNC red side propylene/NO_x experiment of 26 December 1977. This simulation was performed with the full CBM-X mechanism, including the PNA and MPNA reaction cycles. The temperature on this day was extremely low for a smog chamber experiment. The average temperature was 271.5 K, with a maximum of only 275 K. Simulated PNA and MPNA formation begins near the NO_2 maximum concentration. The PNA concentration decreases slowly when the formation reaction is limited as NO_2 concentration and solar intensity approach zero. These results can be compared with those of Figure 6, which presents simulation results for the same mechanism, excluding the PNA and MPNA reactions. Ozone production is overpredicted (O_{3max} = 0.563 ppm) compared with that of the first simulation by 28 percent due to the extra NO_2 and peroxy radicals available at the time when PNA and MPNA would be formed. Under such temperature conditions, the inclusion of PNA and MPNA is obviously needed to properly predict ozone production.

Results from the 14 October 1977 UNC red side experiment are shown in Figures 7 and 8. The average temperature for this experiment was about 288 K with a temperature near 290 K during the simulated PNA peak. Although this is a lower than average temperature for most cases of interest, it is 16 K above the low extreme previously discussed. It is not surprising, therefore, that decomposition of PNA and MPNA is more dominant than during the colder experiment.

Comparison of the predicted PNA curves for the two UNC experiments indicates that both the magnitude and duration of PNA is less than half of that on the warmer day, providing less "storage" of NO_2 and peroxy radicals. In fact, a comparison of Figures 7 and 8 indicates no discernable difference in the predictions of any plotted species other than the oxy acids discussed. Therefore, we feel that the PNA and MPNA reaction cycles need not be considered at the temperatures commonly simulated (greater than 290 K) and we have removed them from the condensed CBM-IV mechanism. For simulations at lower temperature, knowledge of all temperature-dependent chemistry is less definite, but certainly the PNA and MPNA reactions should be included.

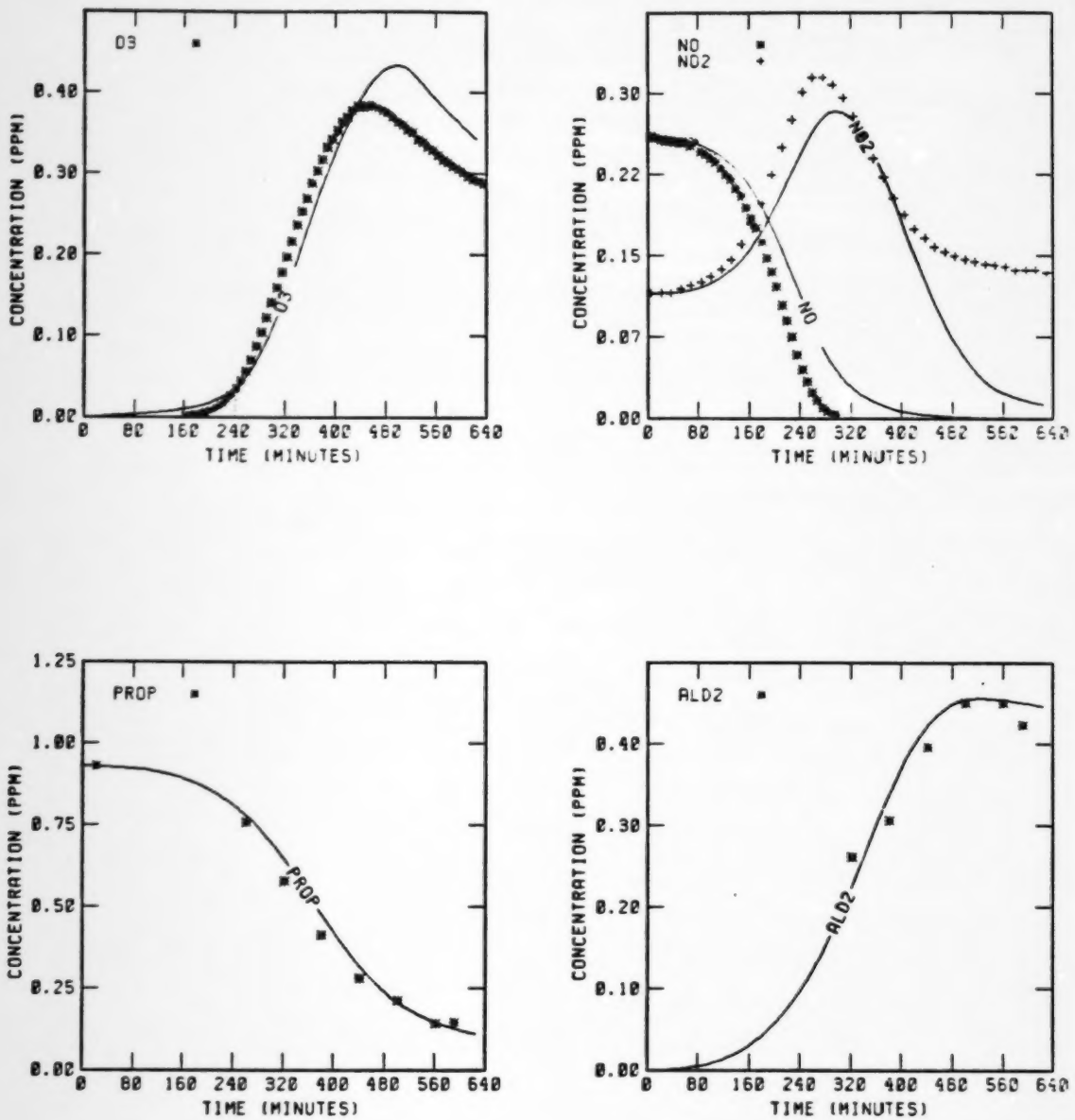

Figure 5. CBM-X simulation results for UNCR 122677 (with PNA and MPNA chemistry).

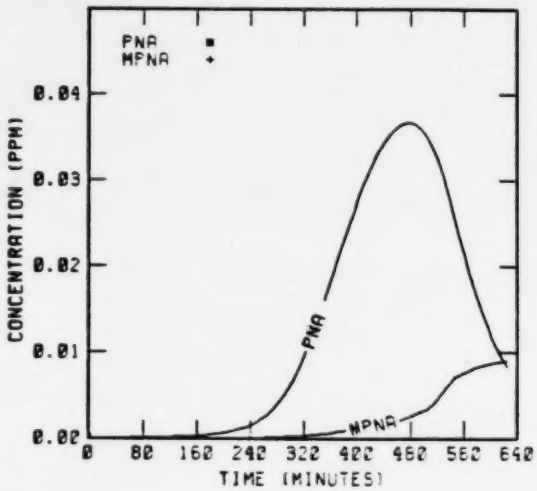

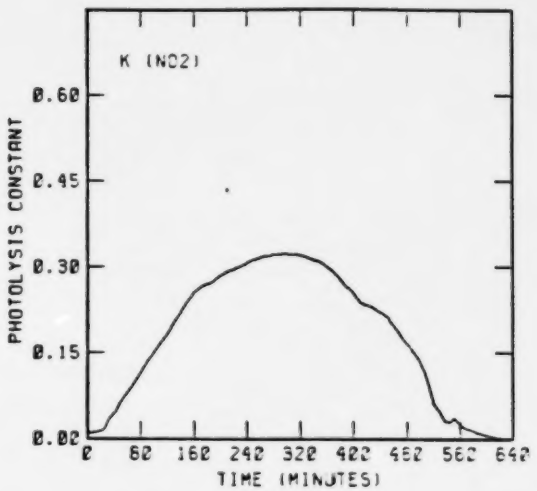

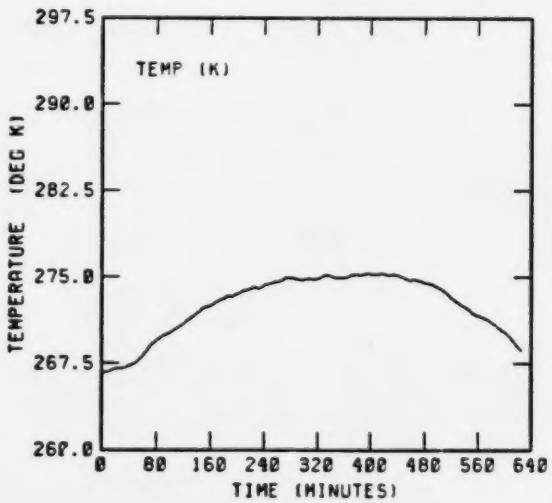

Figure 5. Concluded.

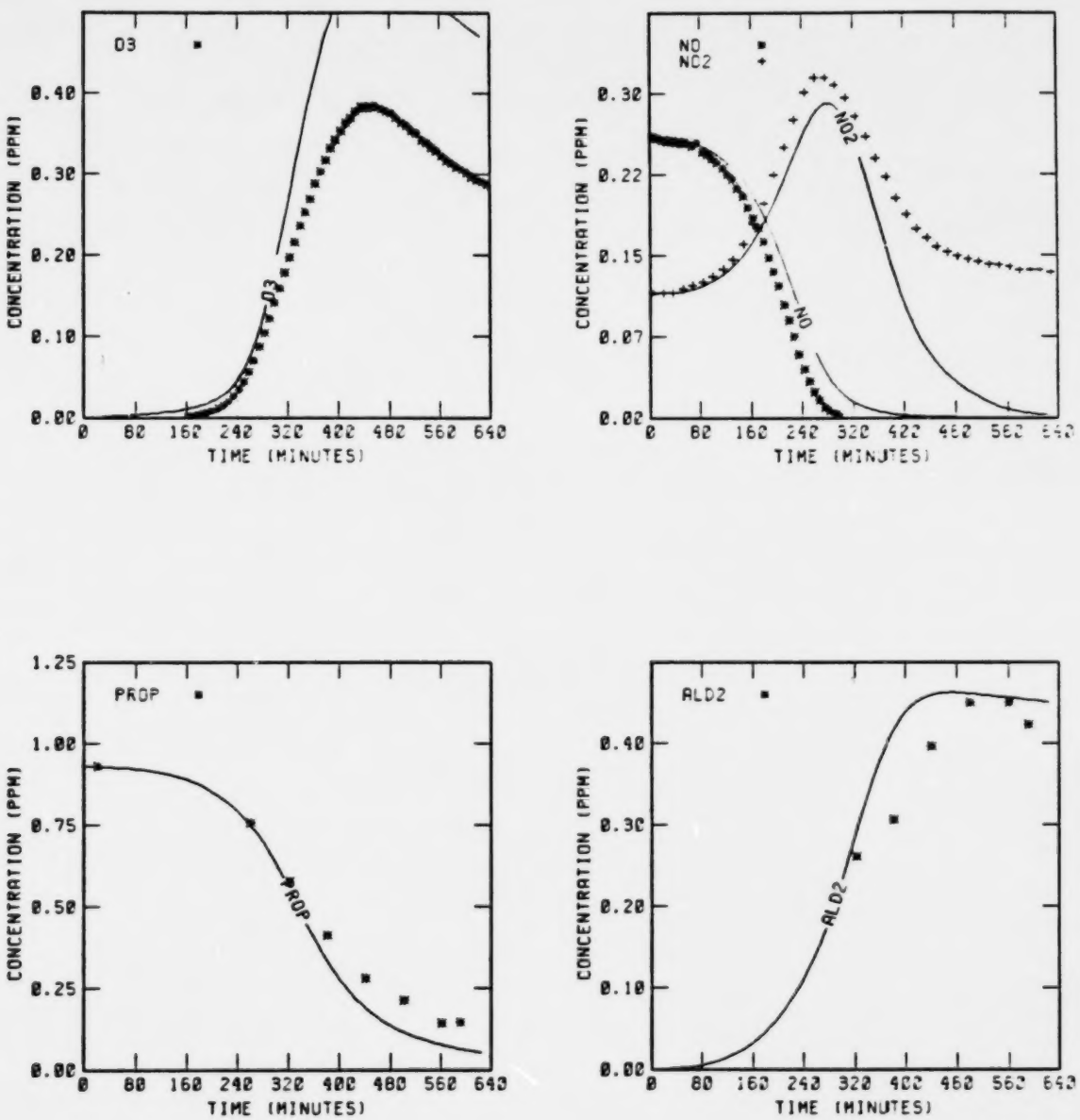

Figure 6. CBM-X simulation results for UNCR 122677 (without PNA and MPNA chemistry).

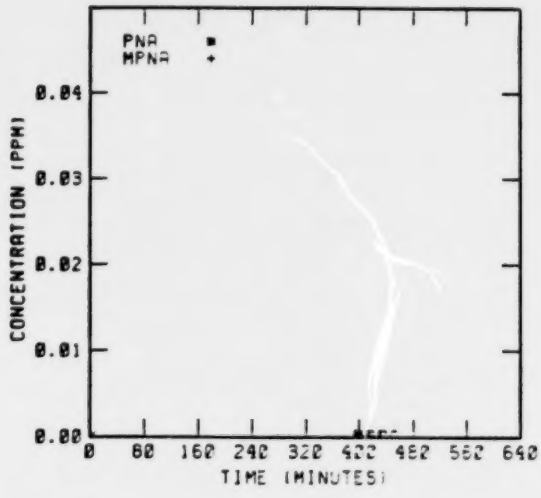

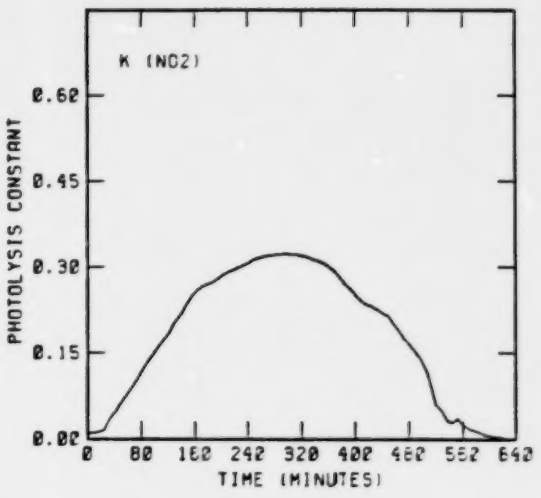

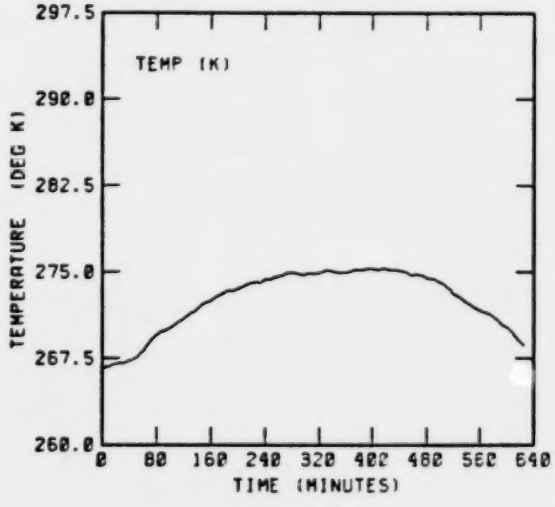

Figure 6. Concluded.

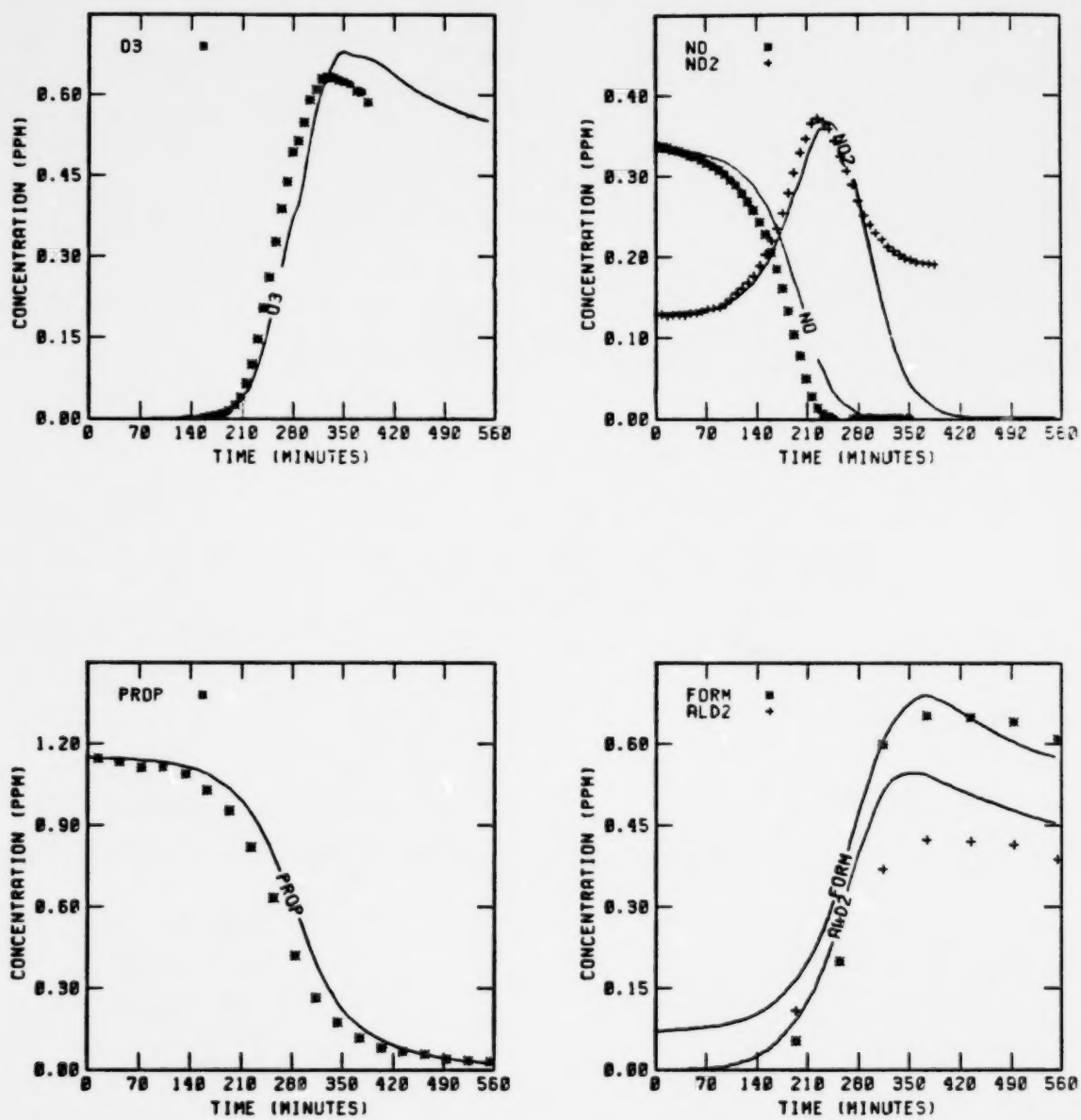

Figure 7. CBM-X simulation results for UNCR 102477 (with PNA and MPNA chemistry).

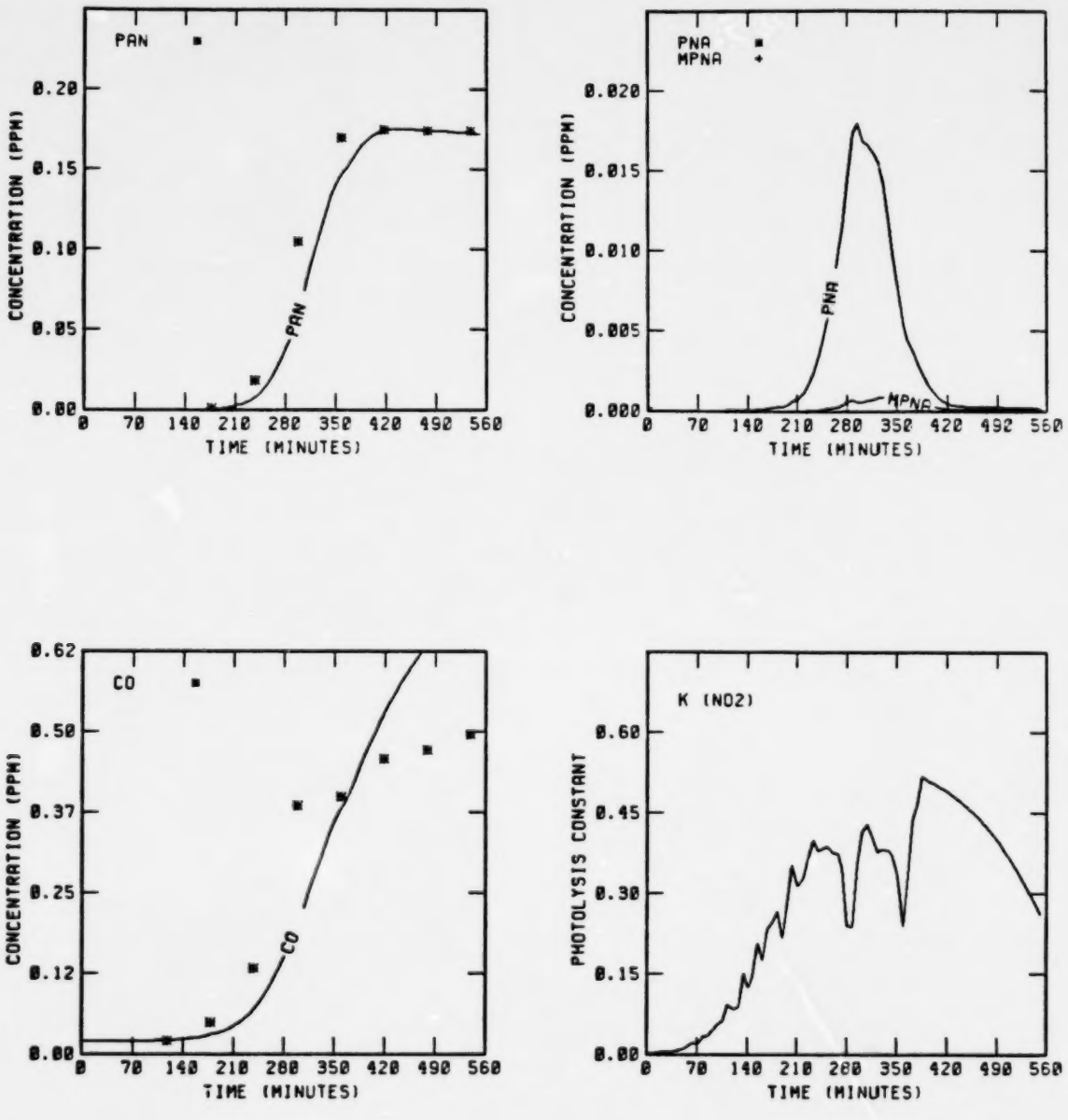

Figure 7. Concluded.

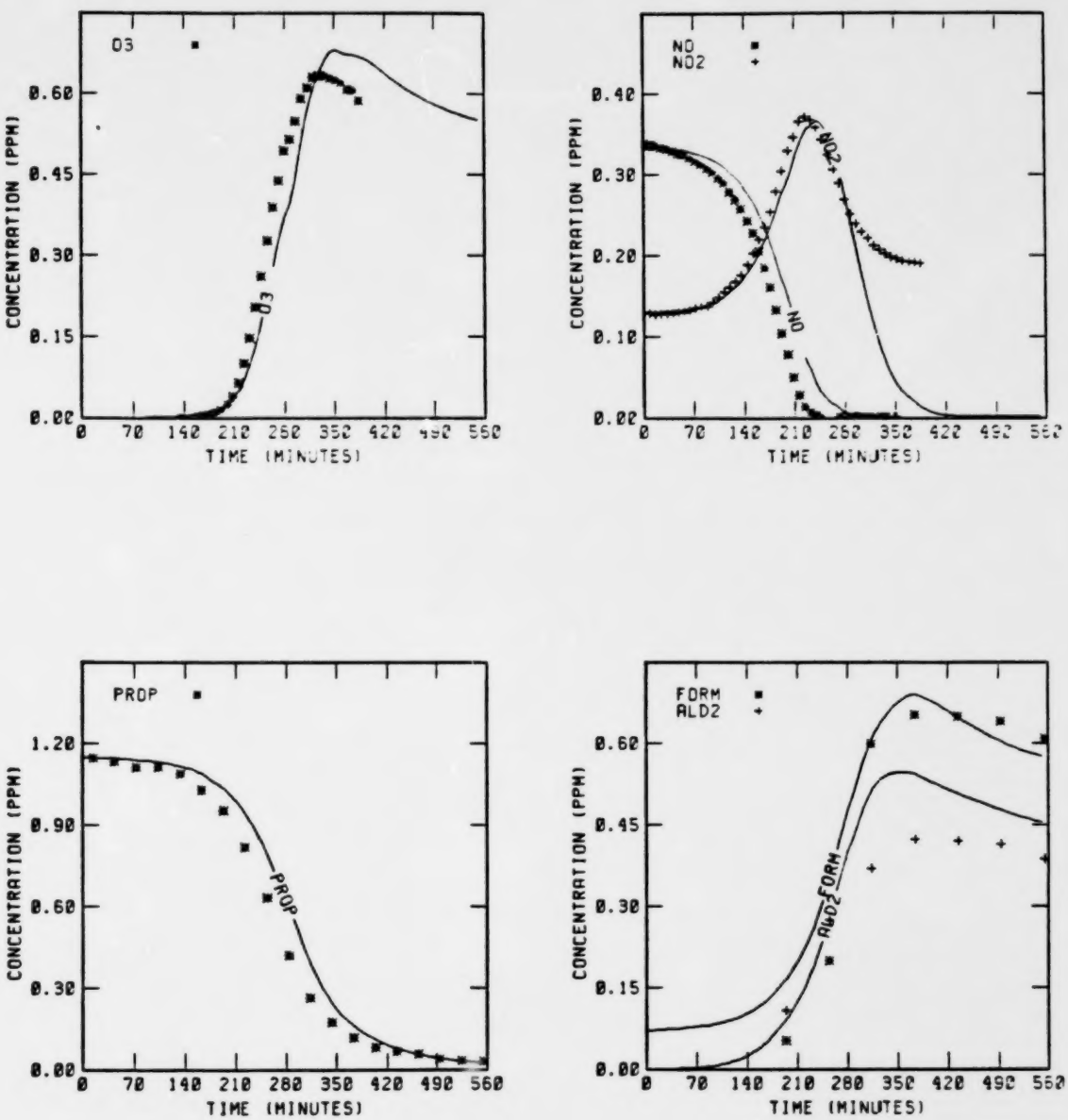

Figure 8. CBM-X simulation results for UNCR 102477 (without PNA and MPNA chemistry).

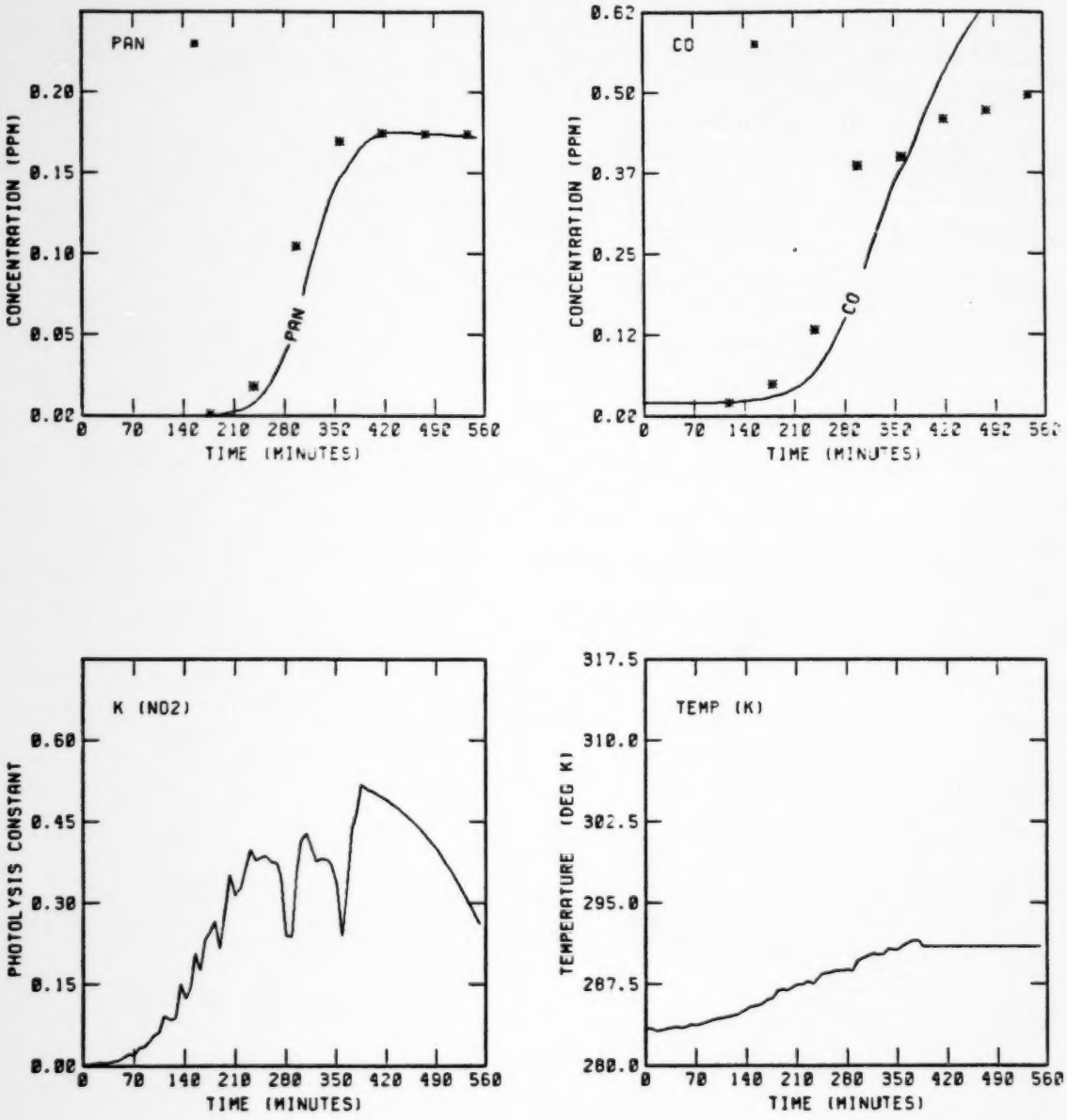

Figure 8. Concluded.

CONDENSATION OF ISOPRENE CHEMISTRY

Although the condensation of isoprene chemistry was minor, that species was not incuded in the UCR and UNC experiments discussed earlier and it is considered separately here. Figure 9 illustrates the results of a simulation of the UNC blue side 16 July 1980 isoprene/NO_x experiment using the isoprene chemistry given in Table 1. Condensation of these reactions for the CBM-IV mechanism required only minor changes to the O, O_3, and OH reactions with isoprene. In all cases, KET was replaced by PAR for the reasons discussed earlier. This change should have little effect on ozone predictions. Figure 10 illustrates the 16 July 1980 results obtained using the CBM-IV isoprene chemistry. There are no obvious differences between the results given in Figures 9 and 10.

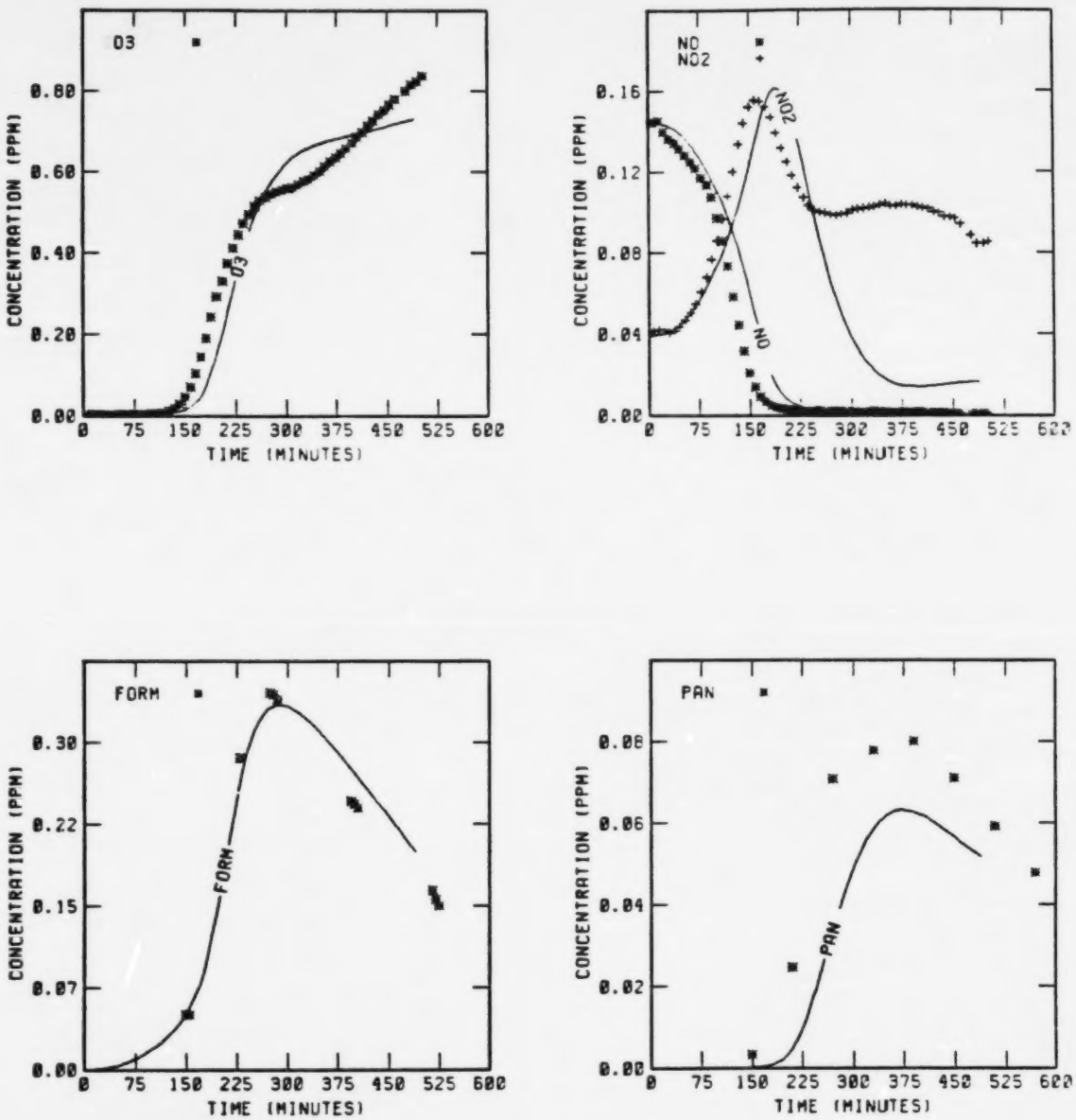

Figure 9. Simulation results for UNCB 71680 using the CBM-RR mechanism.

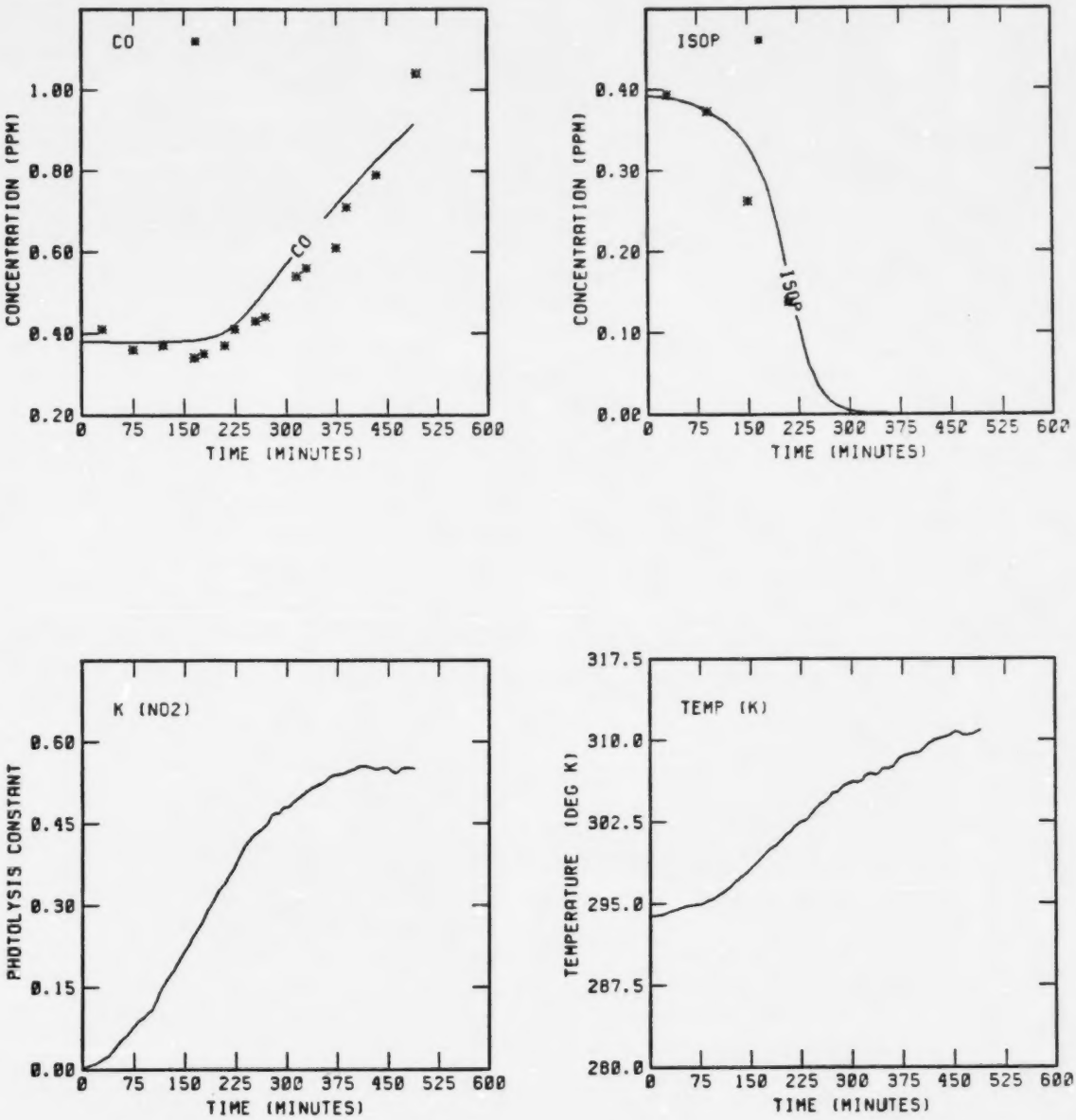

Figure 9. Concluded.

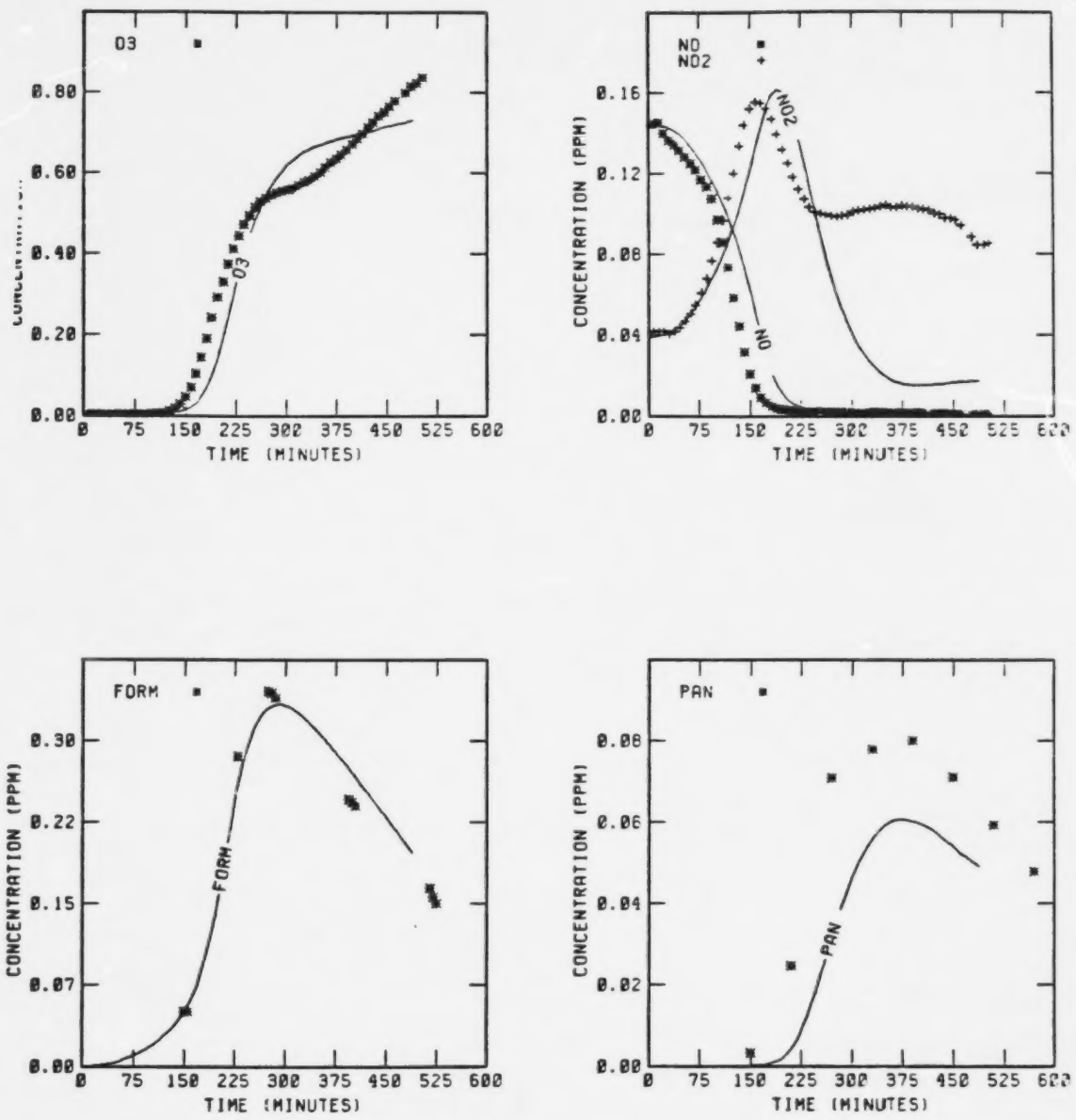

Figure 10. Simulation results for UNCB 71680 using the CBM-IV mechanism.

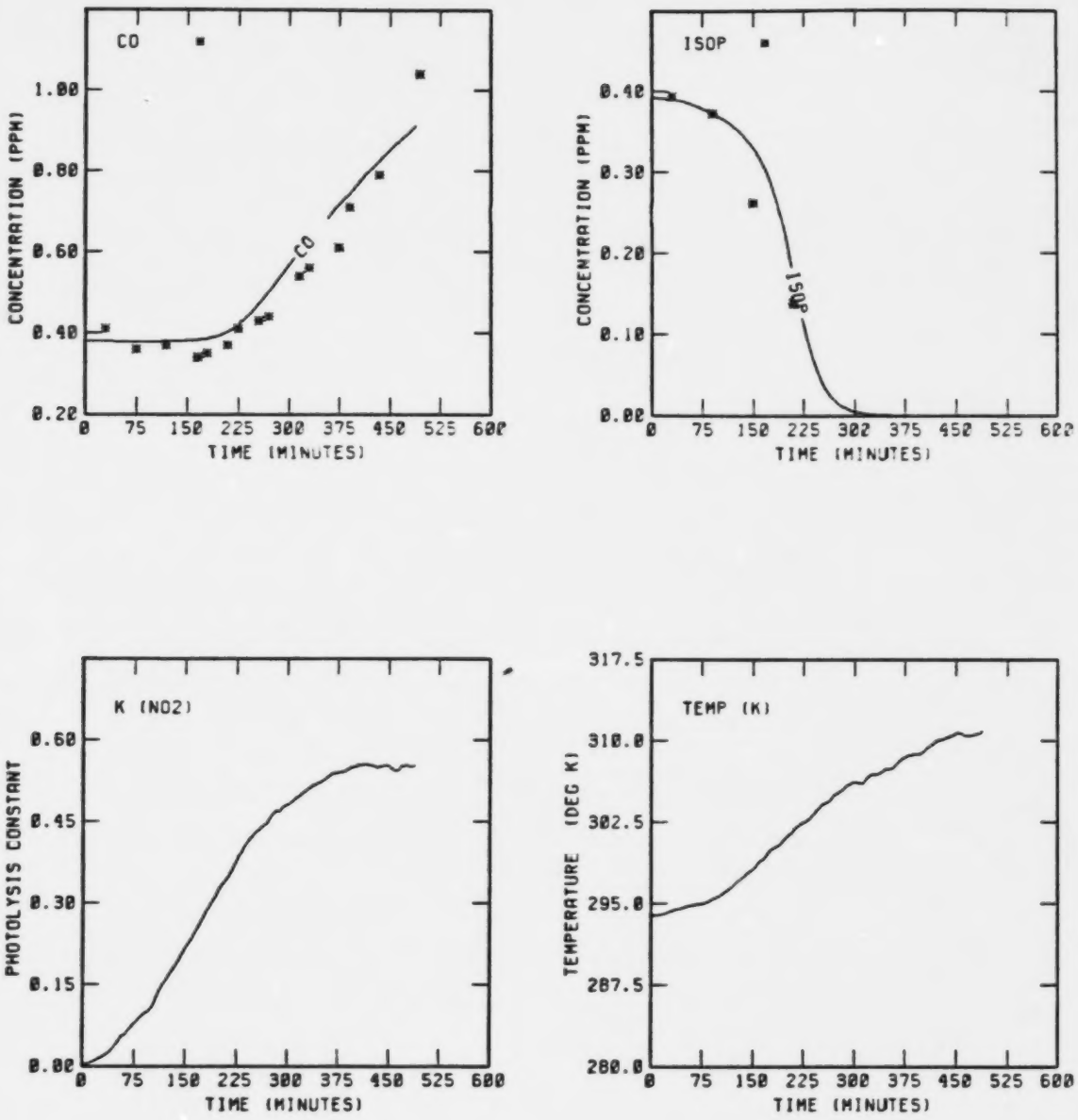

Figure 10. Concluded.

SECTION 4

SUMMARY AND RECOMMENDATIONS

SUMMARY

Under contract to the EPA, Systems Applications has developed a series of urban and regional chemical kinetic mechanisms, each of which describes the formation of photochemical smog from nitrogen oxide and multiple organic precursors. The various versions of the original Carbon-Bond Mechanism (CBM) represent a wide range of detail. The largest and most complex mechanisms--the CBM-X and CBM-XR--are intended for applications on urban and regional scales, respectively. These mechanisms were designed to describe all of the detailed interactions necessary for control strategy analysis in models that do not require condensed chemical schemes because of computer limitations.

The most condensed version of the mechanism series now available is known as CBM-IV. The condensation and testing of CBM-IV is the subject of this report. This mechanism has been carefully tested against results obtained with the expanded CBM and several intermediate mechanisms to ensure that the condensation steps did not contain compensating factors and to verify the performance of the CBM-IV under a range of conditions. CBM-IV differs considerably from previous Carbon-Bond mechanisms even though it is similar in size. All Carbon-Bond mechanisms in the condensation series--CBM-I, CBM-II, CBM-III, and CBM-IV--are of a size suitable for use in large grid models where computational efficiency is required. However, the mechanism condensation approach used prior to the development of CBM-IV was to create condensed reaction subsets that would perform in a manner similar to the larger expanded reaction pathways of specific compounds such as propene, ethene, butane, and toluene. The stoichiometric coefficients were always unit values and these mechanisms were never tested against results obtained with a large complex mechanism designed to simulate urban-like mixtures of hydrocarbons. The CBM-IV, on the other hand, uses extensive and complicated mechanistic structures based on well-founded assumptions.

The condensation of the expanded CBM to CBM-IV was tested in an incremental manner by simulating seven days of outdoor smog chamber data

from two different experimental facilities. These data provided a wide range of time, temperature, light intensity, and concentration conditions for comparing simulation results from increasingly condensed mechanisms with the expanded CBM results. This approach was enacted to minimize compensating errors and to verify the operating boundaries of the mechanism at each condensation step. This development yielded a mechanism containing 28 species and 70 reactions (including isoprene chemistry) compared with 78 species and 170 reactions contained in the CBM-XR.

Because the CBM-IV includes isoprene chemistry, the mechanism is suitable for use in gridded regional oxidant models. With the further addition of sulfur chemistry, along with PNA, MPNA and organic acid chemistry, it may also be suitable for modeling homogeneous gas-phase chemistry in acid rain models. Moreover, additional product species that account for organic nitrates, organic peroxides, or peroxy acids can easily be included in the CBM-IV. However, the CBM-IV must be used with caution under conditions for which it has not yet been tested.

The extensive use of complicated stoichiometric coefficients and other condensation techniques employed in the CBM-IV results in a mechanism that "hides" much of the detail explicitly described in the full CBM-X. That is, the detailed chemistry is usually present in the CBM-IV but mathematically concealed within the stoichiometric parameters. If any improvements or updates to the chemistry should be required, one must first alter the CBM-X before redefining new stoichiometric parameters for the CBM-IV. In addition, the condensation techniques may then need to be retested. Hence, although the CBM-IV may provide the performance of a highly detailed mechanism in an efficient and compact form, all the chemistry is not visible and mechanism updates may require both recalculation of parameters and retesting.

RECOMMENDATIONS

All of the uncertainties in the CBM-X also apply to the CBM-IV. In particular, (1) these mechanisms have not yet been thoroughly tested under dynamic conditions and (2) the ability of the mechanism to predict certain nonozone oxidants such as hydrogen peroxide is uncertain. Smog chamber data with which to test these features is only now becoming available. Dynamic conditions entail the dilution and simultaneous entrainment of fresh and aged pollutants such as occurs under actual smog episode conditions. The dynamic entrainment of organics with varied reactivities also needs further testing. Nevertheless, the CBM-X is the most extensively tested smog mechanism currently available.

Another area needing further study involves the appropriateness of the surrogate approximations used in the CBM, in particular the aromatic species. The CBM-X and CBM-IV treat all aromatics as a mixture of toluene, m-xylene, and paraffins. This may be inappropriate since aromatic hydrocarbons have both a wide range of reactivities and a wide range of reactive products that may not be described by simple surrogate methods. Finally, there may be further stages of condensation possible in which even more detailed chemistry is parameterized by assuming fixed ratios of certain species (e.g., the ratio of toluene to xylene or formaldehyde to other aldehydes).

REFERENCES

Atkinson, R., and A. C. Lloyd. Evaluation of Kinetic and Mechanistic Data for Modeling of Photochemical Smog. Phys. Chem. Ref. Data, 13(2)315-444, 1984

Baulch, D. L., R. A. Cox, R. F. Hampson, Jr., J. A. Kerr, J. Troe, and R. T. Watson. Evaluated Kinetic and Photochemical Data for Atmospheric Chemistry: Supplement II--CODATA Task Group on Gas Phase Chemical Kinetics. Phys. Chem. Ref. Data, 13(4)1259-1380, 1984.

Carter, W.P.L., M. C. Dodd, W. D. Long, and R. Atkinson. Outdoor Chamber Study to Test Multi-Day Effects--Volume I: Results and Discussion. Final Report Cooperative Agreement, U.S. Environmental Protection Agency (CR810260-01), 1985.

Jeffries, H. E., K. G. Sexton, T. P. Morris, M. Jackson, R. G. Goodman, R. M. Kamens and M. S. Holleman. Outdoor Smog Chamber Experiments Using Automobile Exhaust. EPA 600/3-85-032, U.S. Environmental Protection Agency, Research Triangle Park, North Carolina, 1985a.

Jeffries, H. E., K. G. Sexton, R. M. Kamens, and M. S. Holleman. Outdoor Smog Chamber Experiments to Test Photochemical Models: Phase II. EPA-600/3-85-029, U.S. Environental Protection Agency, Research Triangle Park, North Carolina, 1985b.

Kerr, J. A., and J. G. Calvert. Chemical Transformation Modules for Eulerian Acid Deposition Models--Volume I: The Gas-Phase Chemistry. EPA-600/3-85-015, National Center for Atmospheric Research, Boulder, Colorado, 1985.

Killus, J. P., and G. Z. Whitten. Technical Discussions Relating to the Use of the Carbon-Bond Mechanism in OZIPM/EKMA. SYSAPP-84/117, Systems Applications, Inc., San Rafael, California, 1984.

Whitten, G. Z., and H. Hogo. Mathematical Modeling of Simulated Photochemical Smog. EPA-600/3-77-011, U.S. Environmental Protection Agency, Research Triangle Park, North Carolina, 1977.

Whitten, G. Z., H. Hogo, and J. P. Killus. The Carbon-Bond Mechanism: A Condensed Kinetic Mechanism for Photochemical Smog. Environ. Sci. Technol., 14:699, 1980a.

Whitten, G. Z., J. P. Killus, and H. Hogo. Modeling of Simulated Photochemical Smog with Kinetic Mechanisms. EPA-600/3-80-028a, U.S. Environmental Protection Agency, Research Triangle Park, North Carolina, 1980b.

Whitten, G. Z. The Chemistry of Smog Formation: A Review of Current Knowledge. Environ. Int., 9:447-463, 1983.

Whitten, G. Z., J. P. Killus, and R. G. Johnson. Modeling of Auto Exhaust Smog Chamber Data for EKMA Development. EPA-600/3-85-025, U.S. Environmental Protection Agency, Research Triangle Park, North Carolina, 1985a.

Whitten, G. Z., J. P. Killus, and R. G. Johnson. Development of a Chemical Kinetic Mechanism for the U.S. EPA Regional Oxidant Model. EPA-600/3-85-026, U.S. Environmental Protection Agency, Research Triangle Park, North Carolina, 1985b.

Whitten, G. Z., R. G. Johnson, and J. P. Killus. Development of a Chemical Kinetic Mechanism for the U.S. EPA Regional Oxidant Model. EPA/600-3-85/026, U.S. Environmental Protection Agency, Research Triangle Park, North Carolina, 1985c.

Appendix

SIMULATION RESULTS FOR MECHANISM CONDENSATION STEPS

LIST OF FIGURES--APPENDIX A

Number		Page
A-1	Base case simulation results for UCR-80283 two-day experiment	57
A-2	Base case simulation results for UCR-101083 four-day experiment	65
A-3	Base case simulation results for UNC-92081 one-day experiment	81
A-4	Case one simulation results for UCR-80283 two-day experiment	83
A-5	Case one simulation results for UCR-101083 four-day experiment	91
A-6	Case one simulation results for UNC-92081 one-day experiment	107
A-7	Case two simulation results for UCR-80283 two-day experiment	109
A-8	Case two simulation results for UCR-101083 four-day experiment	117
A-9	Case two simulation results for UNC-92081 one-day experiment	133
A-10	CBM-IV (case three) simulation results for UCR-80283 two-day experiment	135
A-11	CBM-IV (case three) simulation results for UCR-101083 four-day experiment	143
A-12	CBM-IV (case three) simulation results for UNC-92081 one-day experiment	159

Appendix A

SIMULATION RESULTS FOR MECHANISM CONDENSATION STEPS

This appendix contains simulation results for three smog chamber experiments (UCR-80283, UCR-101083, and UNC-90281) over four stages of mechanism condensation. Solid lines represent CHEMK simulation results; individual points represent experimental measurements. A discussion of the condensation process with reference to these plots is found in the text.

The primary purpose of the condensation exercise documented in this appendix was to develop the CBM-IV such that each stage of mechanistic compression resulted in nonvarying simulation results. Thus, we include pertinent comparisons between simulation results of different condensation steps rather than between model and measurement values for one step. It is inevitable, however, that these latter comparisons be made since the measurements and model results are presented together. Therefore, we briefly present a few points concerning the experimental data and model results that may keep the reader from misleading observations:

(1) Experimental NO_2 values are often really the sum of NO_2 concentrations and other NO_x species. This is due to the inability of most chemiluminescent NO_x meters to distinguish between NO_2 and other compounds, such as PAN. In the UNC experiment, for instance, the measurements include at least NO_2 and PAN concentrations. A similar situation also appears to occur in the UCR experimental determination of NO_2 in the dark.

(2) Surrogate species, such as OLE and XYL cannot always be directly compared with experimental data (the sum of the presented species) since the chemical nature of the experimental species (related to the individual fractions of the represented species) changes with time. Thus, under extreme conditions (low concentrations--situations in which only one presented species remains), the surrogate species will not always trace the experimental data. Such is the nature of a surrogate representation.

(3) As noted in (2), experimental conditions of low concentrations often yield misleading plots, i.e., relative differences may be large, but the absolute concentrations are very small compared to initial values. For example, in the second-day plots of the UCR data the discrepancies between experimental and predicted OLE concentrations appear large, but the magnitudes of the ordinates of the second-day plots are only 1.3 and 2.7 percent of the first-day values, exaggerating the differences by large factors.

(4) Since H_2O concentrations are input parameters, they were often approximated by linear functions and do not follow measurements traces well.

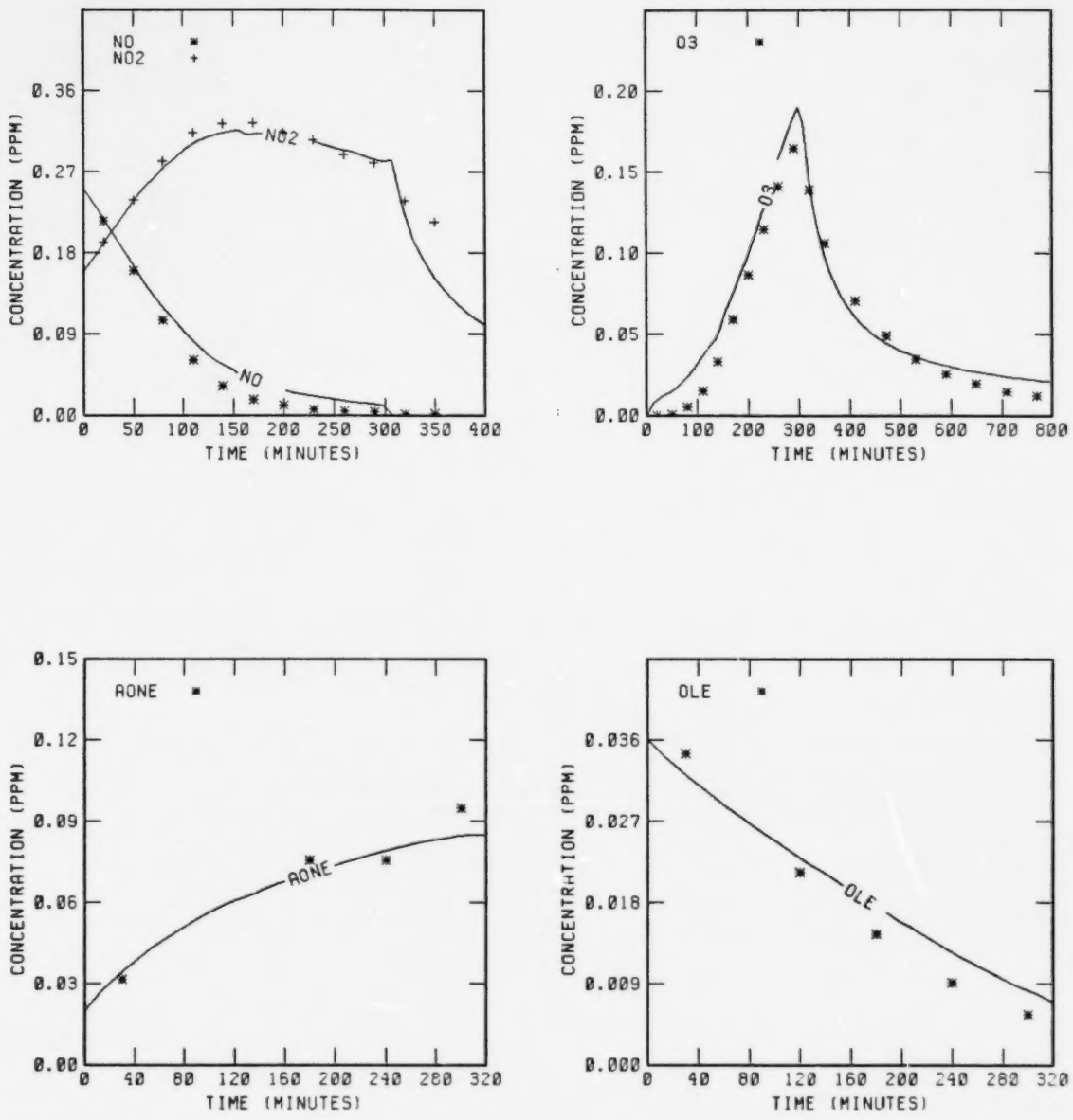

FIGURE A-1. SIMULATION RESULTS FOR OTCR.80283

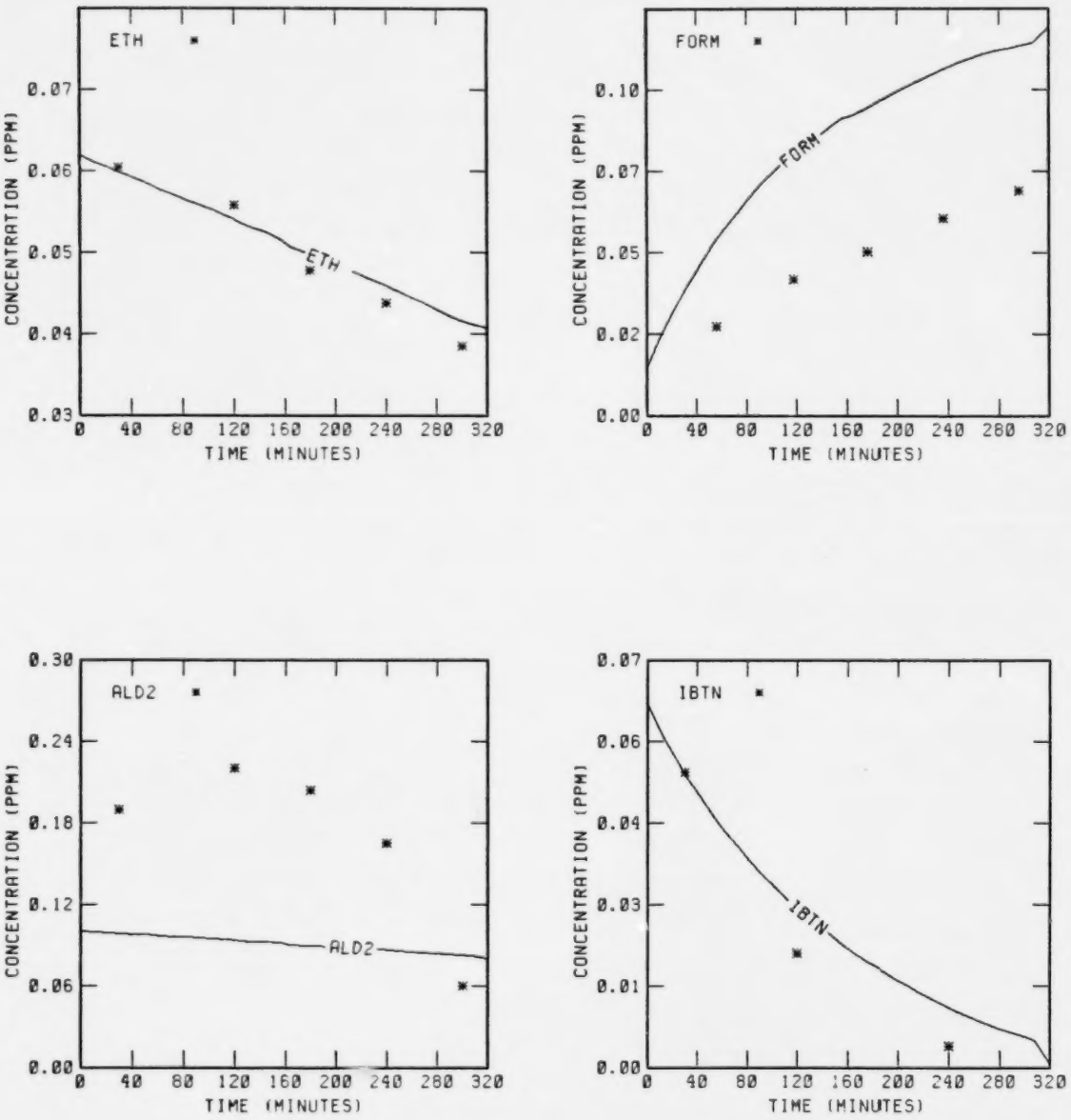

FIGURE A-1. SIMULATION RESULTS FOR OTCR.80283

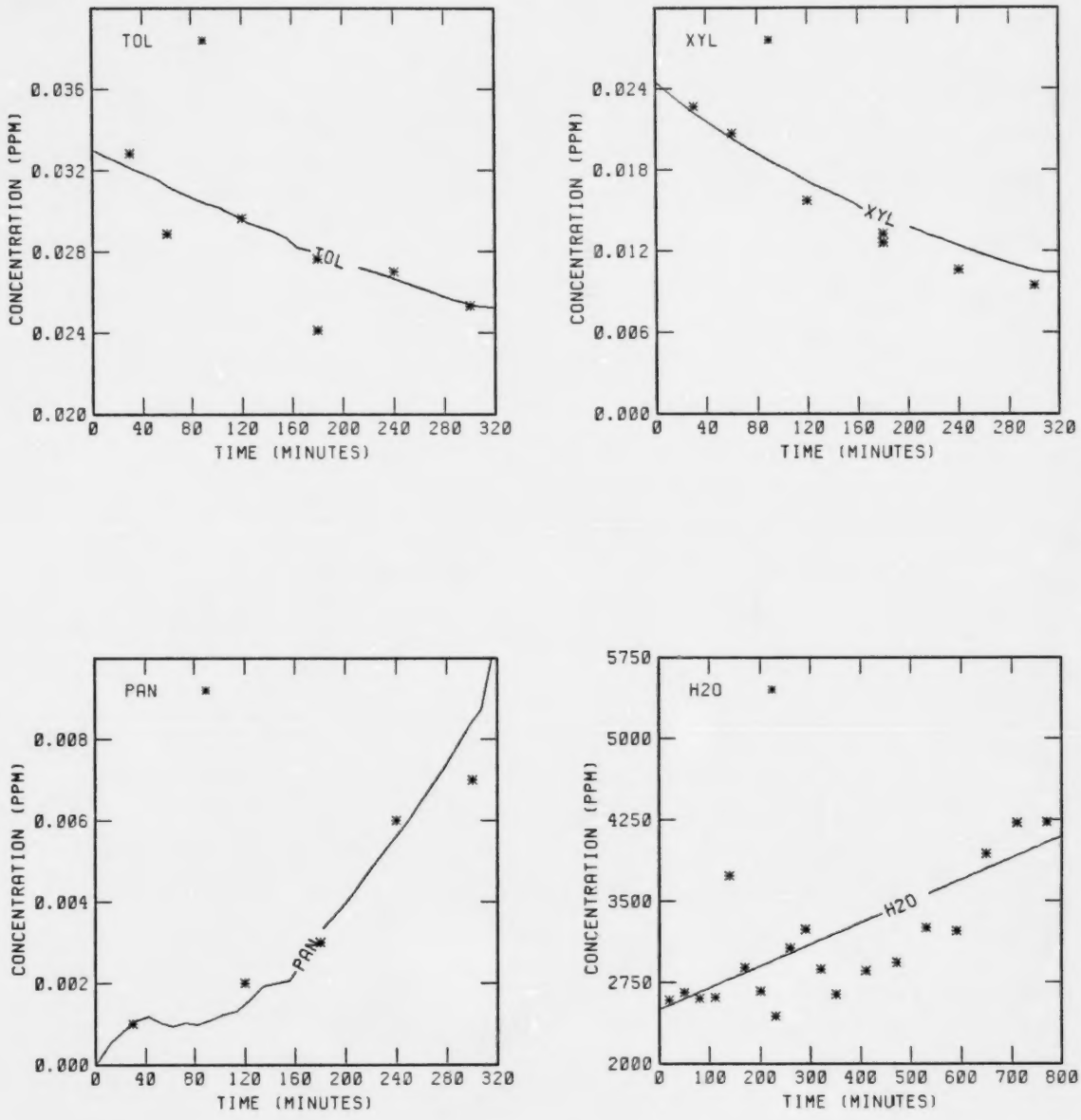

FIGURE A-1. SIMULATION RESULTS FOR OTCR.80283

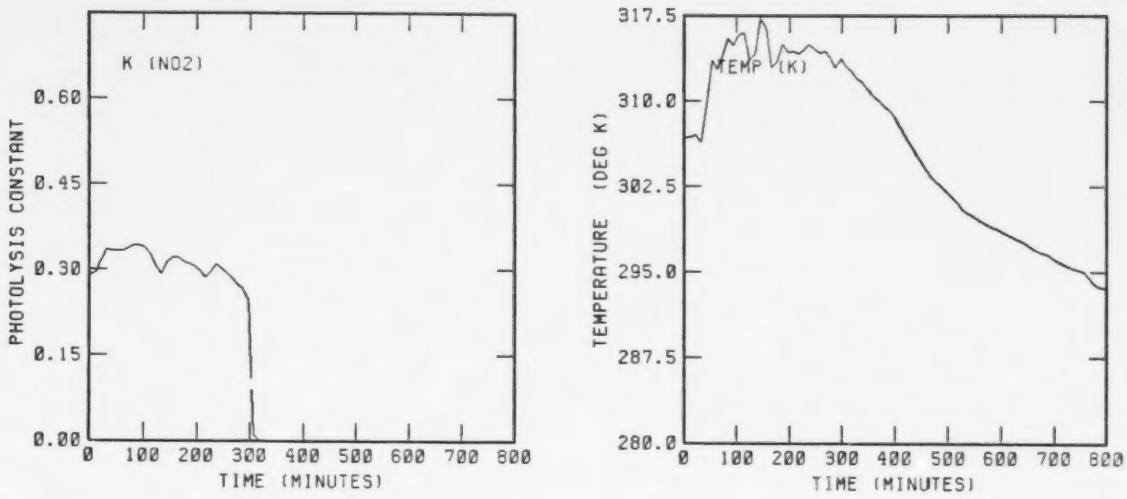

FIGURE A-1. SIMULATION RESULTS FOR OTCR.80283

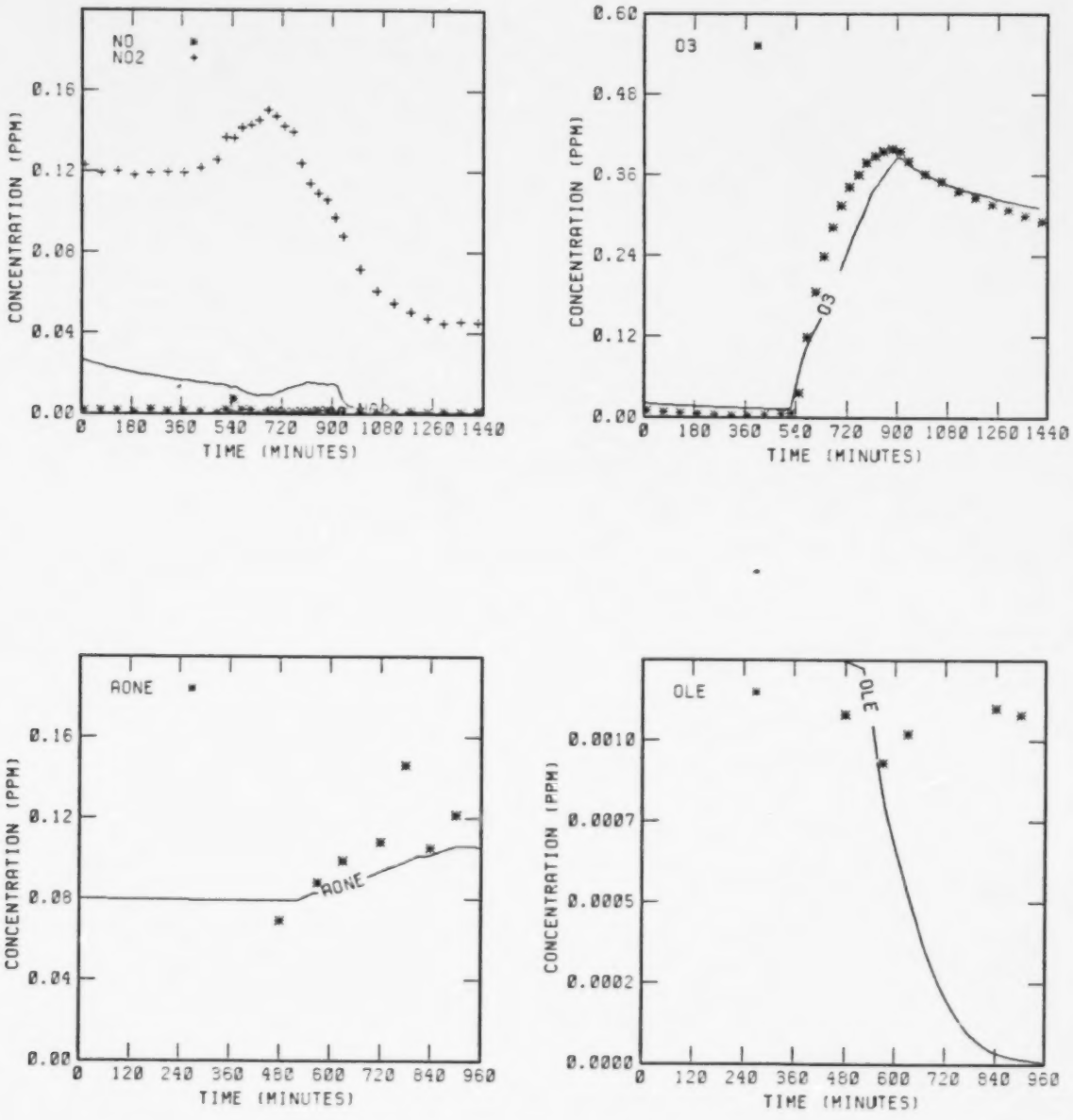

FIGURE A-1. SIMULATION RESULTS FOR OTCR.80383

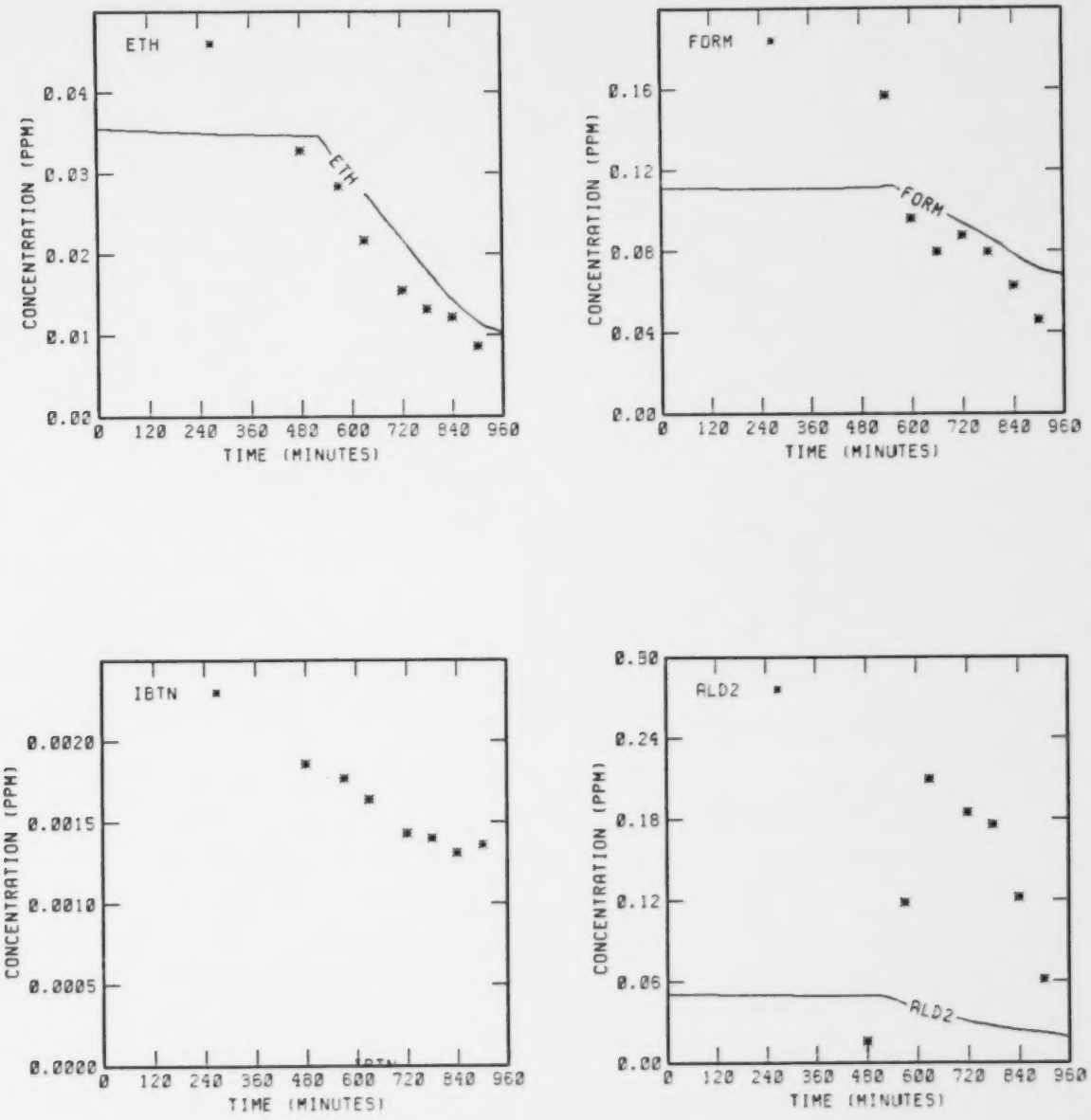

FIGURE A-1. SIMULATION RESULTS FOR
OTCR.80383

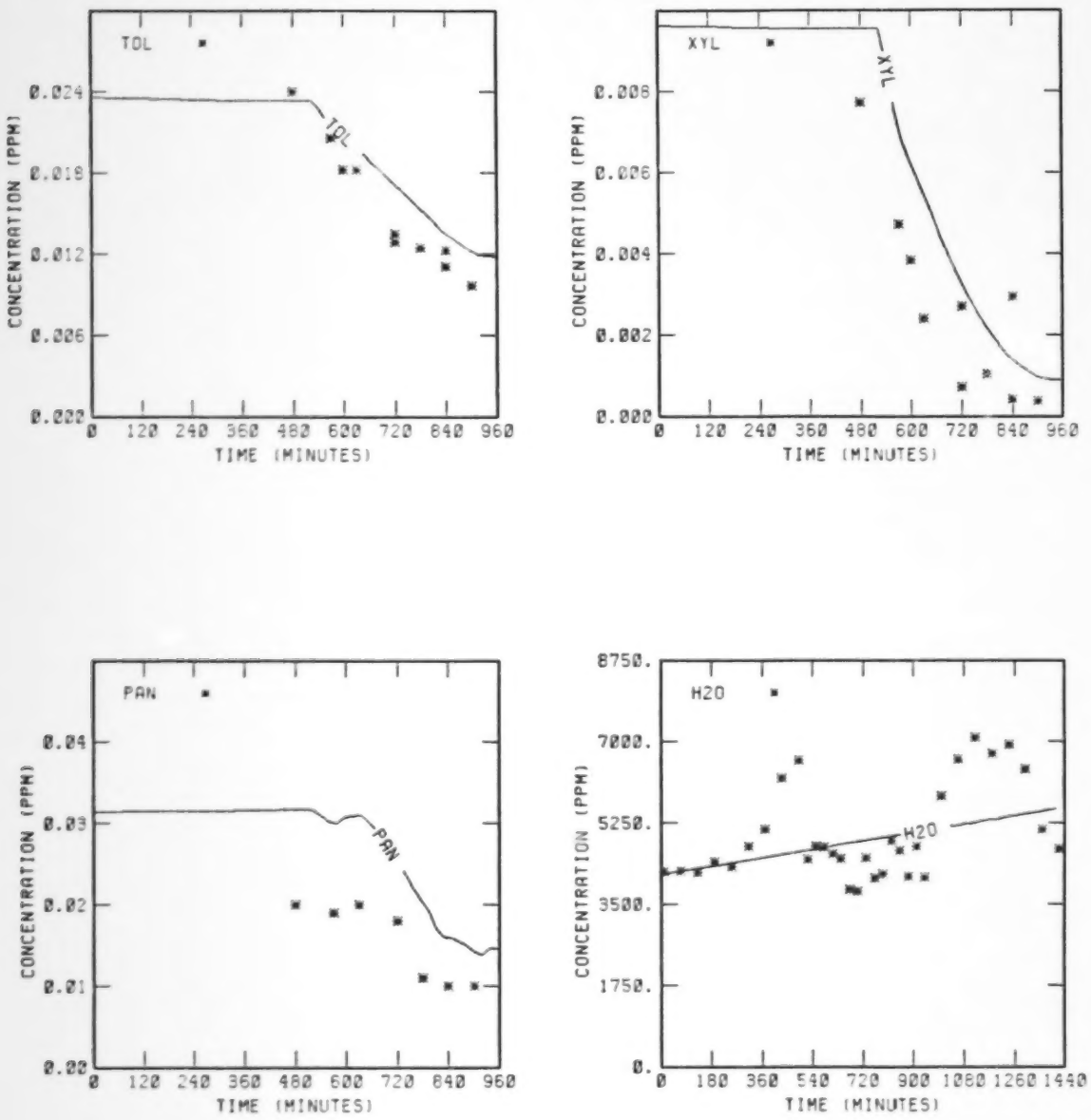

FIGURE A-1. SIMULATION RESULTS FOR OTCR.80383

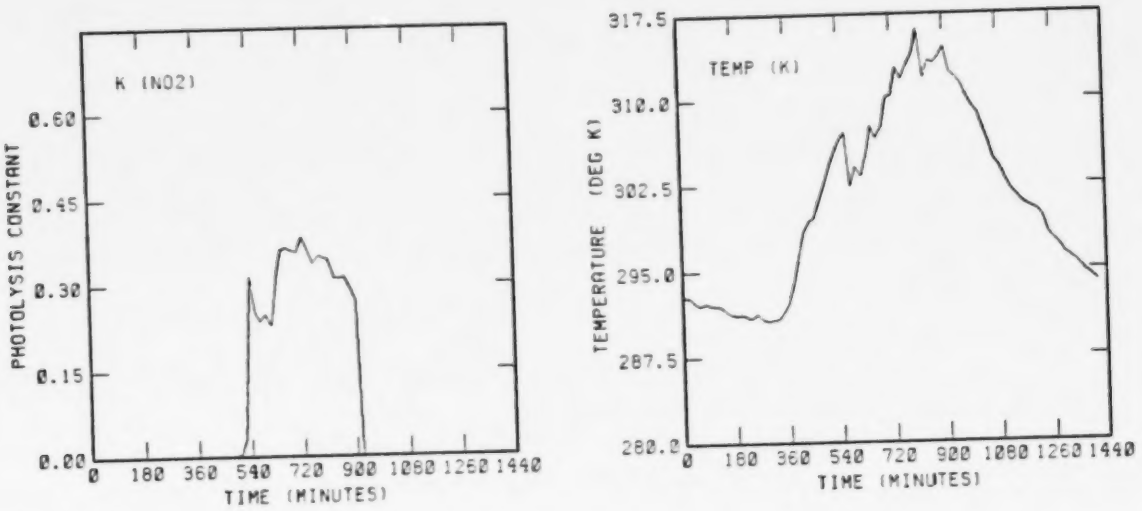

FIGURE A-1. SIMULATION RESULTS FOR OTCR.80383

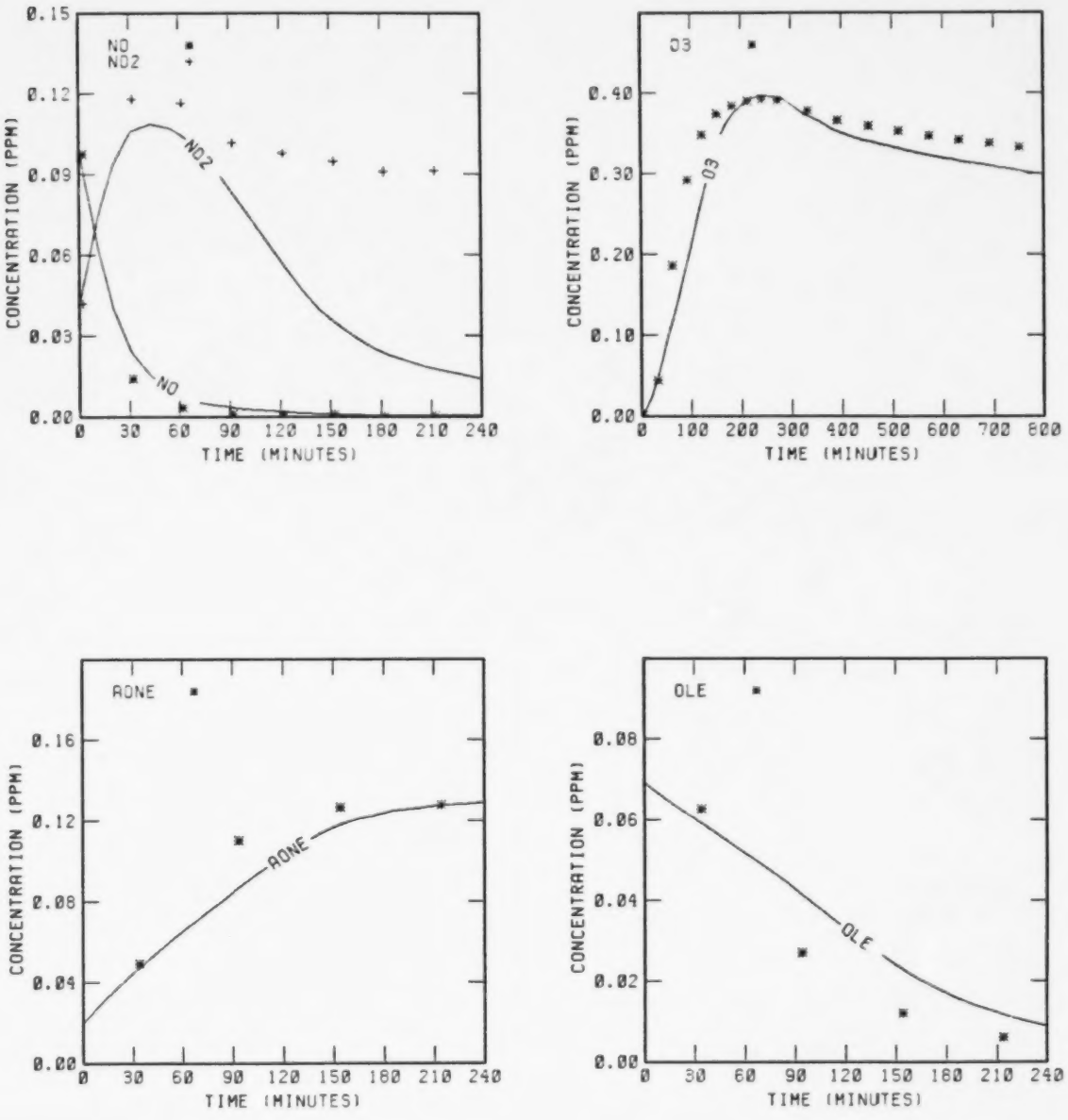

FIGURE A-2. SIMULATION RESULTS FOR
OTCB.101083

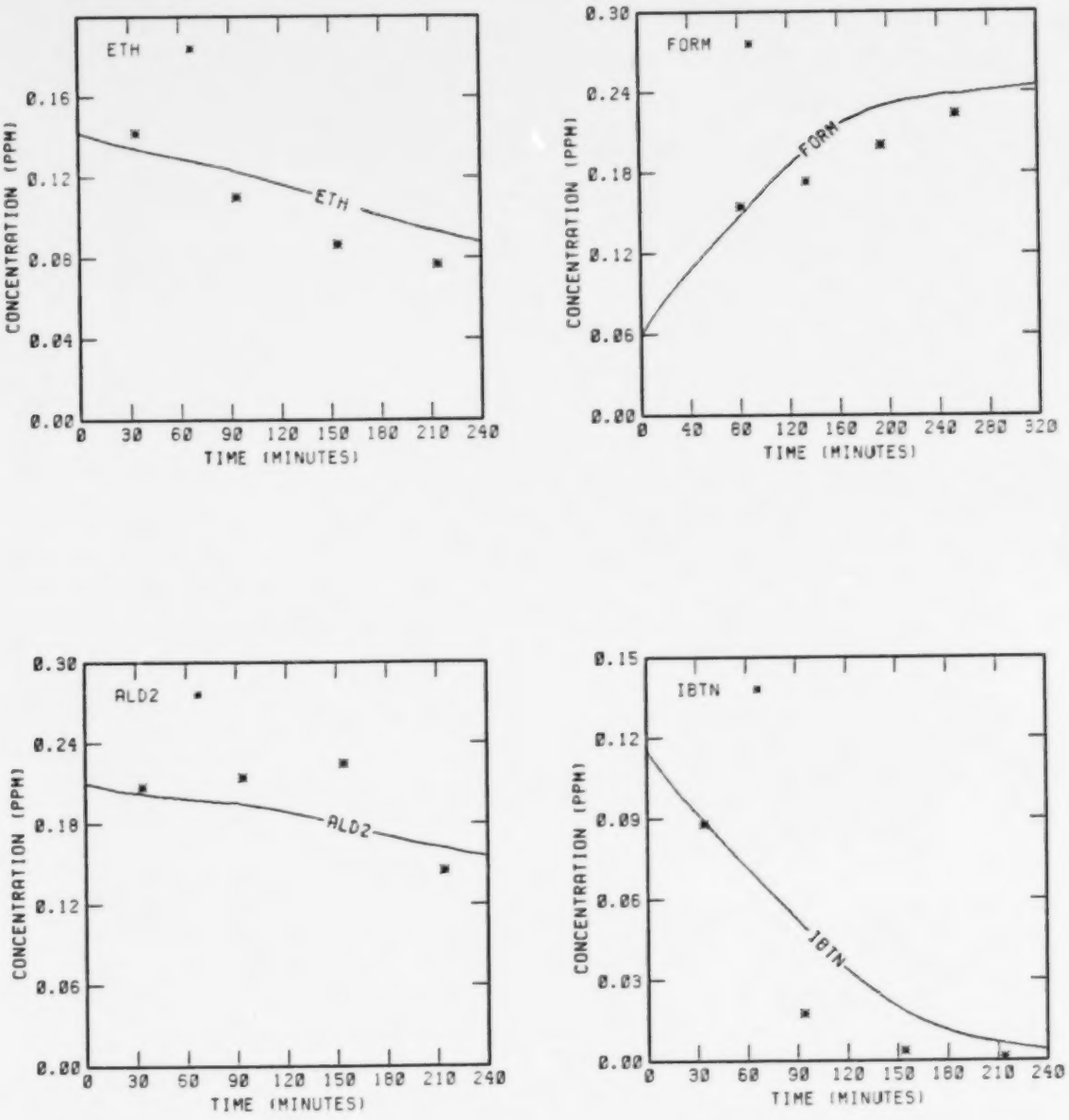

FIGURE A-2. SIMULATION RESULTS FOR OTCB.101083

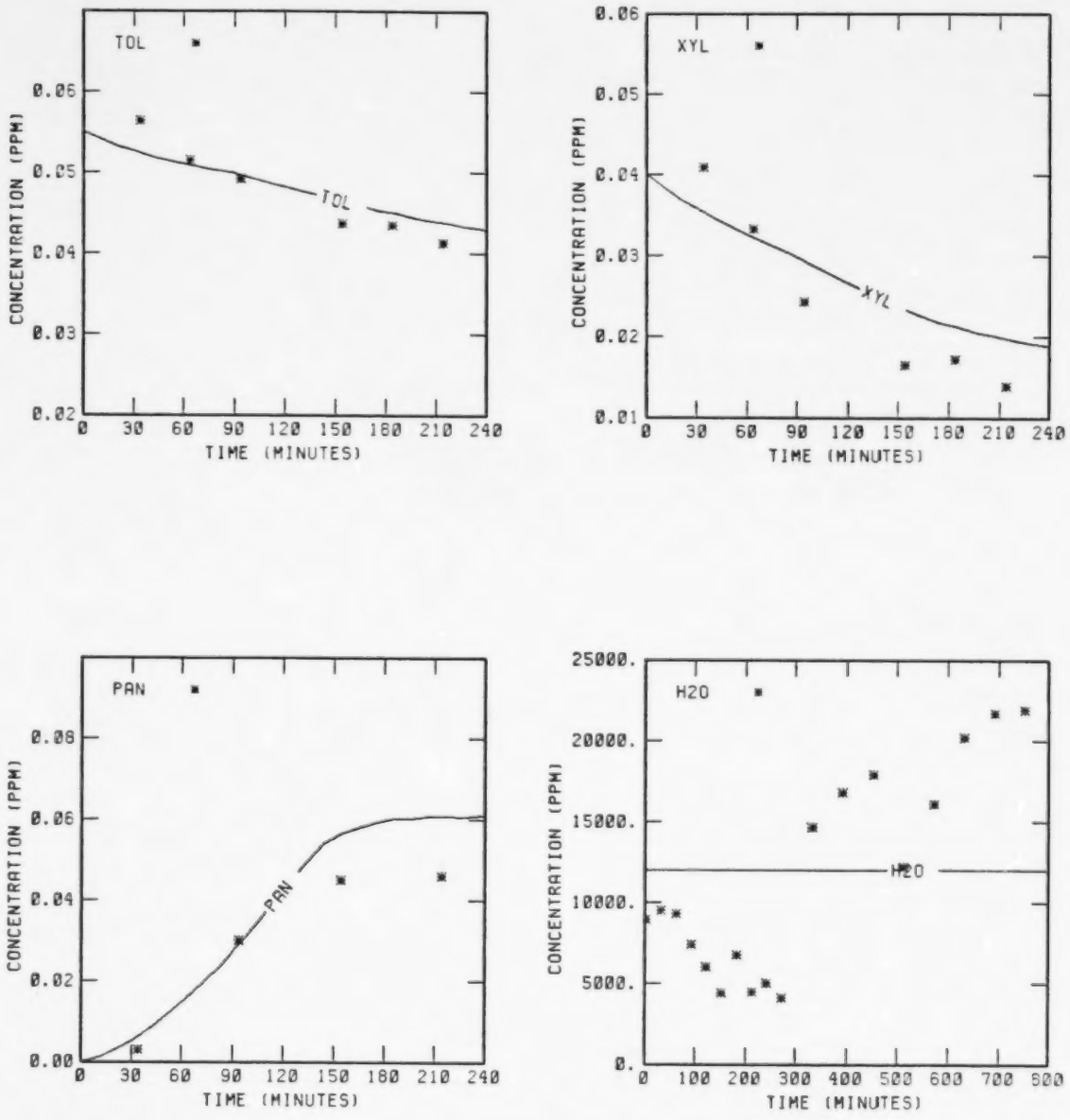

FIGURE **A-2.** SIMULATION RESULTS FOR OTCB.101083

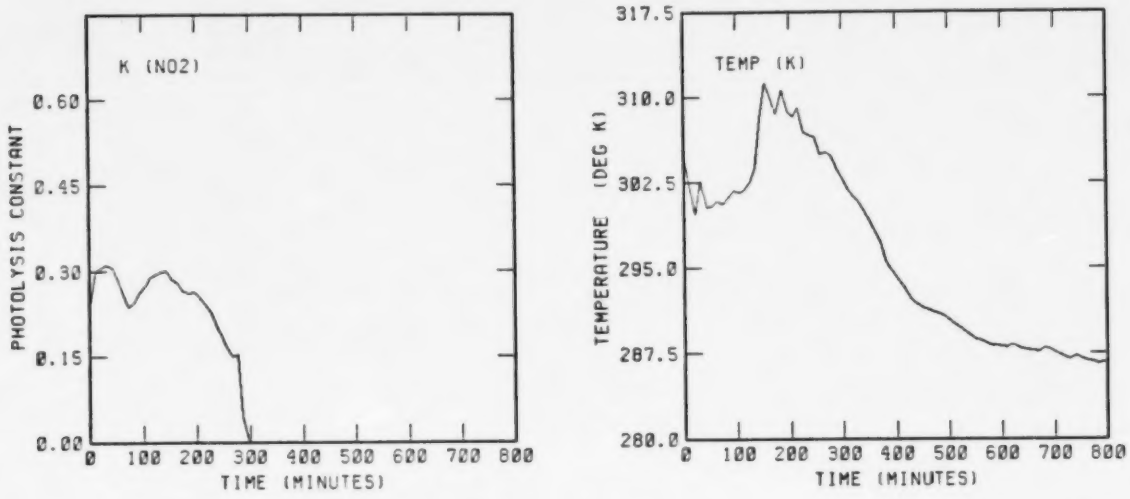

FIGURE A-2. SIMULATION RESULTS FOR
OTCB.101083

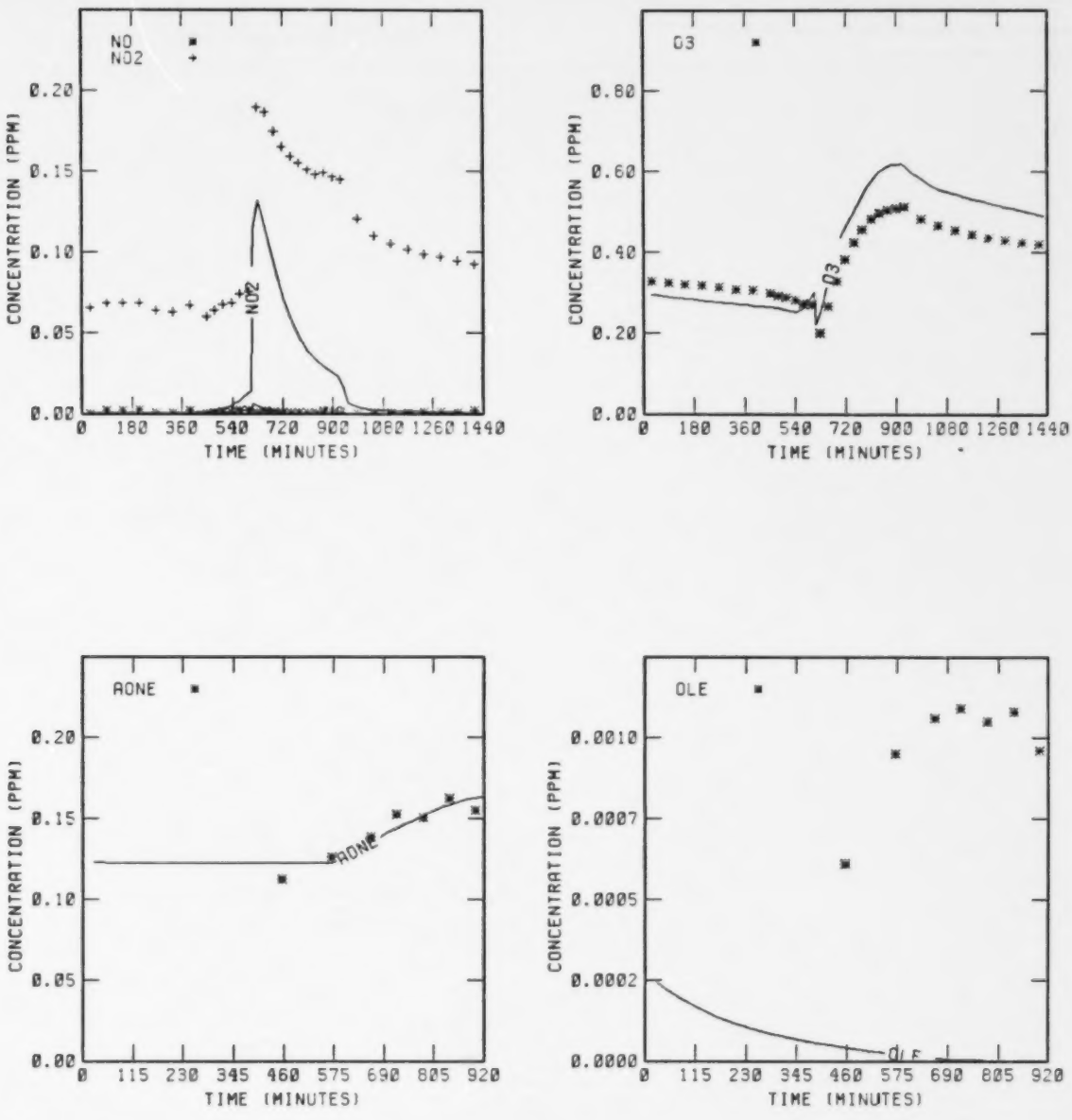

FIGURE A-2. SIMULATION RESULTS FOR
OTCB.101183

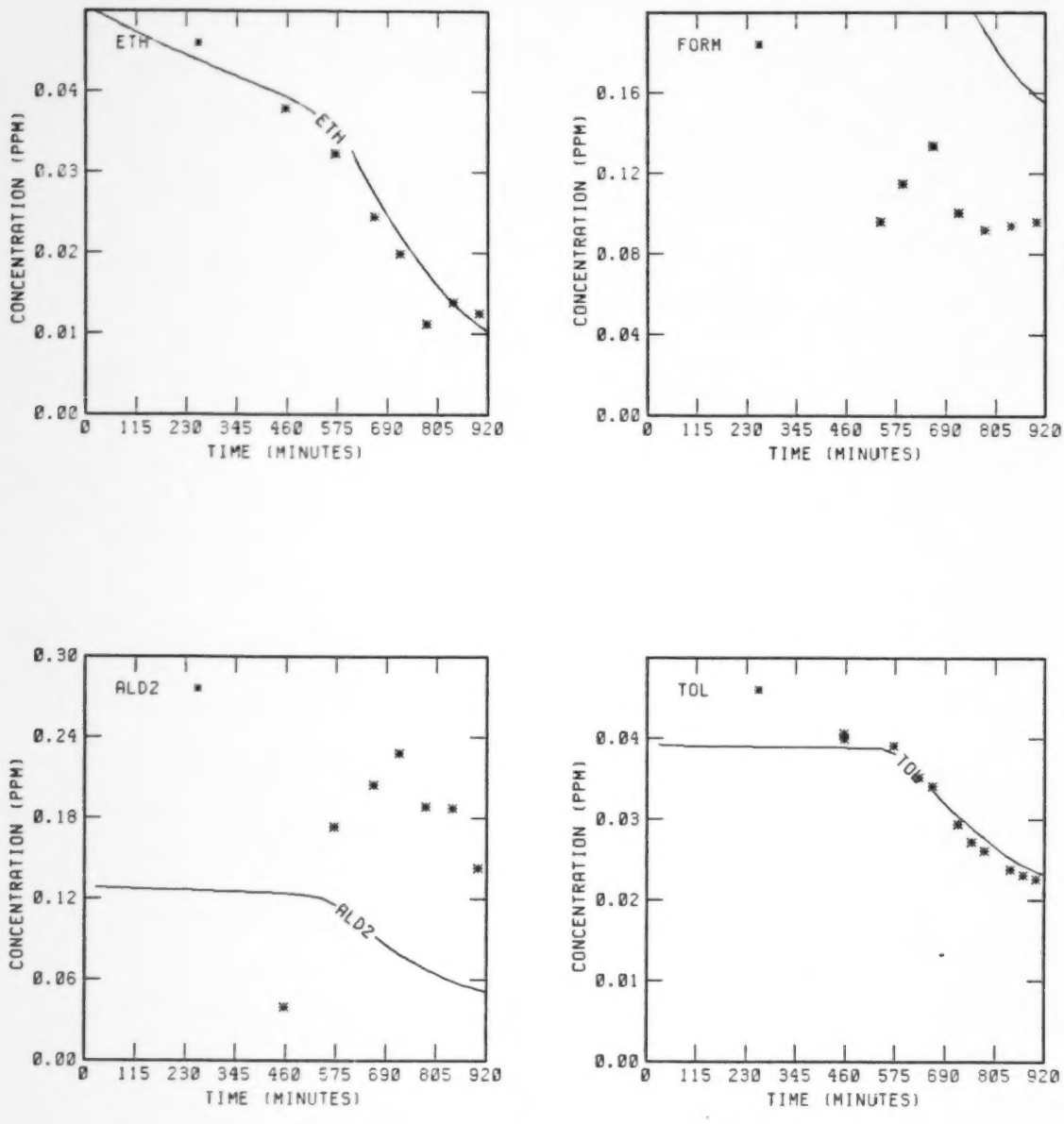

FIGURE A-2. SIMULATION RESULTS FOR OTCB.101183

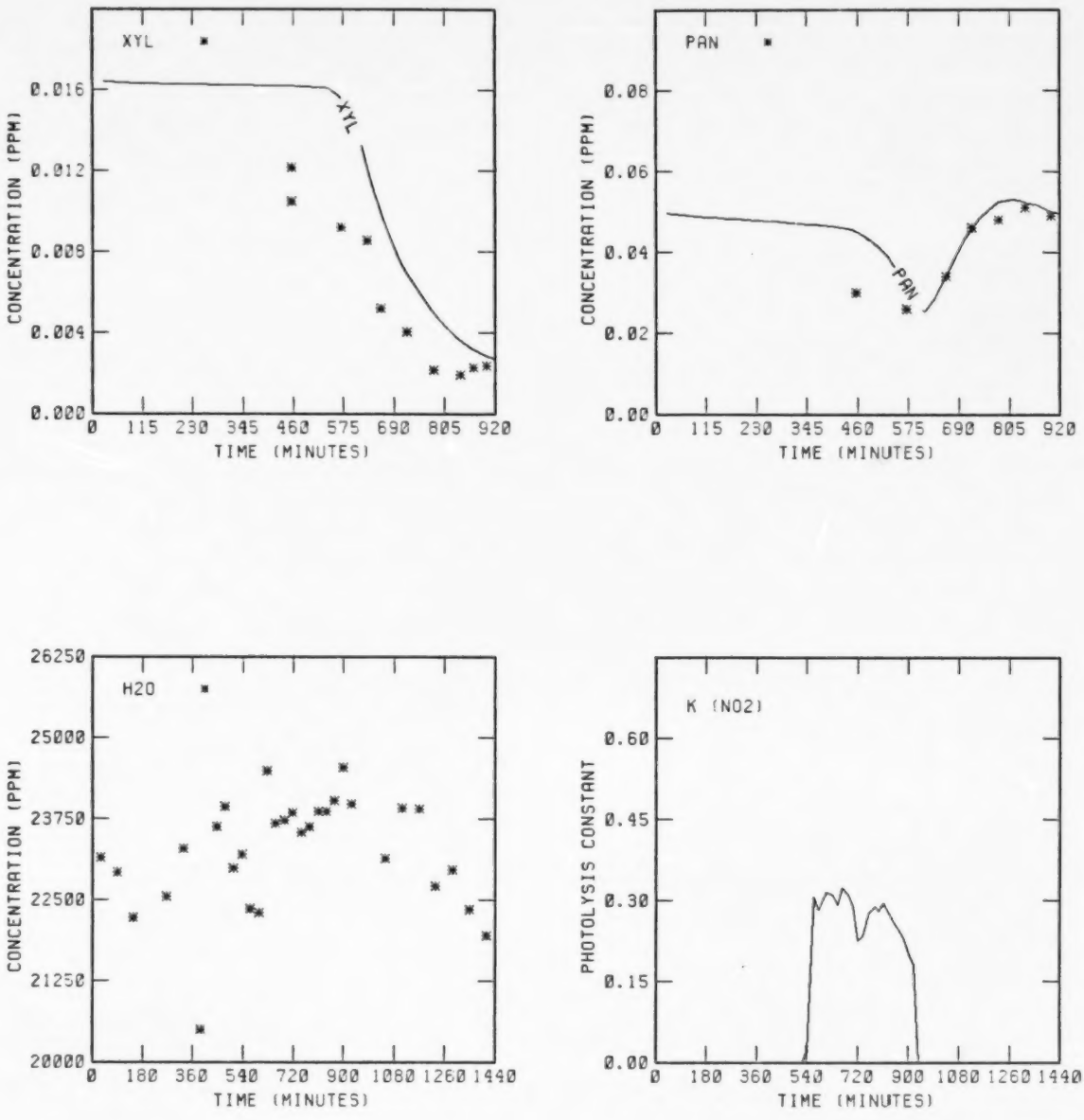

FIGURE A-2. SIMULATION RESULTS FOR
OTCB.101183

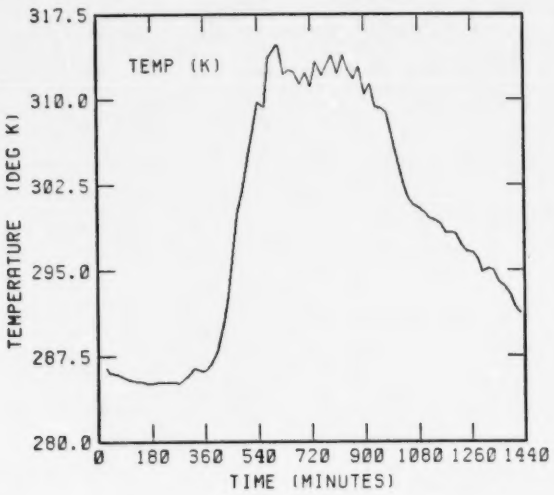

FIGURE A-2. SIMULATION RESULTS FOR
OTCB.101183

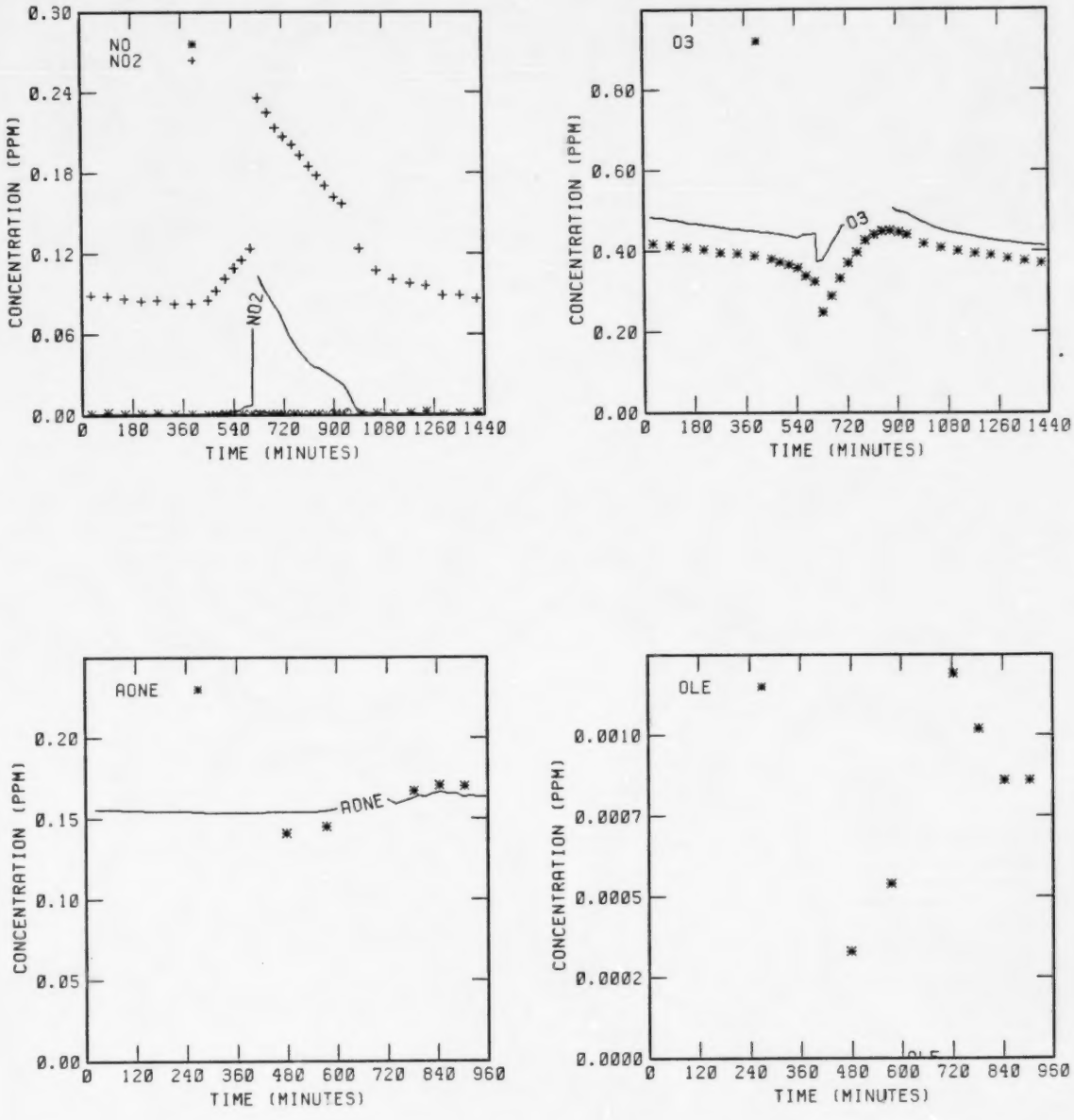

FIGURE A-2. SIMULATION RESULTS FOR OTCB.101283

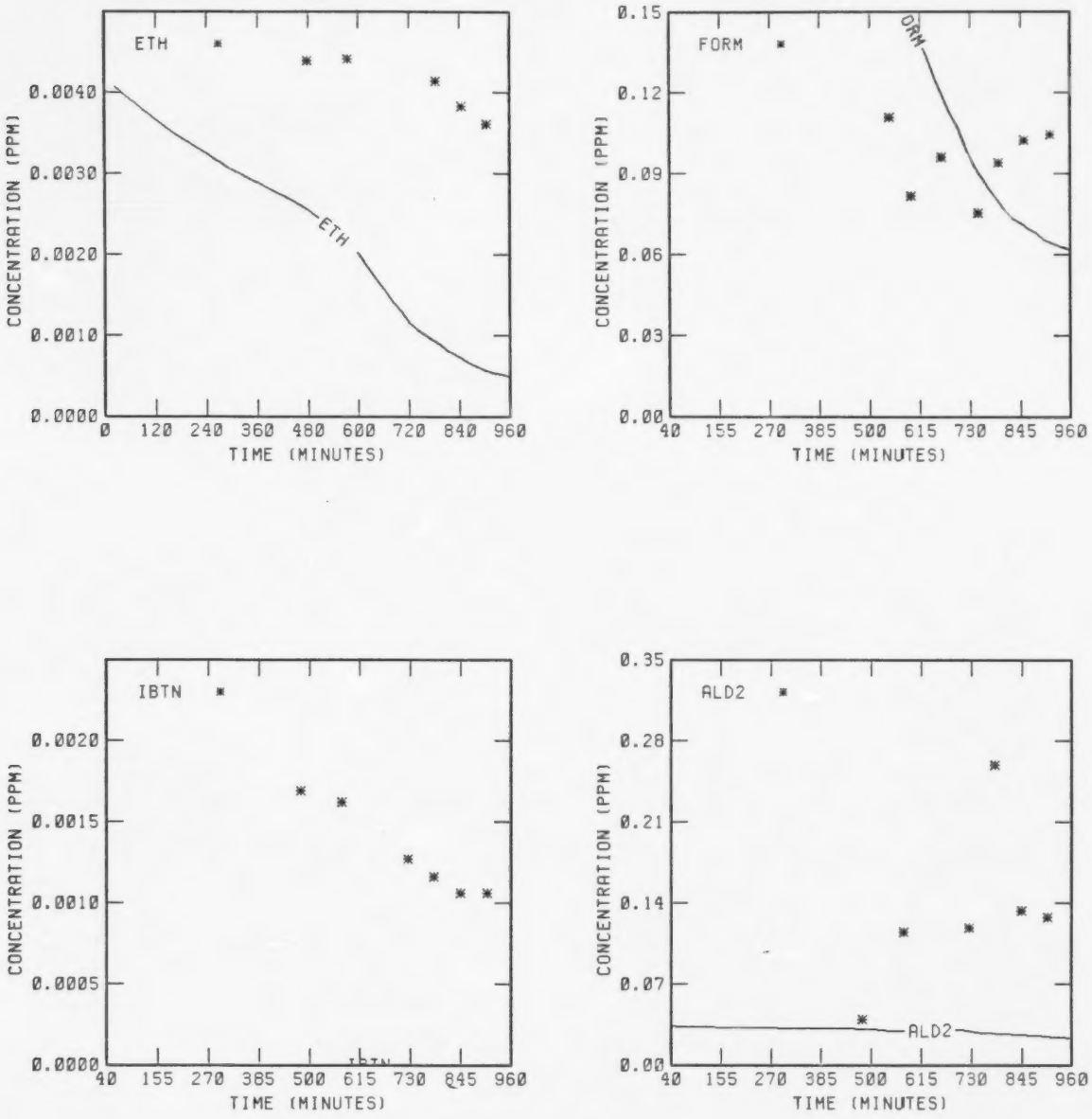

FIGURE A-2. SIMULATION RESULTS FOR
OTCB.101283

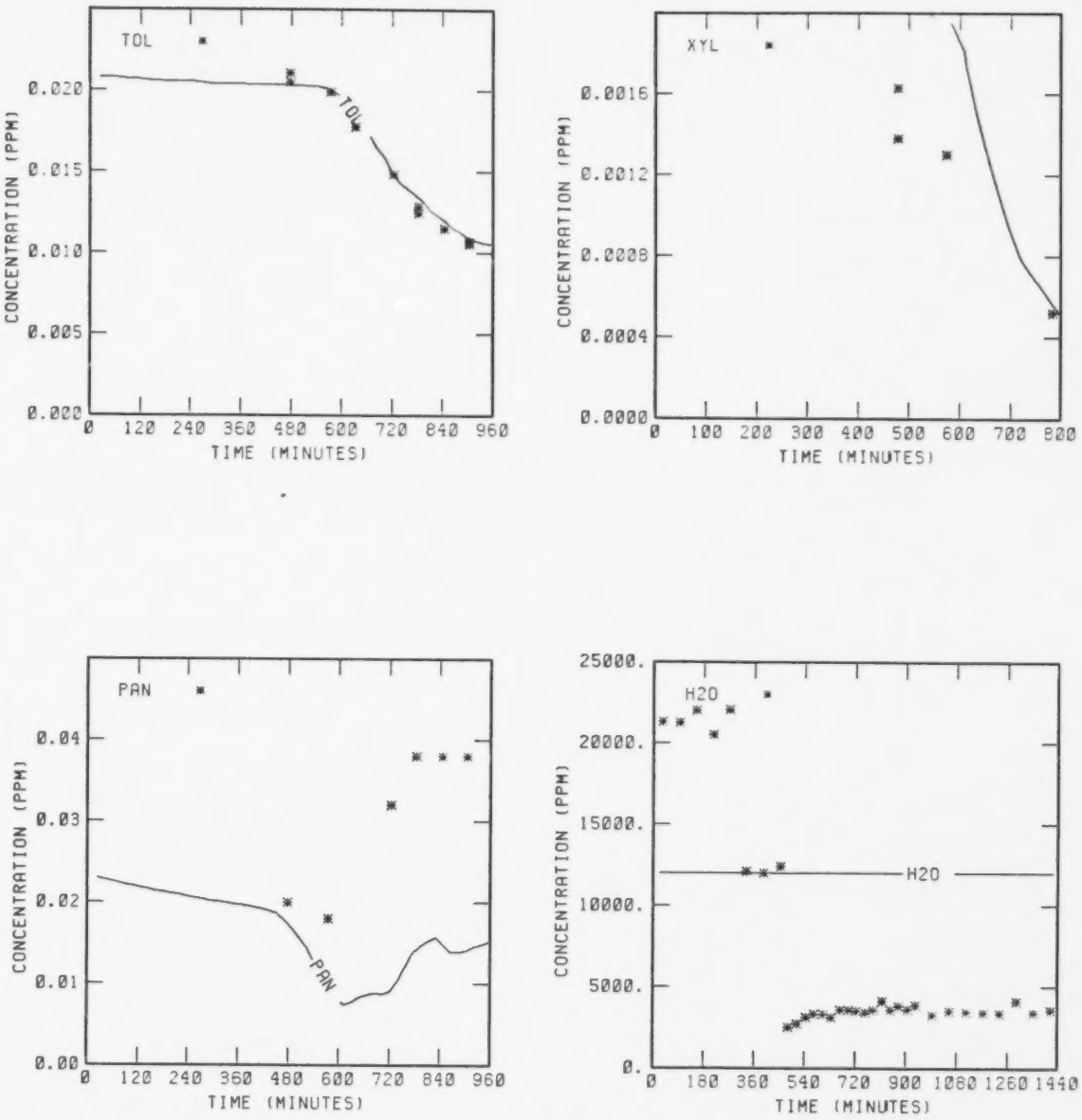

FIGURE A-2. SIMULATION RESULTS FOR
OTCB.101283

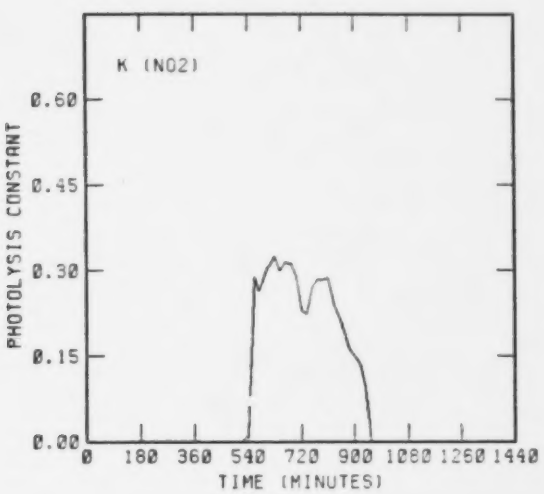

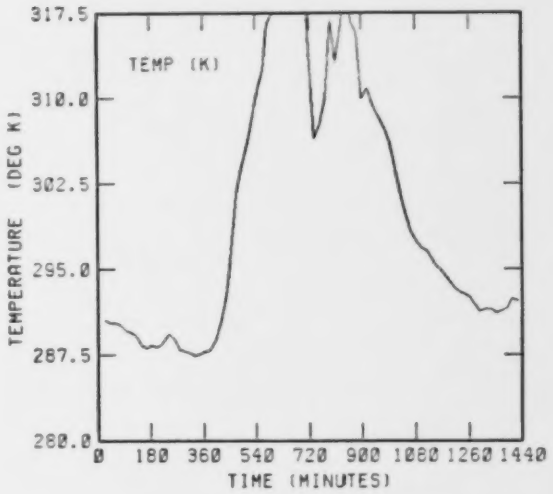

FIGURE A-2. SIMULATION RESULTS FOR OTCB.101283

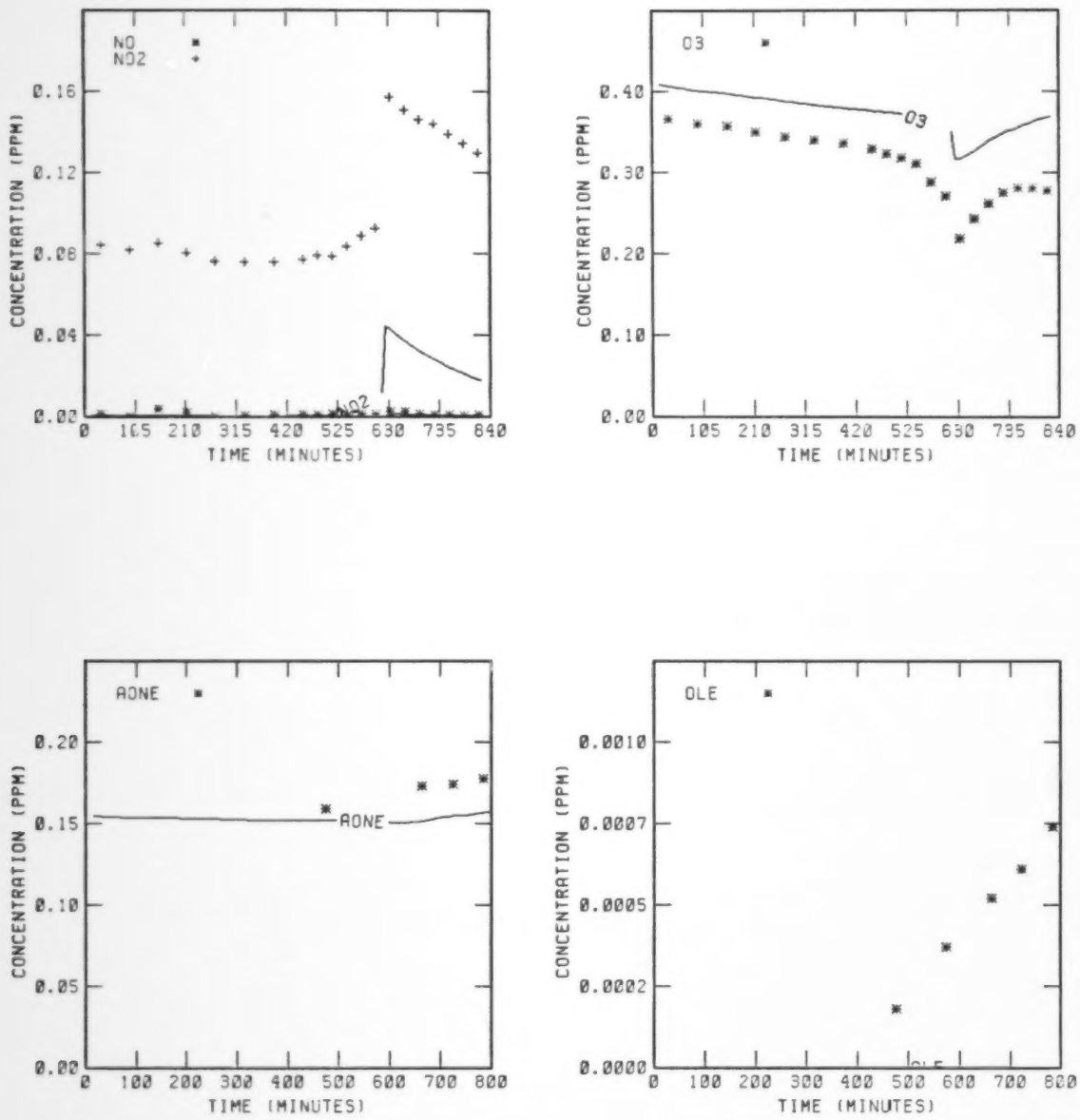

FIGURE A-2. SIMULATION RESULTS FOR OTCB.101383

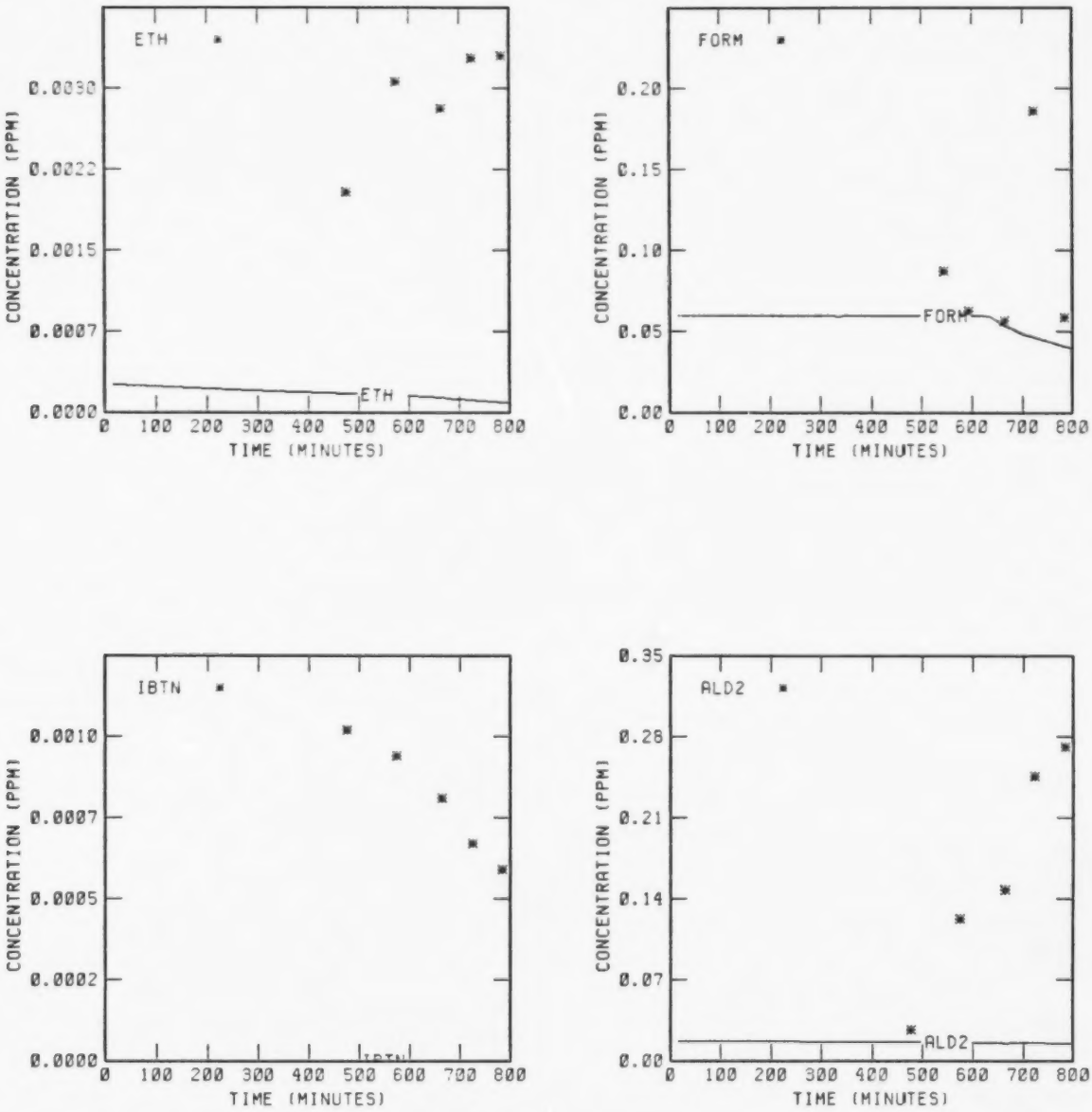

FIGURE A-2 SIMULATION RESULTS FOR
OTCB.101383

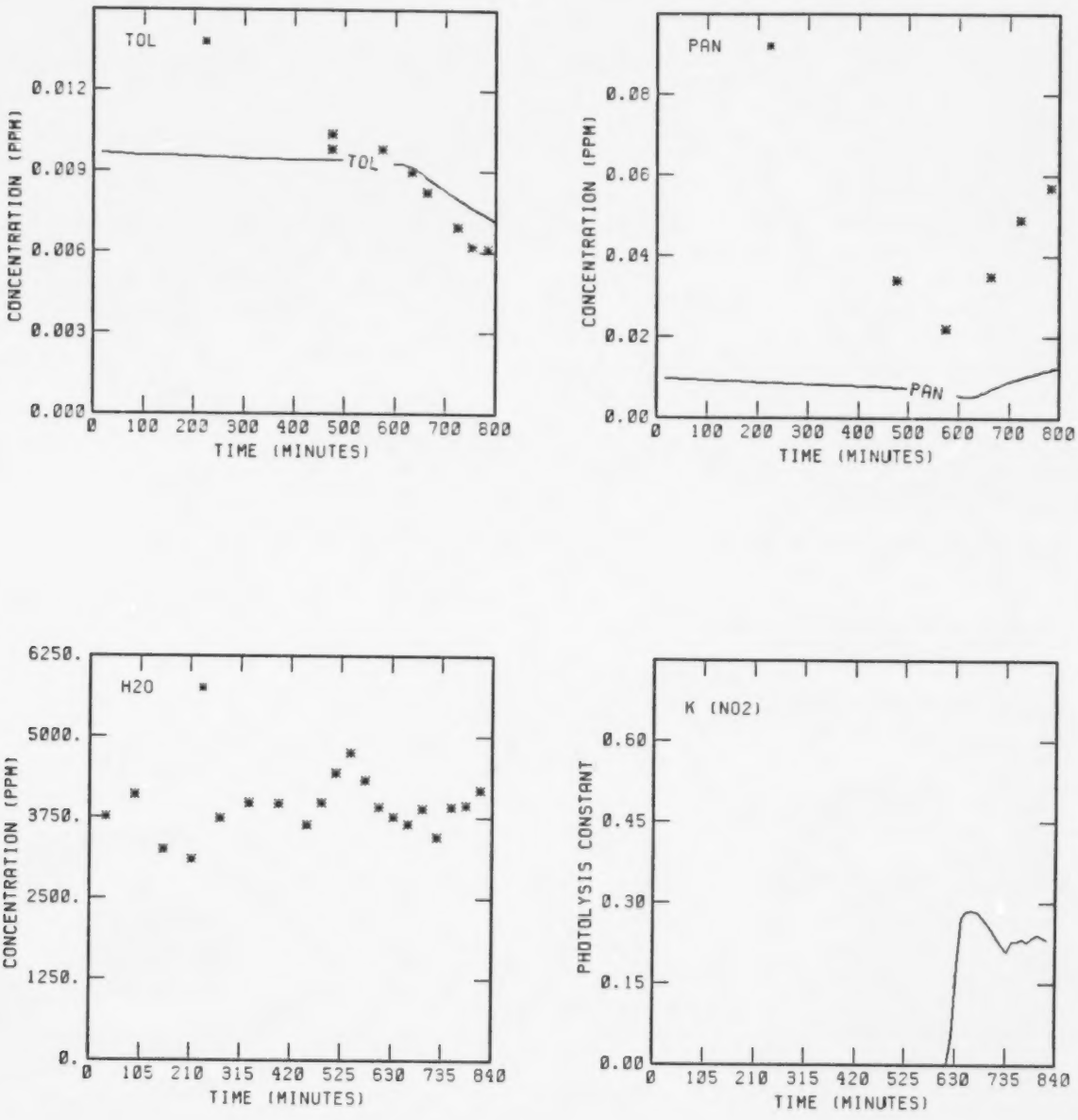

FIGURE A-2. SIMULATION RESULTS FOR OTCB.101383

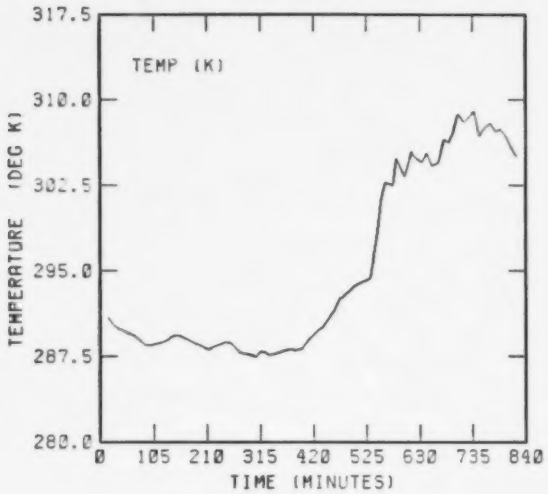

FIGURE A-2. SIMULATION RESULTS FOR
OTCB.101383

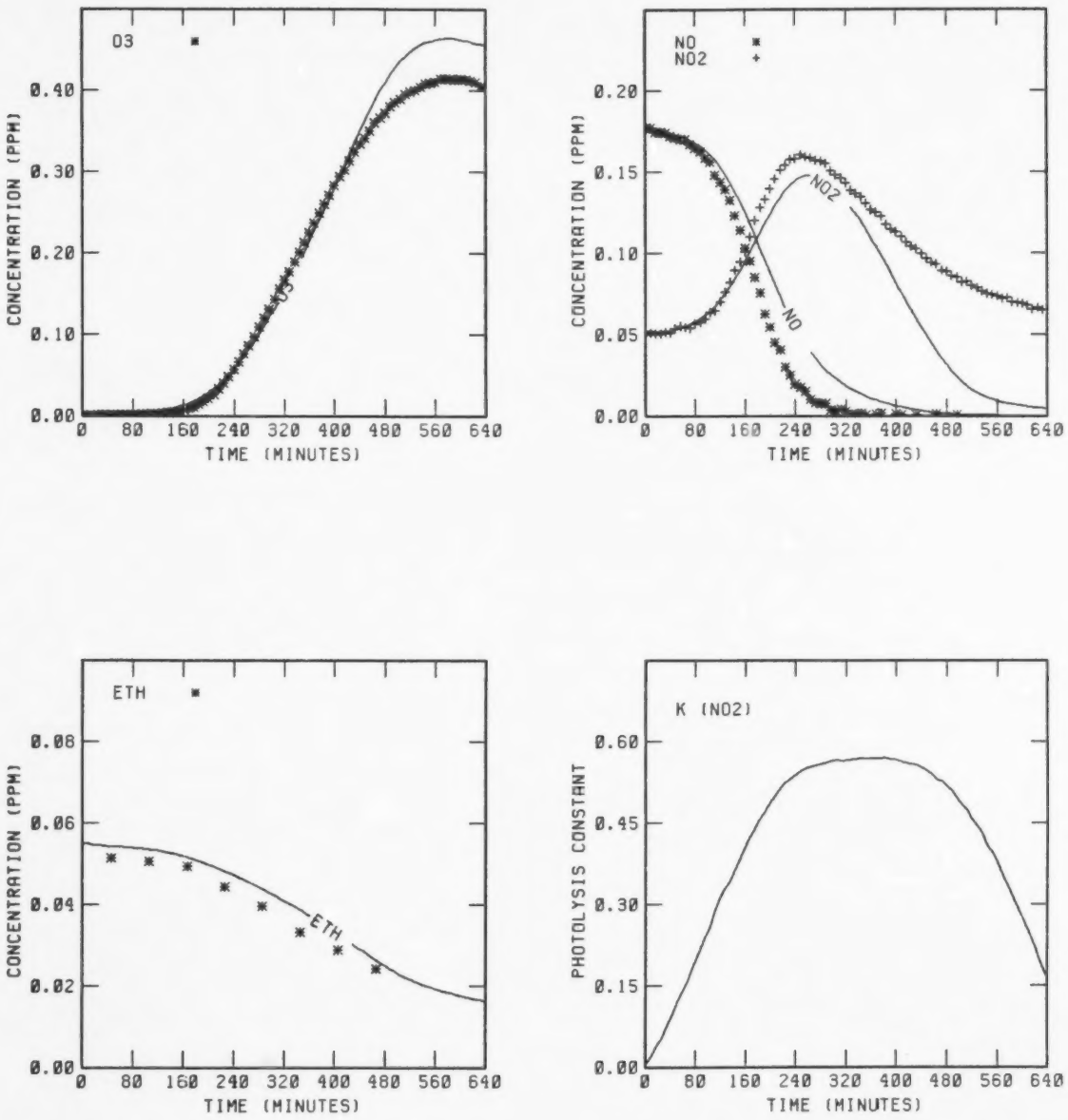

FIGURE A-3. SIMULATION RESULTS FOR
UNCB 92081

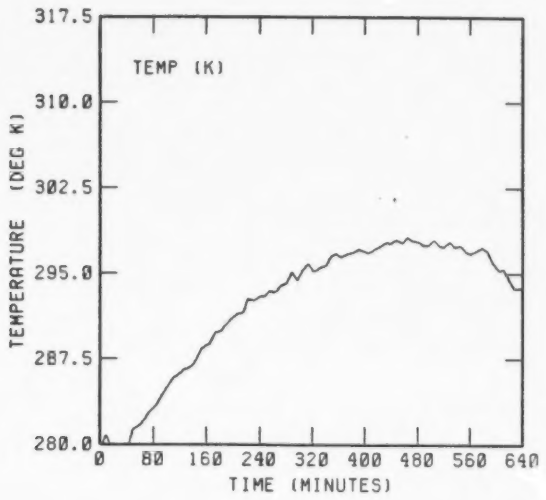

FIGURE A-3. SIMULATION RESULTS FOR
UNCB 92081

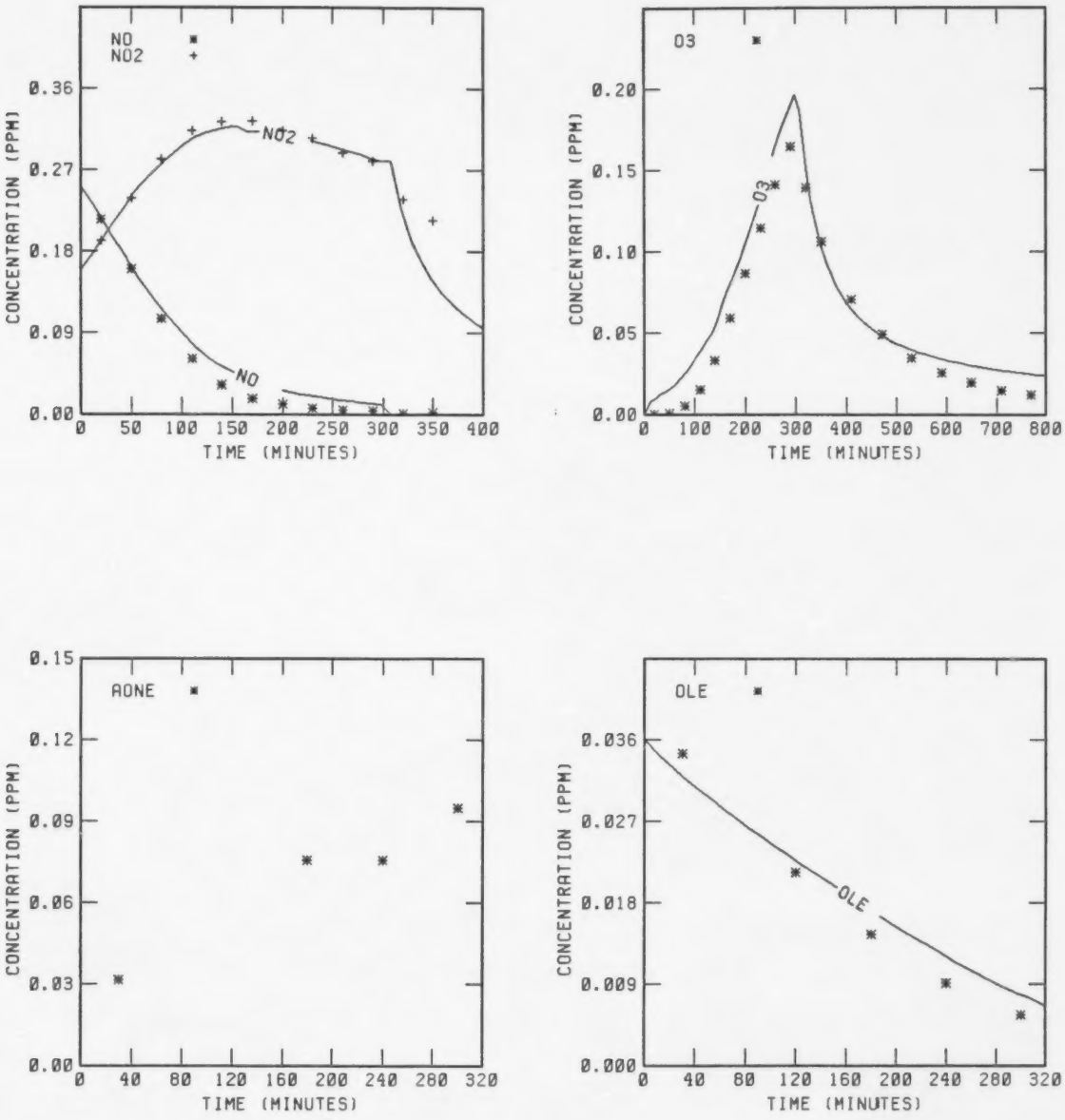

FIGURE A-4. SIMULATION RESULTS FOR OTCR.80283

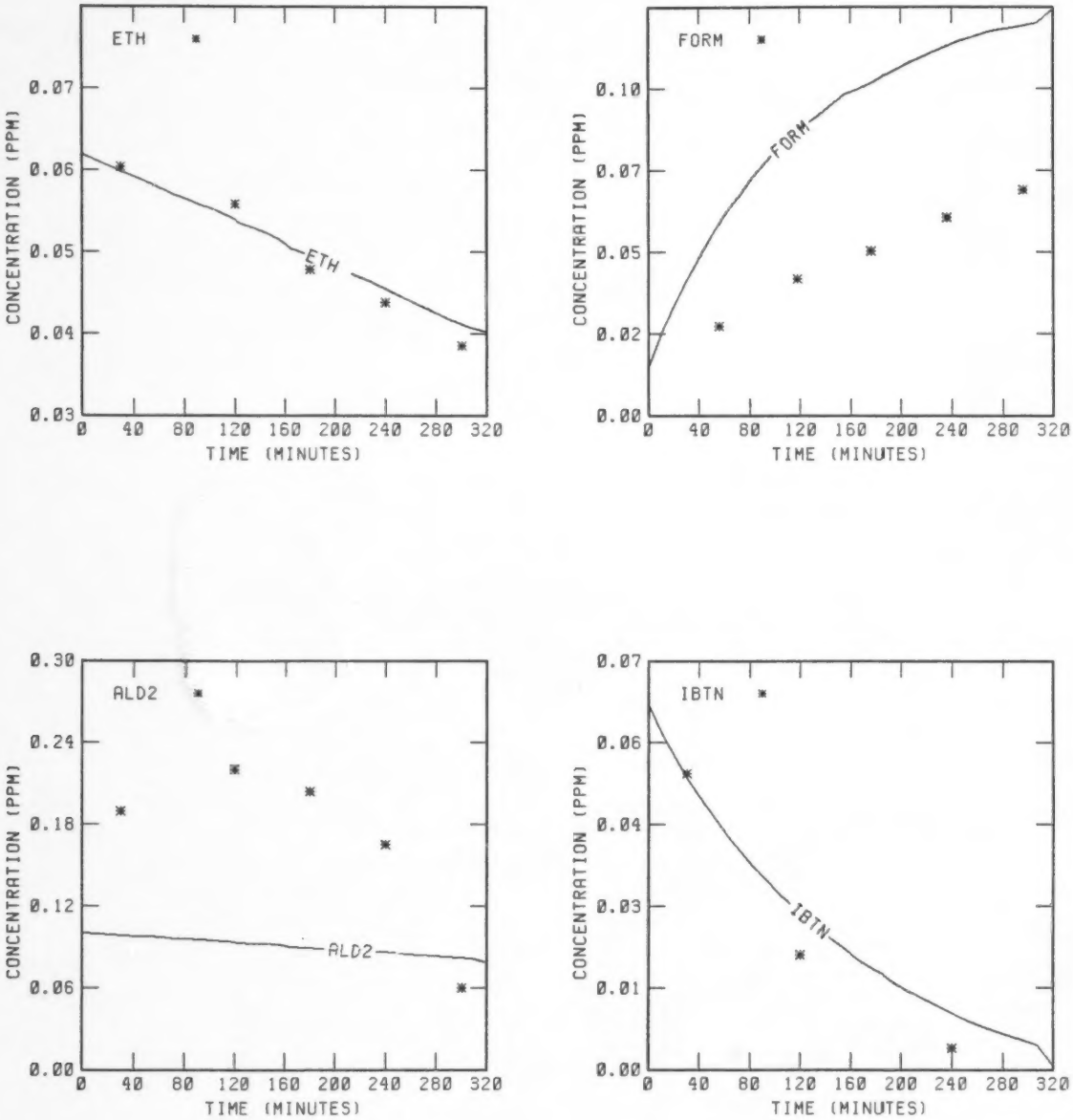

FIGURE A-4. SIMULATION RESULTS FOR OTCR.80283

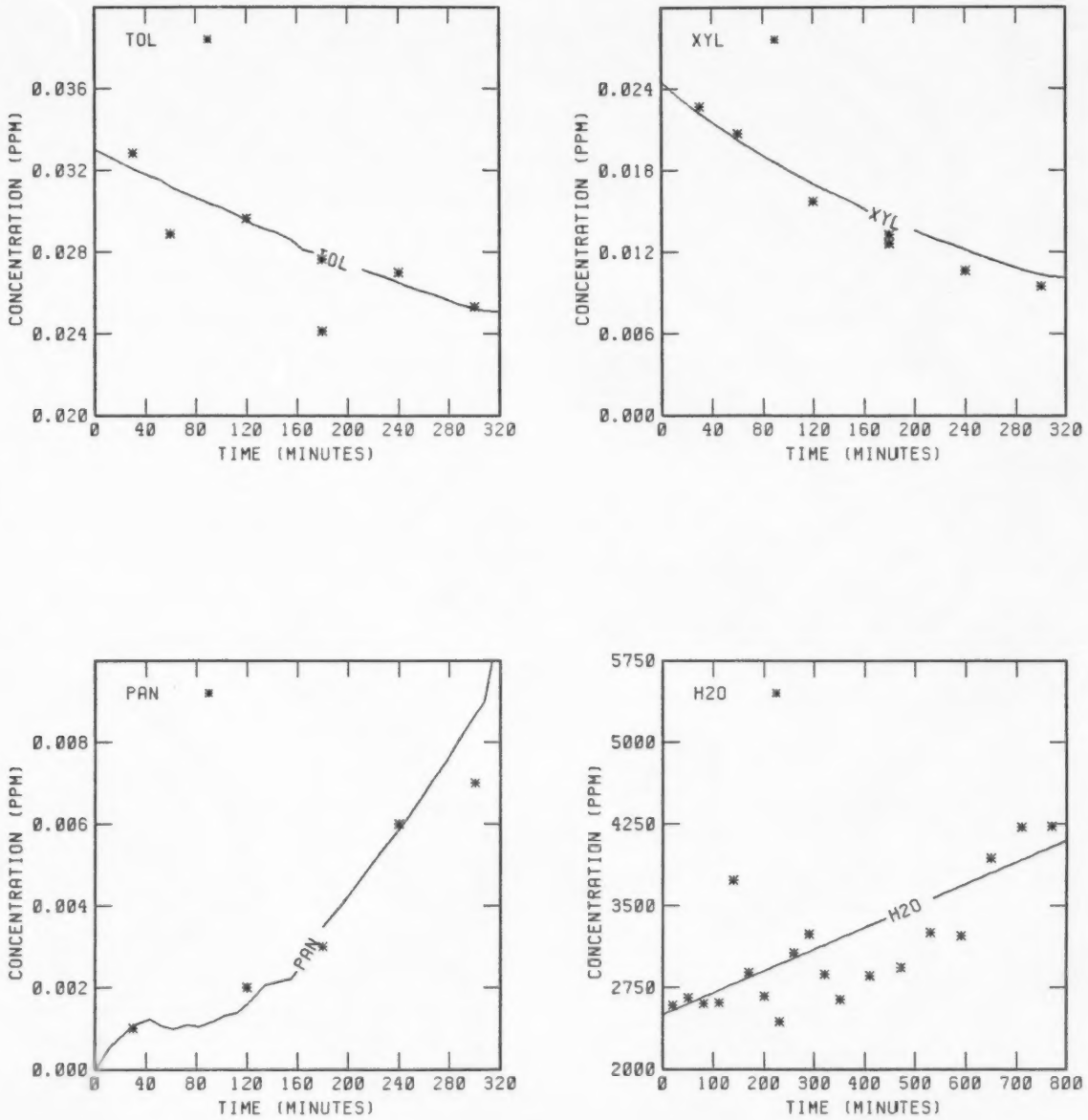

FIGURE A-4. SIMULATION RESULTS FOR OTCR.80283

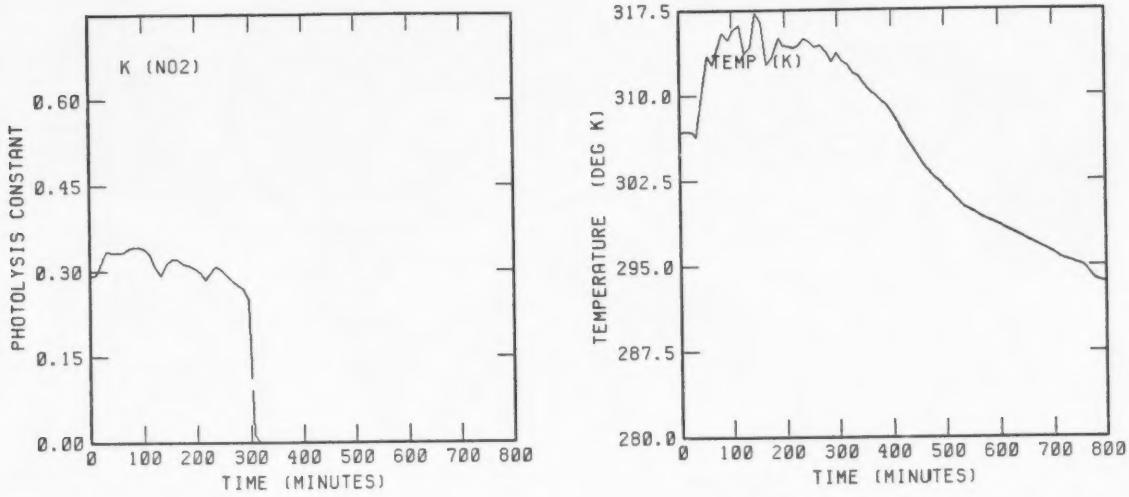

FIGURE A-4. SIMULATION RESULTS FOR OTCR.80283

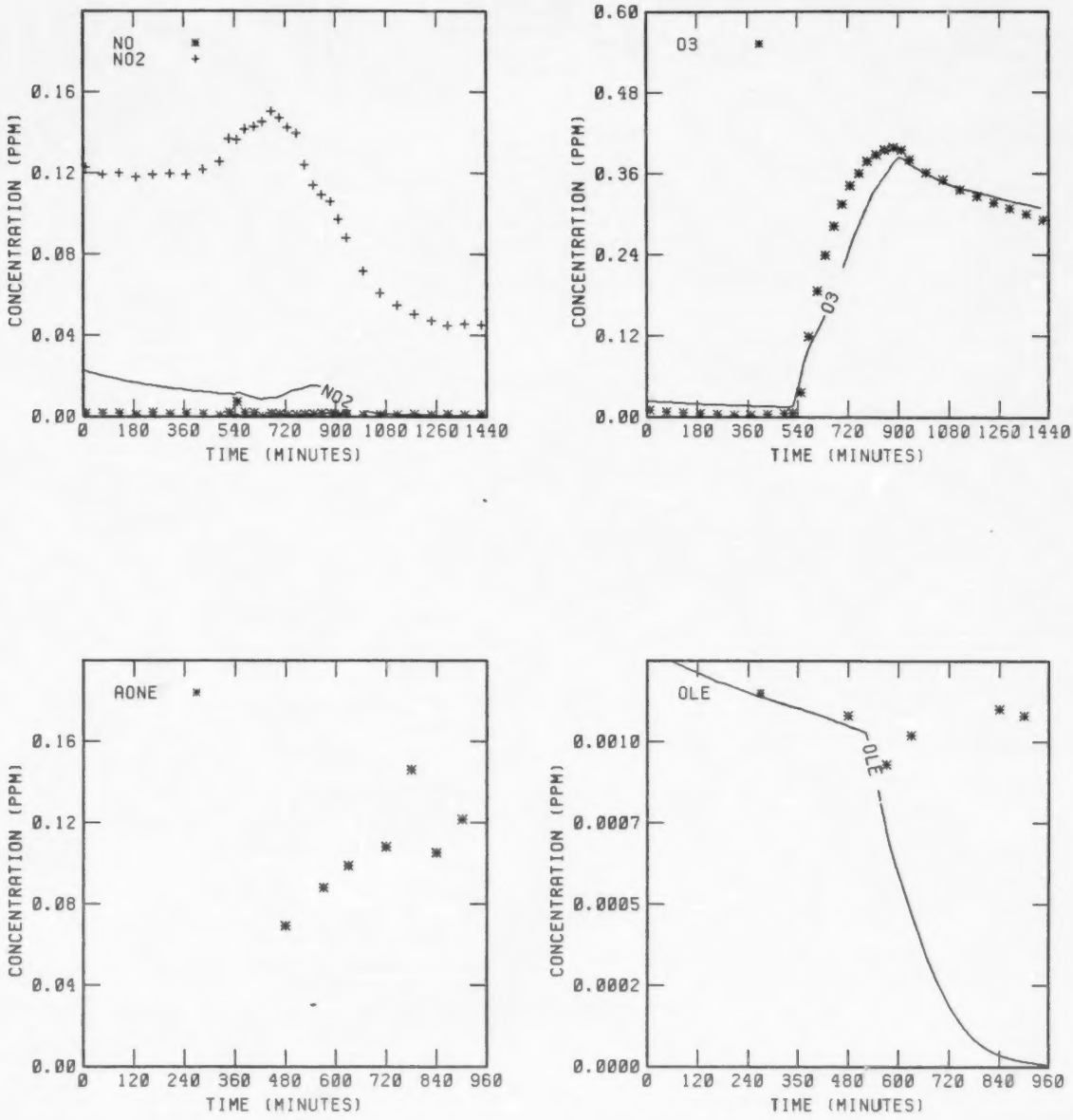

FIGURE A-4. SIMULATION RESULTS FOR OTCR.80383